APPLICATIONS OF NONEQUILIBRIUM STATISTICAL PHYSICS TO ECOLOGICAL SYSTEMS

DISSERTATION

Presented in Partial Fulfillment of the Requirements for

the Degree Doctor of Philosophy in the

Graduate School of The Ohio State University

By

Vishwesha Guttal, M.Sc.

* * * * *

The Ohio State University

2008

Dissertation Committee:

Prof. C. Jayaprakash, Adviser

Prof. David Stroud

Prof. Dick Furnstahl

Prof. Michael Poirier

Approved by

Adviser
Physics Graduate Program

ABSTRACT

Ecological systems such as forest and lakes can exhibit multiple stable states, abrupt transitions and self-organization as a control parameter is varied. Understanding the dynamics of these systems and devising easily quantifiable measures with predictive capabilities using the theoretical tools of stochastic dynamics and nonequilibrium statistical physics form the focus of this thesis.

First, we study simple ecological models with no spatial degrees of freedom, that show a catastrophic transition as a control parameter is varied and propose a novel early warning signal that exploits two ubiquitous features of ecological systems: nonlinearity and large external fluctuations. It is shown that changes in asymmetry in the distribution of time series data, quantified by changing skewness, is an early warning signal of impending regime shifts. Using simple analytical calculations, model simulations that mimic field measurements and an analysis of real data from abrupt climate change in the Sahara, we study the feasibility of skewness calculations using data available from routine monitoring.

Next, we consider a spatially explicit model of collapse of vegetation in one and two spatial dimensions. An analytical calculation based on the mean-field approximation shows that spatial variance and spatial skewness (with an appropriate sign) increase as one approaches the threshold of vegetation collapse. Our numerical calculations show that an increasing spatial variance in conjunction with a reversal in the initial changing trend of spatial skewness is a superior indicator of an impending spatial ecological regime shift when

spatially explicit data are available. These results are shown to hold under several different dispersal kernels such as Gaussian, fat tailed and Cauchy.

Vegetation in semi-arid regions exhibits striking spatial patterns. Theoretical models often ignore the strong fluctuations in parameters such as those arising from seasonality. We present a fully seasonal rainfall model that produces vegetation patterns based on Turing mechanism. We present results for the mean-field and spatially extended versions of the model. We find that the patterns depend on the duration of the wet season even with fixed total annual precipitation (PPT) and our results of maximum vegetation cover as function of PPT is consistent with field observations.

In summary, using theoretical tools of stochastic and nonequilibrium dynamics, we have studied the dynamics of ecological systems showing catastrophic transitions and devised predictive measures which have the potential of practical applications in ecological systems.

Dedicated to my parents

and

to mother earth

ACKNOWLEDGMENTS

I gratefully acknowledge my thesis adviser Prof. C. Jayaprakash for invaluable guidance, for teaching me how to learn physics and for fostering critical thinking in me. He provided academic freedom to pursue my thoughts. In addition, he was always available for advice on career which made a huge difference to me. I have been fortunate to find him as my adviser and it has been a truly enriching experience working under him.

I was privileged to find opportunities to work with Prof. Stroud and Prof. Bundschuh during the initial stages of my graduate school. They have been extremely supportive of me all along and I have learnt a great deal from them. My heartfelt thanks to them.

I would like to thank Prof. Dick Furnstahl and Prof. Michael Poirier for enthusiastically serving on my dissertation committee. I also wish to thank the Department of Physics for providing me the opportunity to be a Teaching Associate during my first two years and for the excellent facilities it has offered for graduate students.

I had a wonderful experience working on a research project with Andrew Nevai and Gregg Hartvigsen. Vikas Malik has been very kind to me in responding to all of my requests on discussions related to Ecology literature and helping me prepare my conference presentations. Paulo D'Odorico, Egbert van Nes, Oliver Lejeune, Marten Scheffer, Gregg Hartvigsen, Sujith Ravi, Nicolas Barbier, Vasilis Dakos, Sonia Kefi, Amitabh Virmani, G. R. Jayanth, Rakesh Tiwari, Srividya Iyer Biswas, Thomas Kleinen and V. Balaji have provided very useful comments on my manuscripts and presentations at various stages.

Many thanks to all these people and several others whom I may have forgotten to name here, for offering help whenever I asked them.

I thank my very close friends Amitabh and Prasoon for being such wonderful friends all along. My housemates at 1531 Worthington - Anand, Dakshinamurthy and Jayanth - have tolerated my extreme dietary restrictions for all these four and a half years and I am indebted to them for their understanding and cooperation. Our daily dinner sessions with discussions on everything under/above the sky provided a perfect recipe for learning filled with laugher.

Thanks to Leena, Tahera, Romel, Fareen, Rakesh and Mehul for making my life at Columbus filled with so much fun.

It would be incomplete to not thank Association for India's Development (AID) for providing me a platform to think critically and act responsibly on variety of social issues.

Last but not the least, no words can thank my parents and family members for their patience while I am out of home for nearly 10 years.

VITA

March 27, 1981	Born - Gangavathi, Karnakata, India
2003	M.Sc., Physics, Indian Institute of Technology, Kanpur
2003 - 2005	Graduate Teaching Associate, Department of Physics, The Ohio State University
2005 - 2007	Graduate Research Associate, Department of Physics, The Ohio State University
2007 - 2008	Presidential Fellow, The Ohio State University

PUBLICATIONS

1. Vishwesha Guttal, C. Jayaprakash, 2008. "Changing skewness: an early warning signal of regime shifts in ecological systems", Ecology Letters, 11:450-460.

2. Vishwesha Guttal, C. Jayaprakash, 2007. "Self-organization and productivity in semi-arid ecosystems: Implications of seasonality in rainfall", Journal of Theoretical Biology, 248: 490-500.

3. Vishwesha Guttal, C. Jayaprakash, 2007. "Impact of noise on bistable ecological systems", Ecological Modelling, 201:420-428.

4. Vishwesha Guttal, Ralf Bundschuh, 2006. "A model for folding and aggregation in RNA secondary structures", Physical Review Letters, 96:018105.

5. Vishwesha Guttal, David Stroud, 2006. "Nonsaturating magnetoresistance and Hall coefficient reversal in a model composite semiconductor", Physical Review B, 76:085202.

6. Vishwesha Guttal, David Stroud, 2005. "A model for a macroscopically disordered conductor with exactly linear high field magnetoresistance", Physical Review B, (Rapid Communications) 71:201304(R).

7. Debashish Chowdhury, Vishwesha Guttal, Katsuhiro Nishinari, Andreas Schadschneider, 2002. "A cellular-automata model of flow in ant-trails: non-monotonic variation of speed with density", Journal of Physics A, 35:L573.

FIELDS OF STUDY

Major Field: Physics

TABLE OF CONTENTS

Page

Abstract ii

Acknowledgments v

Vita vii

List of Tables xii

List of Figures xiii

Chapters:

1. INTRODUCTION 1

    1.1 Background 2
    1.2 Multiple stable states, hysteresis and abrupt flips in ecological systems . 5
    1.3 Focus of the thesis and organization of results 9

2. CHANGING SKEWNESS: AN EARLY WARNING SIGNAL OF REGIME SHIFTS IN ECOLOGICAL SYSTEMS 11

    2.1 Background 11
    2.2 May's one variable model of vegetation collapse 15
        2.2.1 Fokker-Planck analysis: asymmetry in effective potential and time series distribution 16
        2.2.2 Skewness as a measure of asymmetry 19
        2.2.3 Transient or steady state distributions? 22
    2.3 Two variable model of vegetation collapse 25
        2.3.1 Analysis of failure of skewness as an early warning signal 26
    2.4 Two variable parameterized lake model 30

2.5 Analysis of Sahara data . . . 32
2.6 Discussion . . . 35

3. LEADING INDICATORS OF REGIME SHIFTS IN SPATIAL ECOLOGICAL SYSTEMS . . . 39

3.1 Near the critical point of second order phase transition . . . 40
3.2 Indicators of transitions in diffusion model . . . 42
3.2.1 Bifurcation diagram with space and noise . . . 43
3.2.2 Mean field approximation (MFA) to obtain behavior of indicators 45
3.2.3 Dependence of the results on the strength of spatial interactions . 49
3.2.4 Detection and prevention of an impending regime shift in a numerical experiment . . . 52
3.2.5 Semianalytic arguments to show peaking of skewness in a bistable model . . . 56
3.3 Indicators in stochastic partial integro-differential model . . . 58
3.3.1 Mean field approximation (MFA) . . . 59
3.3.2 Semianalytic arguments for spatial indicators . . . 60
3.3.3 Numerical calculations and comparison with results of MFA . . . 62
3.4 Discussion . . . 64

4. SELF-ORGANIZATION AND PRODUCTIVITY IN SEMI-ARID ECOSYSTEMS: IMPLICATIONS OF SEASONALITY IN RAINFALL . . . 68

4.1 Motivation . . . 68
4.2 A model for pattern formation in semi-arid vegetation . . . 69
4.3 The modified model including adaptive nature of plants . . . 74
4.4 Methods . . . 78
4.4.1 Discussion on convergence . . . 78
4.5 Results and Discussion . . . 80
4.5.1 Self-organized pattern formation . . . 81
4.5.2 Insufficiency of PPT in determining the system behavior . . . 83
4.5.3 Maximum productivity as a function of PPT . . . 85
4.5.4 Effect of perturbations on the behavior of the system . . . 88
4.5.5 Limitations . . . 90
4.6 Summary and Concluding remarks . . . 92

5. SUMMARY AND FUTURE WORK . . . 94

5.1 Summary . . . 94
5.2 Future work . . . 95

Appendices:

A. SUPPORTING MATERIALS FOR CHANGING SKEWNESS: AN EARLY WARNING SIGNAL FOR REGIME SHIFTS IN ECOSYSTEMS 98

A.1 Results for the two-variable vegetation model 99
A.2 Validity of asymmetric arguments for coupled multivariable models . . . 102
A.3 Results for the parameterized lake model 105
A.4 Analysis of real data sets 106

B. SUPPORTING MATERIAL FOR SPATIAL INDICATOR CHAPTER 111

B.1 Time dependence of indicators for fixed grazing 112
B.2 Results of dynamic grazing simulations 114
B.3 One point indicators 117

C. SUPPORTING MATERIAL FOR SELF-ORGANIZATION CHAPTER 119

C.1 Jacobian matrix elements 120
C.2 Patterns plotted with scale and in color 122

Bibliography 123

LIST OF TABLES

Table **Page**

3.1 Redistribution kernels and their properties 60

LIST OF FIGURES

Figure **Page**

1.1 Hysteresis in a ferromagnetic material. Photo-Credits: HyperPhysics by Rod Nave, Georgia State University 3

1.2 Landau free energy density for the homogeneous system for different values of applied external magnetic field. The arrows represent the stable macroscopic magnetization for a given applied field. Here, $\alpha = 1.0, \beta = 1.0$. 4

1.3 Terrigenous sediment data indicating climatic shift in Sahara. Circles represent data while connecting line is meant to guide the eye. Note the regime shift occurred around 5500 years before the present day (BP). 8

2.1 Example of a prototypical saddle node bifurcation. The solid lines are stable states, whereas the broken lines are unstable. Arrows indicate the direction of flow of the state variable. 12

2.2 At the center is the bifurcation diagram for May's model (Eq 2.4). The thick lines indicate stable ecological states whereas the dotted line represents the unstable equilibria. The top row shows the change in the effective potential as the control parameter $c \rightarrow c^*$. The bottom row of figures shows that as σ increases, the extent of the region around the minimum explored by the system widens leading to asymmetry. The parameter values are: $r = 1, K = 10, V_0 = 1$. 18

2.3 The plot at the bottom of the panel shows the bifurcation diagram for Eq 2.4. Four subplots at the top of the panel show representative numerical simulation results for the time series and its probability density when the ecosystem is far from and close to the threshold of collapse ($c^* = 2.6$). The asymmetry in the distribution that is clearly visible underlies the indicator of regime shift proposed in thepaper. Simulations were started with the vegetation in the high density state. We choose $\sigma_V = 0.75$, a time step of $dt = 0.01$ for numerical integration and rest of the parameters are as in Fig. 2.2. 20

2.4 Increase in skewness as the ecosystem approaches regime shift via different routes for May's model of vegetation collapse considered in Figure 1. The thick line is the analytical result obtained directly from the stationary probability distribution. The open circles are the average values of skewness obtained by the numerical simulations. Note that we have plotted the absolute value of the average skewness. (a) Approaching the threshold of vegetation collapse by increasing the grazing pressure with fixed external fluctuations $\sigma_V = 0.25$. (b) Approaching regime shift by increasing (noise) fluctuations in the system at $c = 2.0$ (far from threshold). We choose $dt = 0.1$ and rest of the parameters are as in Figure 2.2. 21

2.5 (a) A representative bistable potential. The labels a, b and c correspond to fixed points of the system (b) From left to right: (i) The MFPT to the unstable fixed point from the value V (on x axes). Here, c (maximum grazing rate) = 2.0 and $\sigma_V = 0.75$. The unstable fixed point **b** is at $V = 2$ for this set of parameter values. (ii) The MFPT to the unstable fixed point from the stable fixed point as the grazing rate increases. Here, $\sigma_V = 0.75$. (iii) The MFPT to unstable fixed point from the stable fixed point as the strength of the external fluctuations increase. Here, $c = 2.0$. 24

2.6 An instance where the skewness fails to detect the regime shift. Increase in rainfall rate fluctuations, w, keeping R = 1.5 and $\sigma_B = 0.25$. 27

2.7 Analyzing the failure of skewness as an early warning signal when σ_w increases leading to a regime shift. In all the plots below $R = 1.5$, $\sigma_B = 0.25$ and rest of the parameters are: $\rho = 1.0, \alpha = 1.0, \lambda = 0.12, B_c = 10, B_0 = 1$. (a) Effective potential when the fluctuations in the rainfall rate are absent (*i.e.* $\sigma_w = 0$). (b) The function which modulates the strength of the multiplicative noise. (c)-(e): Effective potential when the fluctuations in the rainfall are present and increasing (from left to right): $\sigma_w = 0.01, 0.10$ and $\sigma_w = 0.25$. 29

2.8 The figures show that changes in the skewness (denoted by γ) can be detected well in advance for a model system which mimics a field measurement scenario. These results are obtained by numerical simulation for the lake model when the nutrient inputs are increased as a function of time towards the eutrophication threshold as described in the text. The initial conditions for simulation are $P(t = 0) = 0.58gm^{-2}$ & $M(t = 0) = 410gm^{-2}$ and a time step of $dt = 0.01$. The moving average skewness has been calculated from data for the previous five years. The dense and the sparse data sets correspond to 100 and 33 measurements of lake water phosphorus concentration (P) per year respectively. Rest of the parameters are:$s = 0.7y^{-1}, h = 0.15y^{-1}, b = 0.001y^{-1}, P_0 = 2.4gm^{-2}, q = 8, \sigma_l = 0.01, \sigma_r = 0.01$ 32

2.9 Analysis of terrigenous sediment data indicating climatic shift in Sahara (a) Time series of terrigenous sediment percentage record from Site 658C off Cap Blanc, Mauritania. Circles represent data while connecting line is meant to guide the eye. Note the regime shift which occurred around 5500 years before the present day (BP). (b) The moving average skewness: for any given time, skewness is calculated from the previous 10 data points. Squares represent computed skewness values with the connecting line meant to guide the eye. 34

3.1 The 'transient' bifurcation diagram for the May's model with space and noise. (a) This plot shows that the qualitative nature of the bifurcation is not affected by the spatial and stochastic fluctuations (b) This plot illustrates that if we wait sufficiently long, the bifurcation diagram shows characteristics of phase diagram of a first order phase transition. 44

3.2 The panels of figures show how the asymmetry in the potential in the landscape picture evolves in the different pathways to regime shifts for a spatially explicit model with diffusion. This is strikingly similar to the ones obtained for the nonspatial model with noise (see Fig. 2.2 in chapter 2) 48

3.3 The rising spatial variance and skewness as the threshold of vegetation collapse is approached in model of Eq 3.9. Parameter values are: $r = 10, K = 10, V_c = 1.0, \sigma_d = 1.0, dx = 0.1, dt = 0.001$. The thick line corresponds to analytical result obtained from the mean field approximation. 50

3.4 Same as Fig 3.3, but scaled by their respective values at $c = 15$. 51

3.5 Effective potential for the spatially explicit model obtained using the mean-field approximation. The potential is shown around the vegetated fixed point as the diffusion constant increases. 52

3.6 Temporal evolution of the system on a two dimensional lattice with (Eq. 3.9) for a situation simulating increasing grazing rate (of 0.1 units every year) observed in the field. Parameter values are as in earlier figures. (a) Temporal evolution of spatial patterns while the grazing rate increases towards the threshold. The brighter color corresponds to higher vegetation densities. (b) Spatial mean, variance and skewness as a function of time. 54

3.7 This plot demonstrates the plausibility of preventing a catastrophic vegetation collapse. Thick line is "business as usual" with an increase of 0.1 units/yr. For the rest, the reduction in grazing rate is initiated an year after the peak of skewness is observed and they are as follows: circles 0.1 units/yr, diamonds 0.2 units/yr, triangles 0.5 units/yr and stars 0.75 units/yr until they decrease to 21 units/yr. 55

3.8 The probability distribution for different values of the control parameter value h. 56

3.9 Variation of mean, variance and skewness. (i-iii) correspond to the potential function of Eq. 3.17 whereas (iv-vi) correspond to Eq 3.18. 57

3.10 Results of spatial indicators for integro-differential model. Comparison between results of mean field approximation and the numerical simulations of Eq 3.19 63

4.1 Patterns of vegetation from Niger (Africa), $12^0 43'$N, $3^0 08'$E. Length scale corresponds to (a) 1 mile (b) 400m (East to West or North to South). Credit Google Earth. Accessed on March 17th 2008. 69

4.2 Bifurcation diagram for the model Eq 4.1 with:$c = 10, g_{max} = 0.05, k_1 = 5, k_2 = 5, r_w = 0.2, W_0 = 0.2, \alpha = 0.2, d = 0.25, D_p = 0.1, D_w = 0.1, D_o = 100, N = 256 \times 256$ and $dx = 1$. For spotted patterns, R=0.75. For Labyrinths, R=1.00. For gapped patterns, $R = 1.25$. 74

4.3 Soil water dependent or seasonal adaptation term $\tau_p(W)^{-1}$. This modulates the growth and decay of plants depending on soil water availability. The markers D and W indicate typical value of this adaptation term during dry and wet seasons, respectively. 76

4.4 Comparison between simulations of pattern formation on a 1 dimensional lattice of 128 spatial grids by two different numerical integration schemes (i) Crank Nicolson implicit scheme and (ii) Fully explicit scheme. For this specific simulation, the rainfall was assumed to be uniform ($N_w = 350d$). The time step for implicit scheme was chosen to be 0.01 of a day where as that for the explicit scheme was chosen to be 0.0001 of a day. Similarly, the results for the seasonal rainfall case with $N_w = 150d$ obtained by different schemes of integration show excellent agreement with each other (within 0.1%). Parameters are: $c = 5, g_{max} = 0.1, k_1 = 5, k_2 = 5, r_w = 0.4, W_0 = 0.2, \alpha = 0.4, d = 0.25, D_p = 0.01, D_w = 0.1, D_o = 100, N = 256 \times 256$ and dx=1. 79

4.5 These figures show the vegetation patterns with and without seasonality in rainfall at the end of 6800 days. The equations 4.17-4.20 were numerically simulated starting with several plant patches on the grid, with soil and surface water set to zero everywhere. Periodic boundary conditions were chosen for all these cases. In this grey scaled picture, darker patch represents bareness whereas the brighter patch indicates presence of vegetation. The length scale of the spatial grid is $128m \times 128m$. Rest of the parameters are as given in Fig. 4.4. 82

4.6 Variation in the productivity of the system as a function of the number of rainy days (N_w) for a given annual precipitation (PPT). (a) The mean-field model productivity is the (rescaled) plant biomass density calculated at the end of 100^{th} rainy season ($t = 34800\,days$) starting with a nonzero plant density. Here, $R_{rc} = 10\,mm\,day^{-1}$, $P_{scaling} = 160\,g\,m^{-2}$ (b) The productivity in the spatial model computed as the percentage of land area covered by plants at the end of the 20^{th} rainy season ($t = 6800\,days$). Here, $R_{rc} = 3.25mm\,day^{-1}$. For both the plots, we have set the total number of days in an year to be 350, $PPT = 350\,mm\,year^{-1}$ and all other parameters are as indicated in 4.4. The circles are the data points obtained from numerical simulations and the dotted line, obtained by linear interpolation between two consecutive data points, is meant to guide the eye. 84

4.7 The maximum productivity of the system as a function of the annual precipitation (PPT). For a given PPT, we calculate the productivity (as in Fig 4.6) as a function of N_w and extract the maximum value and display it as a function of PPT. (a) The mean-field results, where productivity is the (rescaled) plant biomass density. (b) The spatial model results, where the productivity is the percentage of land area covered by plants. For both the plots, all parameters are as of those in Fig 4.6. 86

4.8 Productivity in the spatial model, i.e, fraction of area covered by plants, as a function of time in the scenario of increased variation in interannual rainfall fluctuations (N_w). We have chosen $PPT = 250\,mm\,year^{-1}$. The number of rainy days is generated according to uniform random number distribution with mean $\langle N_w \rangle = 75\,days$ and a variation of 75% around the mean. . . . 89

A.1 (a) The bifurcation diagram as a function of the rainfall rate R. Here, $R_1 = 1.06$ and $R_2 = 2.0$. Increase in the skewness as the threshold to regime shift is approached in different ways for the two variable vegetation model. The open circles are the average value of skewness obtained by the numerical simulations. The dotted line is meant to guide the eye. Note that we have plotted the absolute value of the (average) skewness. (b) Approaching the threshold by reduction in rainfall rate with $\sigma_B = 0.25$ and $\sigma_w = 0.01$ (c) Increase in external fluctuations (σ_B) with $R = 1.5$ (far from threshold of vegetation collapse) and $\sigma_w = 0.01$. 100

A.2 More results of the two variable vegetation model (a) and (b): Nullclines (indicated by think lines) and fixed points (at the intersection of nullclines; stable fixed points are represented by full circles whereas the unstable fixed point is an open circle) are shown in the top row. The bottom row shows the time series distribution for a representative simulation. 101

A.3 Plots of the direction field for the two variable vegetation model. The dottel lines represent the nullclines of the system. The point of intersection of nullclines is the vegetated fixed point. The short segment of lines represent the strength of the direction field (*i.e.* velocity at any point n the phase plane. (a) Far from bifurcation: R=1.5 (b) Close to the bifurcation: R=1.10. The bifurcation occurs at R=1.06. 104

A.4 Results for the parameterized lake eutrophication model (see chapter 2, section 2.4) (a) The bifurcation diagram for Lake eutrophication model as a function of nutrient loading. The thick lines represent the stable oligotrophic and eutrophic states whereas the broken lines represent the unstable state. The two bifurcation points correspond to $l \approx 0.5$ and $l \approx 0.95$. (b) Absolute value of the average skewness of lake model as obtained by numerical simulations, as we approach the threshold due to increased nutrient loading. Calculation of skewness are performed for 500 time units and then averaged over 200 such simulations. 105

A.5 Analysis of terrigenous sediment data indicating climatic shift in Sahara (a) Time series of terrigenous sediment percentage record from Site 658C off Cap Blanc, Mauritania [1]. Circles represent data while connecting line is meant to guide the eye. BP stands for 'before present'. (b) The moving average variance: for any given time, variance is calculated from the previous 10 data points. (c) The moving average skewness: for any given time, skewness is calculated from the previous 10 data points. 109

A.6 Analysis of total phosphorous concentration data obtained at one station (Sandusky Bay) in Lake Erie [2] (a) The time series of the data from 1997 to 2006 in units of mg/litre. (b) The moving average skewness, calculated from the preceding 100 data points. 110

B.1 Spatial mean, variance and skewness for different kernels. (a) Gaussian Kernel: Parameters are: $dx = 0.1, dt = 0.1, N = 16384, \sigma = 0.1, \sigma_c = 1.0$. (b) Fat tailed kernel: $\theta = 0.1$ and all other parameter values are same as the previous plot. 112

B.2 To study the temporal dependence of mean, variance and skewness for far from and close to bifurcation for spatial model with diffusion. Parameter values: $N = 128 \times 128, dx = 0.1, dt = 0.001, D = 0.001, r = 10, K = 10, \sigma_c = 4.0$. As (b) clearly indicates, even if the grazing parameter is a constant and has not yet crossed the mean-field threshold for collapse, various moments show a time dependence and the system ultimately collapse to a low density vegetated state. 113

B.3 Spatial variance and skewness with 95% CI for $D = 0.01$. The full results are shown in Chapter 3, Fig. 3.6. We assume that the data points thus obtained form independent set of random numbers. The error bars for the skewness are obtained by $\gamma_{actual} \pm 1.96 * sde$ where sde is the standard error given by $sde = \sqrt{6/N}$ where N is the total number of data points available for the calculation [3]. For this specific simulation, we find that changes in variance and skewness can be reliably detected for data collection at 16×16 or more spatial points. 114

B.4 Results of dynamic simulation with D=0.001. Parameters are: $r = 10, K = 10, V_0 = 1, \sigma_c = 4.0, c(t = 0) = 15.0$. The grazing rate is incremented discretely by 0.2 units every year until it reaches 26 and is kept constant thereafter. (a) Full spatial patterns. (b) Moments as a function time, with right panel zoomed in just prior to the transition. (c) Variance and skewness with 95% CI. 115

B.5 Same as Fig B.4, except for $D = 0.1, \sigma_c = 2.0$. Unlike previous cases, we find that changes in variance and skewness can be reliably detected for fewer data collection points (at 8×8 or more). 116

B.6 One point indicators (variance and skewness) with diffusion. 117

C.1 These figures show the state of the vegetation patterns at the end of 20^{th} rainy season (t=6800 days). The equations (1-3) were numerically simulated using fully explicit scheme on a $128m \times 128m$ spatial grid starting with plant peaks (P=20) at 10% of the grids, with soil and surface water set to zero everywhere. Periodic boundary conditions were chosen for all these cases. The animation showing how the pattern varies with seasonality is available as online. The length of the rainy season was set to $N_w = 150$ days. All other parameter values are as indicated earlier. (a) Spotted pattern at $R = 2.4\, mm\, d^{-1}$. (b) Labyrinthine pattern at $R = 2.8\, mm\, d^{-1}$ and (c) Gap pattern at $R = 3.25\, mm\, d^{-1}$. 122

CHAPTER 1

INTRODUCTION

Ecological systems exhibit fascinating dynamical behaviors and spatial patterns such as cycles in populations of snowshoe hare[4], chaotic population dynamics of crabs, flour beetles and planktonic communities [5, 6, 7], threshold dynamics in diseases, invasive species and ecosystems states of coral reefs, lakes and forests [8, 9, 10, 11], regular spatial patterns in vegetation, salt marshes, mussel beds and coat of animals [12, 13, 14, 15]. These examples form only the tip of the iceberg. These behaviors are governed by nonlinear and stochastic dynamics with interactions occurring at multiple scales and exhibiting emergent properties at macroscopic scales.

One of the foremost challenges in ecology involves understanding the complex systems using simple mathematical models and devising theories which can be helpful in making reliable predictions. Nonlinear dynamics and statistical physics provide an excellent set of tools in that direction. The focus of this thesis is to devise such predictive measures and to understand the dynamics of ecological systems which show abrupt transitions between their states, using techniques of nonequilibrium statistical physics. In the next section, I will motivate the topic of the thesis by providing theoretical and empirical support for the 'existence of multiple stable states and threshold dynamics in ecosystems.

1.1 Background

Consider a tropical forest ecosystem, for example, where a large number of individuals interact with each other through processes such as birth, death, competition and spatial spreading to maintain biodiversity and processes such as water and nutrient cycles at the ecosystem scale. Identifying an appropriate spatial and temporal scale is a key step if one is interested in applying the tools of physics and mathematics in studying them [16]. Clearly, the systems under consideration show complex dynamics, but the importance of studying such systems through simple ideas of nonlinear dynamics and statistical physics has been appreciated only recently [17]. Ecology (more generally, biology) has often been considered as a descriptive science looking for seemingly endless details. However, ecology is perhaps the most quantitative branch of all of biology and some of the most profound and successful ideas are based on strong theoretical foundations.

The earliest theoretical work in ecology on the growth of population were developed by Thomas Malthus in 1798 and Pierre-Francois Verhulst in 1835. This was later followed by the work on spread of infectious diseases by Donald Ross and the predator prey dynamics by Lotka and Volterra during early 20th century [18, 19, 20]. The work of Evelyn Hutchinson and Robert MacArthur during 1960's provided a major thrust on theoretical work in ecology [21, 22, 23, 24]. The phenomenon of deterministic chaos which arose from studies of simple mathematical models of population dynamics in 1976 by Robert May attracted wide attention not only of ecologists, but also the physicists and mathematicians [17]. Since then a number of empirical and theoretical studies have underlined the role of nonlinearity leading to multiple stable states [9, 25, 26, 27, 28] and the importance of spatial scale [16, 29, 30, 31, 32, 33, 34] in ecological systems.

In multistable systems the initial conditions or the history along with randomness decide which of those available states is occupied by the system. Importance of multiple stable states and the role of chance in deciding the fate of the final state of the system is well established in statistical mechanics [35, 36, 37]. The classical example of a physical system

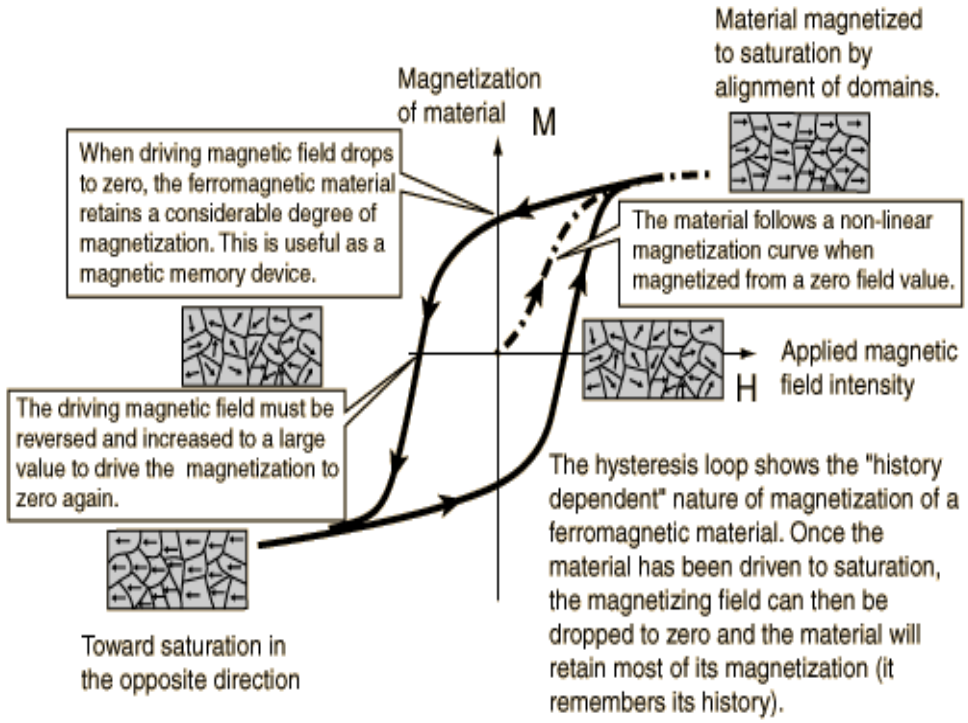

Figure 1.1: Hysteresis in a ferromagnetic material. Photo-Credits: HyperPhysics by Rod Nave, Georgia State University

showing hysteresis is a ferromagnetic material. When an external field is applied, the magnetic domains of the material align themselves along the direction of the field. The alignment continues to sustain itself substantially even when the magnetic field is turned off because it costs energy to disalign the domains. When the magnetic field is reversed beyond a certain threshold, the alignment switches to the new direction of the magnetic

field. This hysteretic property, a nonequilibrium phenomena, is at the heart of innumerable applications including magnetic tapes and hard discs. This is shown in Fig. 1.1.

In a ferromagnetic system, the magnetic domains or spins interact in such a way that aligning along the same direction as its neighbors is energetically favorable. For a coarse

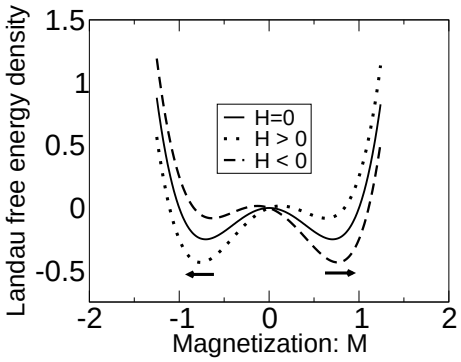

Figure 1.2: Landau free energy density for the homogeneous system for different values of applied external magnetic field. The arrows represent the stable macroscopic magnetization for a given applied field. Here, $\alpha = 1.0, \beta = 1.0$.

grained magnetic spin density denoted by $M(x,t)$, the Landau free energy can be written as:

$$\mathcal{F} = \int_V d^d x[-HM - \alpha M^2 + \beta M^4 + (\nabla M)^2] \tag{1.1}$$

and the free energy density for the homogeneous system is shown in Fig 1.2 as the external magnetic field varies.

The global minima of the Landau free energy, for any given magnetic field, corresponds to the thermodynamically stable state. In thermodynamic limit, as the magnetic field changes sign, the macroscopic magnetization changes discontinuously leading to a first order phase transition. However, the system can stay in a metastable state for substantially long times because of the low probability in being able to cross the strong barrier to reach

the global stable state. In other words, when the metastable state has long lifetimes, we may consider it as 'stable' on the timescales of interest. This leads to the nonequilibrium phenomena of hysteresis where the reversal of magnetic field does not lead to immediate reversal of alignment of magnetic domains. An 'effective potential' analogous to the Landau free energy (even though a free energy itself has no interpretation in an ecological system) can be defined for simple models of dynamical systems. We repeatedly use this intuitive picture of the effective potential in this thesis to study the dynamics of ecological systems.

1.2 Multiple stable states, hysteresis and abrupt flips in ecological systems

The plausibility of multiple stable states in ecological systems was perhaps first suggested by Lewontin in 1969 in order to explain the observed structure of communities [25] (community is defined as "an assemblage of populations of different species, interacting with one another" [38]). In his own words "...that history is relevant to present state of populations, species and communities, and that their present state can not be adequately explained without reference to specific historical events. This is equivalent to saying that multiple state states...exist". One of the first empirical studies to evaluate such a hypothesis was performed by Sutherland in 1974 on a fouling community – a complex assembly of living organisms such as ascidians, bryozoans and muscles found on sides of docks, marinas, harbors, etc. This work, however, was severely criticized by Connell and Sousa in 1983 for not considering the criteria of stability carefully [39]. The main argument being that in most of those studies an alternative state did seem to occur, but within relatively short time scales it settled back to the original state. Such a dynamics can occur even in presence of a limit cycle or as transient dynamics and hence the stability of the alternative state was not convincingly established.

It is clear from the effective potential picture that signatures of multiple stable states can be established by showing the following: (i) Different initial states lead to different final states and those states are stable with respect to (small) perturbations. (ii) (Large) perturbations can trigger shift to another permanent state. (iii) Hysteresis in response to changing conditions in forward and backward directions. Demonstrating these conditions through controlled experiments in real ecological systems is difficult. Additionally, false positives can not be easily ruled out because the results obtained at shorter time and length scales typical to experimental studies may not necessarily be extrapolated to ecosystem scales.

Long term studies now provide better evidence for the existence of multiple stable states and abrupt changes between them. Some of the well studied systems are marine, lake and semi-arid ecosystems. An analysis of 100 environmental time series in North Pacific ocean showed evidence for abrupt changes in several variables on two occasions: first in 1977 and the second in 1989. Remarkably, the latter shift did not lead the system to return to pre-1977 conditions [40].

Lakes are perhaps the best studied ecosystems in this context. Long data sets are available from a number of shallow lakes in the world. The main driving parameter of ecosystem functioning is the nutrient input (such as Phosphorus and Nitrogen) which can be easily measured. A pristine lake is transparent with low nutrient and algal concentrations, high fish and macrophyte vegetation. Such a state can make a transition to a turbid water state due to increased nutrients into the lake. A study of 100 year long data from Lake Takern and Lake Krankesjon in Sweden is reported to have "spontaneously switched" between two states of "clear" and "turbid" water [41]. The large shallow lake Apopka in Florida (USA) underwent a transition to a turbid state during a hurricane in 1948 where as

Lake Tamnaren near Stockholm and Rice Lake near Wisconsin turned turbid due to changes in water levels [42, 43, 44]. In many of these observations, the clear water state could only be restored at much lowers levels of nutrient inputs than the critical value at which transition to turbid water state took place [45, 46, 9]. These examples provide evidence for abrupt transitions and hysteresis, thus strengthening the hypothesis of alternative stable states. Experimental work show that a clear water state is stabilized by macrophyte vegetation which promote processes to clear the water and therefore provide themselves an access to better sunlight at the bottom of lakes. On the other hand, a turbid water leads to poor availability of light killing nearly all of the macrophyte vegetation and the life supported by it [47]. Such positive feedback mechanisms in which each state self-stabilizes are common features of ecosystems showing multiple stable states.

The most striking example of large scale change in the ecosystem state occurred in the Sahara (North Africa), the most recent one being at around 5500 years before present day (BP) [1]. Geological data support that Sahara was sufficiently humid and even hosted large perennial lakes such as Lake MegaChad spanning $330,000 km^2$ area [48, 49, 50]. The data shown in Fig. 1.3 corresponds to a well-dated record of terrigenous sediment deposition and it indicates an abrupt termination of humid periods resulting in collapse of vegetation and desertification. Note that the terrigenous sediment acts as a proxy to the climate of Sahara. The complete transition from a vegetated state to the current arid state happened in a span of decades to centuries, a relatively short time period if compared with the time scales at which each of the state is stable. The driving force of the transition is the summer insolation which is known to slowly change due to earth's orbital precession [51]. Climate models indicate a strong sensitivity of monsoons to summer insolation: an 8% reduction in insolation (expected change due to orbital precession) can lead to 40% reduction in the

rainfall [52, 53]. The abrupt response of the ecosystem is attributed to the highly nonlinear positive feedbacks between reduced regional precipitation and loss of vegetation cover [54].

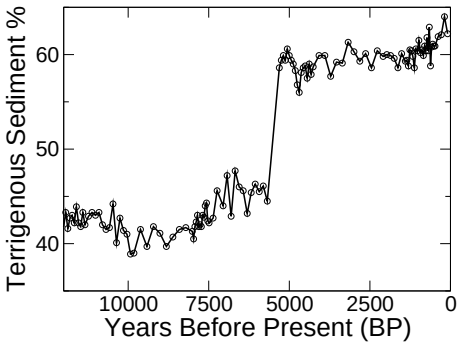

Figure 1.3: Terrigenous sediment data indicating climatic shift in Sahara. Circles represent data while connecting line is meant to guide the eye. Note the regime shift occurred around 5500 years before the present day (BP).

It is now widely accepted that many ecological systems as well as social and economic systems undergo abrupt transitions beyond a threshold, also referred to as a tipping point [9, 10, 55, 56, 57]. Other examples include marine ecosystems [58, 59, 60, 61], ponds [62, 63], forests [64, 65], rivers [66] abrupt loss of biodiversity in coral reefs [67, 68, 69, 70], preferential states of soil moisture [71], and trophic cascades [72, 73]. Existence of alternative stable states has been shown in many lab cultures containing single or multiple species [74, 75, 76, 77, 78, 79].

Simple mathematical models in conjunction with empirical studies have provided useful insights into both the feedback mechanisms that stabilize alternative stable states in a number of ecosystems and the occurrence of critical thresholds beyond which regime shifts occur [8, 45, 80, 81, 82, 83, 84]. However, such a thorough enumeration across wide spectrum

of ecological systems is practically an impossible task. Therefore, an important task in ecology is to develop predictive measures of proximity to a tipping point which do not depend on the detailed understanding of ecological processes. If these indicators can be easily and reliably computed by a simple analysis of data available from routine monitoring, they can be employed as early warning signals of impending catastrophic transitions with potential applications in conservation of ecosystems.

1.3 Focus of the thesis and organization of results

The aim of this thesis is two fold. The first aim is to develop leading indicators of proximity to a threshold which can serve as early warning signals of an impending transition. The second one is to study the dynamics of bistable ecological systems in presence of temporal and spatial fluctuations. We don't necessarily, however, separate the two aspects and they are often intertwined and presented simultaneously. To study these issues, we will employ the mean-field-models with stochasticity and the spatially extended stochastic models using reaction-diffusion and integro-differential equations. We perform a combination of analytical and numerical calculations to establish various results.

The main theme of the next two chapters is on developing leading indicators of regime shifts in ecological systems. In chapter 2, using simple nonspatial models of bistable ecological systems, we propose that changing skewness of the time series distribution is an early warning signal of impending regime shifts. In chapter 3, we consider a spatially explicit model of regime shifts in ecosystems. Using a mean-field approximation and numerical simulations, we show that spatial variance and spatial skewness calculated from the probability distribution of the instantaneous spatial pattern are reliable indicators of proximity to a threshold. While establishing these results on the predictive measures, we also present

results on the dynamics of bistable systems under the influence of space and noise. We show that the qualitative nature of the bifurcation diagram (specifically, the coexistence or the bistable region) remains unchanged on spatial and temporal scales of ecological interest, although there is only one stable state in the thermodynamic limit.

In chapter 4, we switch to a spatially extended model of semi-arid ecosystems where the vegetation exhibits self-organization due to limited resource availability. We adopt a model that produces spatial patterns due to Turing instability and study the implications of strong seasonal fluctuations in the driving parameter and the limiting resource, which is rainfall.

We compare our results with field data in two instances. In chapter 2, we calculate the moving average skewness of Sahara climatic data which exhibited catastrophic transition from a vegetated to desert state around 5500 years ago. We find that the data is not sufficiently resolved and hence we were unable to find a trend in skewness prior to the regime shift. In chapter 4, we compare the results of maximum vegetation cover with the recently published data from Savanna grasslands and find a reasonably good agreement [85].

Chapter five presents a brief summary of the research work and scope for future work.

CHAPTER 2

CHANGING SKEWNESS: AN EARLY WARNING SIGNAL OF REGIME SHIFTS IN ECOLOGICAL SYSTEMS

2.1 Background

In this chapter, using simple models of ecological systems showing bistability, we present changing skewness of time series distribution to be a leading indicator of an impending regime shift. This section provides the background and present several recently proposed indicators. This will be followed by establishing changing skewness as an early warning signal of regime shifts by studying three different ecological models of varying complexity. In section 2.2, we will present analysis for one variable model where an effective potential can be defined. In section 2.3, we present results for a more complex two variable model of vegetation collapse where no effective potential exists and we analyze a case of failure of skewness to detect an impending regime shift. Next, in section 2.4, we present results for a two variable model of a lake model parameterized to a real lake. This is followed by a simple analysis of real data in section 2.5 followed by discussion and concluding remarks. The results of work has been published in *Ecology Letters*.

Several indicators that can potentially determine the proximity to a transition point have been recently suggested in simple models. A common aspect of all the models is

that they show a regime shift via a saddle node bifurcation in which a stable fixed point disappears by merging with an unstable fixed point as we vary one of the model parameters. Saddle node bifurcations, also referred to as fold bifurcation or blue sky bifurcation, are widely employed to model regime shifts in ecology. A prototypical example of this bifurcation is given by [86]:

$$\dot{X} = r - X^2 \tag{2.1}$$

where r is the control parameter of the system. The fixed points of the system are obtained by setting the right hand side to zero. This system has two fixed points for $r > 0$; one stable ($X_s^* = \sqrt{r}$) and the other unstable ($X_u^* = -\sqrt{r}$). As shown in Fig. 2.1, the bifurcation occurs at $r = 0$. Even though this model does not have any fixed points for $r < 0$, in a full model of the ecological system of interest to us (i.e., the ones which show bistability) there will be a discontinuous jump to a new fixed point for negative values of r.

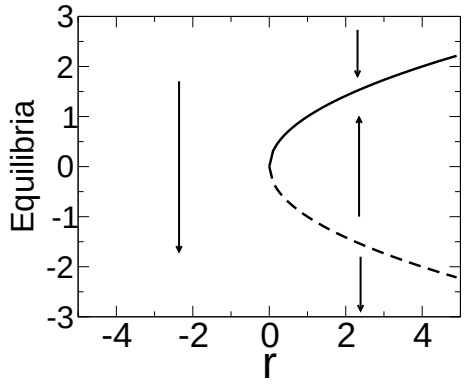

Figure 2.1: Example of a prototypical saddle node bifurcation. The solid lines are stable states, whereas the broken lines are unstable. Arrows indicate the direction of flow of the state variable.

As we approach the bifurcation from positive values of r, the dynamics of perturbation from the stable fixed point within a linear approximation can be written as:

$$\dot{x} = -\alpha x + \eta(t) \tag{2.2}$$

where $x = X - X_u^*$, $\alpha = 2\sqrt{r} > 0$ and $\eta(t)$ is a Gaussian white noise process satisfying $\langle \eta(t)\eta(t') \rangle = \sigma^2\, \delta(t - t')$. The noise term represents random fluctuations acting on the ecological system (originally not included in Eq. 2.1). In terms of the new parameter α, the bifurcation occurs at $\alpha = 0$. The Eq. 2.2 is the famous Ornstein-Uhlenbeck stochastic process [87, 88]. The correlation function ($C(\tau)$) and the spectral function ($S(\omega)$) for this process in the steady state are given by [88, 89]:

$$C(\tau) = \langle x(t)x(t+\tau) \rangle = \frac{\sigma^2}{2\alpha} e^{-\alpha|\tau|} \qquad S(\omega) = \int_{-\infty}^{\infty} e^{-i\omega\tau} C(\tau) d\tau = \frac{\sigma^2}{\omega^2 + \alpha^2} \tag{2.3}$$

where the angular brackets represents average over all realizations of noise.

The variance or the amplitude of fluctuation of the time series is given by $C(\tau = 0) = \sigma_x^2 = \frac{\sigma^2}{2\alpha}$. The correlation time τ_c can be defined by $C(\tau) = C(0)e^{-\tau/\tau_c}$; hence $\tau_c = 1/\alpha$ and this can be interpreted as the typical recovery time of the system when perturbed from the stable state. From these expressions it is clear that the variance σ_x^2, the recovery time τ_c and the strength of the peak of power spectrum $S(\omega = 0)$ increase as we go towards the bifurcation. All these quantities can be easily evaluated from the time series of the dynamical variable, more specifically the ecological variable of interest and they have been suggested to be leading indicators of regime shifts in ecological systems [90, 91, 92, 93, 94]. Since these indicators were obtained through a linear analysis, we refer to them as 'linear indicators'. Note that even though the expression in Eq 2.3 show that these indicators diverge in steady state as we go towards a threshold (i.e., $\alpha \to 0$), this is not true when

the system shows an alternative stable state for $r > 0$, a scenario applicable to ecosystems. See the section 2.2.3 for a discussion.

These features of indicators which arise near a threshold can be intuitively understood by the reduction in the curvature (flattening) of the potential that determines the dynamics as the bifurcation point is approached in one-variable models. The potential for the system in the linear approximation is given by $U(x) = \frac{\alpha}{2}x^2$ (see next section) and its curvature by α which goes to zero at the bifurcation. This flattening leads to a substantial reduction in the recovery rate of the system from a perturbation. In addition, as one approaches a regime shift, the potential picture of the ecosystem dynamics exhibits a pronounced asymmetry around the stable state. In contrast to the flattening of the potential which is obtained by a linear analysis, the asymmetry arises due to nonlinear effects and hence presents a new way of devising an early warning signal. We exploit the impact of large external fluctuations and asymmetry in the landscape on the dynamics of the ecosystem and show that a changing skewness (a measure of the changing asymmetry) of the time series can be an effective early warning signal of regime shifts. In general, regime shifts can occur either due to the approach to a threshold point as an external parameter is varied or due to increased width of the external noise distribution [9, 95]. Whereas the existing set of indicators can serve as warning signals typically only for the former scenario, it is shown that a changing skewness is a promising indicator for both routes to regime shift. We provide an intuitive understanding of these results and discuss the issues related to the feasibility of computing skewness in empirical data sets by analyzing data from climatic shift in the Sahara and total phosphorus concentration data from a tributary to Lake Erie.

Three ecological model systems we consider differ in their complexity, the nature of the noise, the details of ecological feedback mechanisms: two of them model the vegetation

collapse in semi-arid regions and another, a parameterized model of lake eutrophication [8, 96, 97, 95]. More specifically, an effective potential can be obtained for a simple one variable model of vegetation collapse whereas the two variable model does not have this feature, but incorporates important ecological feedback mechanism. The lake model is parameterized to a lake in Wisconsin. This allows us to check the utility of asymmetric indicator in different contexts and at different levels of modeling approximations.

2.2 May's one variable model of vegetation collapse

The first model describes the dynamics of a logistically growing population V with rate r and carrying capacity K under a grazing pressure which is quadratically increasing for small population densities and saturates to a maximum rate of c for higher population densities [8, 96]:

$$\frac{dV}{dt} = rV(1 - \frac{V}{K}) - c\frac{V^2}{V^2 + V_0^2} + \eta_V(t) \tag{2.4}$$

where $\eta_V(t)$ is Gaussian white noise i.e., $\langle \eta_V(t)\eta_V(t')\rangle = \sigma_V^2\delta(t - t')$. The bifurcation diagram for the deterministic limit of the model (henceforth referred to as the mean-field model) is shown in Fig. 2.2. The mean-field version has been applied in a variety of ecological contexts [8, 98, 99, 100, 101], but we view it as a model of vegetation (V denotes the biomass density) in semi-arid regions so as to make contact with the second model we have studied. The vegetation biomass is measured in the units of V_0 and the system exhibits abrupt vegetation collapse as the maximum grazing rate, c, increases beyond a threshold given by $r(1 + K^2/4)/K$. For the specific values of parameters we have chosen, the system exhibits a bistable region with coexisting bare and vegetated states for $1.8 < c < 2.6$. We are interested in predicting the vegetation collapse that occurs as we approach the bifurcation at $c^* = 2.6$.

We justify our choice of additive noise fluctuations as follows: The grazing parameter c represents the density of an herbivore population, for example [8]. The population of the herbivore is a dynamical variable in itself, but we have not written down an explicit governing equation for its dynamics. Instead, we assume that the time scale on which grazing population changes is relatively short compared to time scales of interest in the dynamics of vegetation. We then approximate it to be fluctuating around a mean value, like a Gaussian. The resulting noise structure would then be $\eta_V(t)V^2/(V_0^2+V^2) \approx \eta_V(t)$ since we are only interested in the dynamics of the fully vegetated ($V \gg V_0$) system prior to a transition. Such an approximation to additive noise has the advantage that we can interpret it as occurring due to variety of external fluctuations, including those in grazing, that affect the growth rate of the vegetation. If we are in the low vegetated state, a similar approximation yields an additive noise, but with a prefactor of ≈ 0.2 for the specific parameter values we have chosen in the model. However, with the additive noise fluctuations in the low vegetated state, the system may fluctuate to negative values of V which is not ecologically meaningful. Thus, one must include the multiplicative noise term.

2.2.1 Fokker-Planck analysis: asymmetry in effective potential and time series distribution

The description of the stochastic system such as Eq. 2.4 is obtained by the probability density of the state variable. In order to avoid writing the full expression from Eq 2.4, we consider following simpler notation and this can be easily applied to other one variable models. We denote the state of the ecosystem by x and let the dynamics be described by:

$$\dot{x} = f(x) + g(x)\eta(t) \tag{2.5}$$

where $\eta(t)$ is a Gaussian white noise process with variance σ^2, *i.e.,* $\langle \eta(t)\, \eta(t') \rangle = \sigma^2 \delta(t - t')$. When $g(x)$ is a constant, the noise enters the dynamical equation additively independent on the state of the system x; for example, the noise term $\eta_V(t)$ in May's vegetation model. Such a noise is said to be *additive*. If, on the other hand, $g(x)$ is not a constant, then the strength of the noise depends on the state of the system and it is said to be *multiplicative* (see the lake model in section 2.4).

Next, we describe the evolution of the probability density of the state variable by Fokker-Planck equation [102]. Using the Ito-interpretation for the stochastic differential equation 2.5, the probability density evolves in time according to [88, 102]:

$$\frac{\partial P(x,t)}{\partial t} = -\frac{\partial}{\partial x}\Big[f(x)P(x,t)\Big] + \frac{\sigma^2}{2}\frac{\partial^2}{\partial x^2}\Big[g(x)^2 P(x,t)\Big]. \tag{2.6}$$

See section 2.6 for a discussion on the choice of Ito versus the Stratanovich calculus. To obtain the stationary probability distribution, we set $\partial P_s(x,t)/\partial t = 0$. We can then solve the above equation to obtain

$$P_s(x) = N \exp\Big(-\frac{2}{\sigma^2}U(x)\Big) \tag{2.7}$$

where N is the normalization constant and $U(x)$ is the effective potential given by

$$U(x) = -\int_{x_0}^{x} \frac{f(x) - \sigma^2 g(x) g'(x)}{g(x)^2}\, dx. \tag{2.8}$$

For the case of additive noise, taking $g(x) = 1$, we find $U(x) = -\int_x f(y)dy$ which gives us the shape of the potential. For the multiplicative noise, as is clear from the full expression of the effective potential in Eq. 2.8, the shape of the cup can be nontrivially altered depending on the functional form of $g(x)$ and the strength of the fluctuations σ [89].

Let us now turn back our attention to analyzing the dynamics of the system near the bifurcation, but now include nonlinear term (in contrast to Eq. 2.2) to obtain:

$$\dot{x} = -\alpha x + \beta x^2 + \eta(t) \tag{2.9}$$

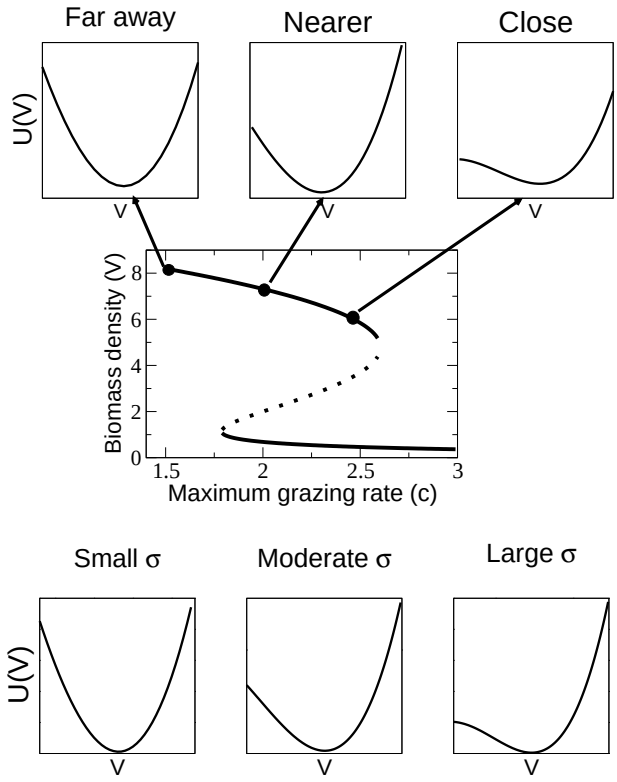

Figure 2.2: At the center is the bifurcation diagram for May's model (Eq 2.4). The thick lines indicate stable ecological states whereas the dotted line represents the unstable equilibria. The top row shows the change in the effective potential as the control parameter $c \to c^*$. The bottom row of figures shows that as σ increases, the extent of the region around the minimum explored by the system widens leading to asymmetry. The parameter values are: $r = 1, K = 10, V_0 = 1$.

The corresponding potential is given by: $U(x) = \frac{\alpha}{2}x^2 - \frac{\beta}{3}x^3$. Clearly, the potential is not an even function of x anymore and hence exhibits an asymmetry. The expression for steady-state probability distribution of time series, $P_s(x) = N \exp(-\frac{2}{\sigma^2}U(x))$, clearly shows that an asymmetric potential leads to an asymmetric stationary time series distribution. It is illustrated in Fig. 2.2 which shows how the asymmetry arises in two different routes to regime shift for May's model. As one approaches the threshold, the basin of attraction shrinks and flattens and the asymmetry in the bowl becomes pronounced. Therefore for a

fixed small variance of an additive noise term, the measured asymmetry will increase. On the other hand, consider the case in which the system is relatively far from the threshold. For small noise, the system explores a relatively narrow region which is symmetric around the minima. However, as the external fluctuations increase, the asymmetric effects of the effective potential on the dynamics can become measurable. Next, we focus on measuring this asymmetry.

2.2.2 Skewness as a measure of asymmetry

The skewness, denoted by γ, is a dimensionless measure of the degree of asymmetry of a probability distribution. Given a probability distribution $P(x)$, with mean μ and standard deviation σ, the skewness is defined as the scaled third moment about the mean:

$$\gamma = \frac{\int_{\mathbf{R}} (x-\mu)^3 \, P(x) dx}{\sigma^3} \tag{2.10}$$

where $\mathbf{R}$ is the range or support of the probability distribution. The skewness vanishes for distribution symmetric about the mean and is positive or negative for an asymmetric distribution with a tail above or below the mean respectively.

We begin by showing that qualitative changes in the shape of the distribution are observed in the time series of the state variable as one approaches a threshold point. We illustrate this using the results of numerical simulations of the one-variable vegetation model of Eq 2.4. The stochastic differential equation is solved numerically by a simple Euler algorithm which is first order accurate in time [88, 102]. The solution for a particular time sequence of noise values obtained by our numerical simulation corresponds to the time series data of the ecological variable collected in field. The plots of time series of the state variable, the vegetation biomass density, and the corresponding probability distributions are shown in Fig. 2.3. The distribution is symmetric at $c = 1.5$ far from the threshold. As the

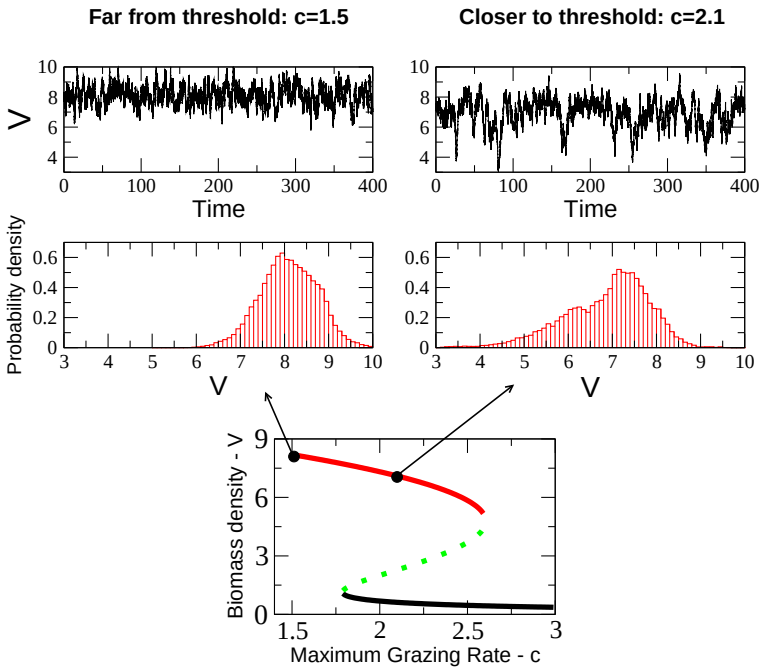

Figure 2.3: The plot at the bottom of the panel shows the bifurcation diagram for Eq 2.4. Four subplots at the top of the panel show representative numerical simulation results for the time series and its probability density when the ecosystem is far from and close to the threshold of collapse ($c^* = 2.6$). The asymmetry in the distribution that is clearly visible underlies the indicator of regime shift proposed in thepaper. Simulations were started with the vegetation in the high density state. We choose $\sigma_V = 0.75$, a time step of $dt = 0.01$ for numerical integration and rest of the parameters are as in Fig. 2.2.

threshold value is approached, the distribution develops a visible asymmetric tail. For this specific model simulation, substantial asymmetry is observed at $c = 2.1$, relatively far away from the bifurcation ($(c^* - c)/c^* \approx 20\%$). We emphasize that the probability distributions being shown in this and the later ones below are *not* the steady state distributions, but only a local equilibrium or transient distribution. See section 2.2.3 for a discussion.

In Fig. 2.4, we plot the absolute value of the average skewness in two scenarios corresponding to different routes to a regime shift. The skewness is calculated for a time series of length 2000 time units. We then average the skewness over 100 such realizations.

In both the plots, the open circles represent the average values of skewness obtained by numerical simulations. The solid line represents the analytical calculations obtained by a direct evaluation of skewness of the corresponding stationary probability distributions. We have calculated the analytical value of skewness by performing the integration (Eq. 2.10) in the region $\mathbf{R} = (x_l, x_m)$ around the stable fixed point x^* such that $x_l = x^* - 2\sigma_V$ and x_r is determined by numerically solving the equation $P_s(x_r) = P_s(x_l)$ (see section 2.2.3).

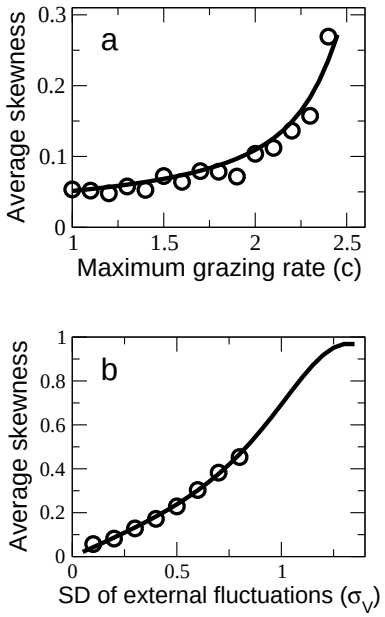

Figure 2.4: Increase in skewness as the ecosystem approaches regime shift via different routes for May's model of vegetation collapse considered in Figure 1. The thick line is the analytical result obtained directly from the stationary probability distribution. The open circles are the average values of skewness obtained by the numerical simulations. Note that we have plotted the absolute value of the average skewness. (a) Approaching the threshold of vegetation collapse by increasing the grazing pressure with fixed external fluctuations $\sigma_V = 0.25$. (b) Approaching regime shift by increasing (noise) fluctuations in the system at $c = 2.0$ (far from threshold). We choose $dt = 0.1$ and rest of the parameters are as in Figure 2.2.

In the first scenario, the variance of the external noise is held constant and the grazing rate c is varied. The skewness of the time series distribution as a function of the bifurcation parameter c, shown in Fig. 2.4(a), increases slowly up to $c = 2.0$. However, as the grazing rate is tuned closer to the threshold value from $c = 2.0$ to 2.6, the skewness increases substantially. Thus, an increase in skewness foreshadows the vegetation collapse and serves as an early warning signal of the regime shift.

In the second route, increasing the external noise by increasing the standard deviation, σ, of the Gaussian noise distribution, leads to a regime shift even if the system is far from the bifurcation [95]. In Fig. 2.4(b), we plot the skewness, with a fixed grazing rate at $c = 2.0$, as σ is varied. Clearly, the skewness increases as the noise level increases. This is an intrinsic dynamical effect since the external noise distribution is Gaussian and symmetric.

We have checked that the features reported above hold for the model with no additive noise but noise in either the growth rate r or the grazing rate c. In the former case the skewness though large far from equilibrium, increases substantially as the bifurcation is approached, thus serving as an early warning signal.

2.2.3 Transient or steady state distributions?

In all the calculations shown above, we have calculated the skewness of non-steady state probability distributions. This applies if one were to calculate other indicators as well, even though the theoretical calculations (Eq 2.3) were based on a steady state analysis. The steady state calculation of probability distributions (Eq. 2.7) for a bistable system includes the ecological transition itself. Obviously, such a calculation is not useful for the purposes of ecological forecasting. We refer to the non-steady state probability distribution prior

to the transition as the *transient distribution*. In the transient approximation, the 'linear indicators' do not possess the divergences as predicted by Eq. 2.3. Note that skewness is not divergent even under those ideal conditions. However, if we are not too close to a regime shift, the trends of changes in the indicators calculated from the transient distribution may be observable and this has been demonstrated for skewness in this paper and for other indicators in earlier studies [91, 93, 94].

Clearly, as we move closer to the threshold, there are higher chances that the system escapes to an alternative stable state much before the characteristics of the transient state can be reliably measured. For this reason, we do not show data for $\sigma > 0.8$ in Fig. 2.4(b). A simple heuristic argument suggests that if the strength of noise fluctuations $\sigma_V^2 > \Delta U$, where ΔU is the potential barrier (analogous to activation energy in reaction kinetics), the time required to make a transition can be relatively small. We have studied this more carefully as follows: Starting from the vegetated state the system will eventually make a transition to the bare state in the presence of Gaussian noise. In a random process with a given initial condition the first occurrence of an event such as reaching a specific value is known as the "first passage time" [88, 103]. When averaged over many realizations, we obtain the *mean first passage time* (MFPT). The MFPT in our problem is the average time interval over which the system remains in the vegetated state; more generally, the time scale on which a regime change is likely to occur. In all of our calculations if the MFPT is smaller than a certain length of time interval we have chosen (2000 time units for May's model), we do not compute skewness. The details of MFPT are calculated as below.

Once again we resort to a simpler notation. We suppose that the dynamics of a system is described by the following stochastic differential equation:

$$\dot{x} = f(x) + \eta(t) \tag{2.11}$$

where $\eta(t)$ is as usual taken to be a Gaussian white noise with variance σ^2. We assume that $U(x)$ is a bistable potential (the results hold for any other potential as well). Fig. 2.5(a) shows a representative bistable potential with stable fixed points at a and c and an unstable fixed point at b. Our interest is in calculating the average time the system stays in the basin of attraction of one of the stable states, say that of state a.

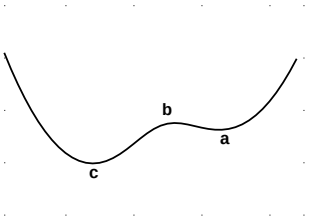

(a)

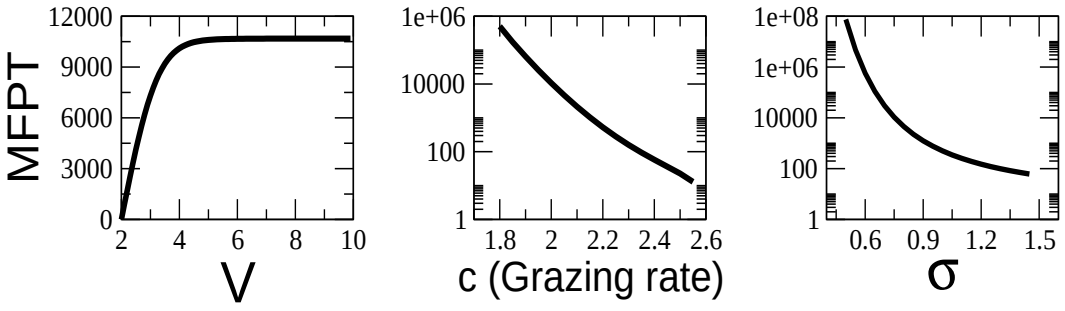

(b)

Figure 2.5: (a) A representative bistable potential. The labels a, b and c correspond to fixed points of the system (b) From left to right: (i) The MFPT to the unstable fixed point from the value V (on x axes). Here, c (maximum grazing rate) $= 2.0$ and $\sigma_V = 0.75$. The unstable fixed point **b** is at $V = 2$ for this set of parameter values. (ii) The MFPT to the unstable fixed point from the stable fixed point as the grazing rate increases. Here, $\sigma_V = 0.75$. (iii) The MFPT to unstable fixed point from the stable fixed point as the strength of the external fluctuations increase. Here, $c = 2.0$.

To do so, we assume that the basin of attraction of state a extends from ∞ up to b. Define $T(x)$ as the mean first passage time to state b starting at $x > b$. Then it can be shown that $T(x)$ follows the following ordinary differential equation [88]:

$$f(x)\frac{dT(x)}{dx} + \frac{\sigma^2}{2}\frac{d^2T(x)}{dx^2} = -1 \tag{2.12}$$

with the boundary conditions: $T(b) = 0$ and $\frac{dT(x=\infty)}{dx} = 0$ (*i.e.,* a reflecting boundary at $+\infty$).

We use Mathematica to solve the above equation for the May's vegetation model of Eq. 2.4 [8]. The results for MFPT are shown in Fig 2.5. Note that MFPT drops substantially as one approaches a threshold keeping the fluctuations constant or as the external fluctuations increase at a fixed distance from threshold. If the time scale of observation is more than the MFPT, then the transient approximation fails and we do not show results corresponding to those.

2.3 Two variable model of vegetation collapse

We check the applicability of our proposal in a more complex model of vegetation dynamics given by:

$$\frac{dw}{dt} = R - \alpha w - \lambda w B + \eta_w(t) \tag{2.13}$$

$$\frac{dB}{dt} = \rho w B(1 - \frac{B}{wB_c}) - \mu\frac{B}{B + B_0} + \eta_B(t) \tag{2.14}$$

Here the soil water w increases due to rainfall at a rate R, decreases due to evaporation ($-\alpha w$ term) and uptake by vegetation($-\lambda w B$ term.) The vegetation biomass B grows logistically under the grazing pressure as in the previous model. We have included fluctuations in the rainfall rate whose standard deviation is σ_w and the effect of external fluctuations (with strength σ_B) on the biomass growth rate.

This model obviously differs from the one variable model by including an explicit water-vegetation feedback mechanism. An important technical difference, however, is that an effective potential can not be defined for this model. This can be seen as follows: Using a simpler notation of $\dot{x_1} = f_1(x_1, x_2) + \eta_1(t)$ and $\dot{x_2} = f_2(x_1, x_2) + \eta_2(t)$, we can write the Fokker-Planck equation for this coupled system:

$$\frac{\partial P(x_1, x_2, t)}{\partial t} = -\sum_i \frac{\partial}{\partial x_i} f_i \, P + \frac{1}{2} \sum_{i,j} \sigma_{i,j}^2 \frac{\partial}{\partial x_i \partial x_j} P \tag{2.15}$$

where $\langle \eta_i(t) \eta_j(t') \rangle = \gamma_{ij} \delta(t - t')$. For Eq. 2.13, $\gamma_{i,j} = \delta_{ij} \sigma_i^2$. The condition for the existence of potential is that we can write $\mathbf{f} = \{f_1, f_2\} = -\nabla U(x_1, x_2)$. A necessary condition for the existence of potential function U is:

$$\frac{\partial f_j}{\partial x_i} = \frac{\partial f_i}{\partial x_j} \qquad \forall \; i, j \tag{2.16}$$

It can be easily verified that the above condition is not satisfied for Eq 2.13. However, we recall that our proposal of skewness as an indicator of regime shift depended on the existence of asymmetry in the potential. Nevertheless our calculations (see Appendix A.1) show that the results of skewness continue to hold for this model as well. It is possible to devise an intuitive understanding of how the asymmetry arises by considering the vector field that represents the "forces" that determine the rate of the change of the dynamical variables (see Appendix A.2).

2.3.1 Analysis of failure of skewness as an early warning signal

Our calculations for the two variable model show that skewness may fail to signal a regime shift in certain circumstances, especially when large external fluctuations are drivers. We find that for large, but constant values of fluctuations in rainfall σ_B, an increasing external fluctuations σ_w can easily drive a regime shift. However, skewness fails

to increase as the strength of the fluctuations increase(shown in Fig. 2.6). In this section, we present a heuristic argument and its mathematical underpinning to understand the failure of skewness as an early warning signal.

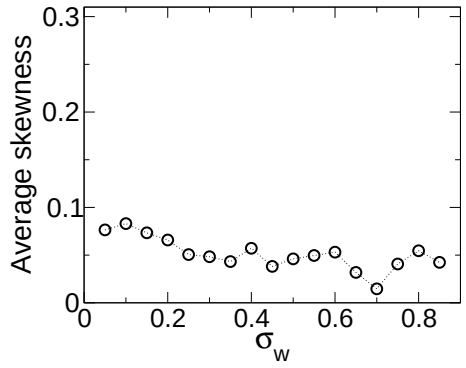

Figure 2.6: An instance where the skewness fails to detect the regime shift. Increase in rainfall rate fluctuations, w, keeping R = 1.5 and $\sigma_B = 0.25$.

In the model above, the soil water w equilibrates on time scales of a few hours to days which is much faster compared to the biomass density which grows on the scale of months to years. Thus, we make the so called quasi-static approximation by setting $dw/dt = 0$ and substitute the corresponding equilibrium value of w in Eq. 2.13 to obtain the reduced equation:

$$\frac{dB}{dt} = \rho B\Big(\frac{R}{1+\lambda B} - \frac{B}{B_c}\Big) - \mu\frac{B}{B+B_0} + \sigma_B\,\eta_B(t) + \tilde{\sigma_w}\tilde{\eta}_w(t)\rho\frac{B}{1+\lambda B} \tag{2.17}$$

$$= f(B) + \sigma_B\,\eta_B(t) + \tilde{\sigma_w}\,\tilde{\eta_w}(t)g(B) \tag{2.18}$$

$$\text{s.t.} \qquad f(B) = \rho B\Big(\frac{R}{1+\lambda B} - \frac{B}{B_c}\Big) - \mu\frac{B}{B+B_0} \quad \& \quad g(B) = \rho\frac{B}{1+\lambda B} \tag{2.19}$$

where $\tilde{\sigma_w}$ and $\tilde{\eta_w}$ are appropriately renormalized quantities representing the fluctuation in rainfall rate in the reduced equation. The reduced equation for the biomass density has a multiplicative as well as the additive noise term. We explain below how the multiplicative

noise term reduces asymmetry in the time series distribution by heuristic arguments as well as a direct calculation of the effective potential for the reduced equation given above.

Since above equation consists of both an additive and multiplicative noise, consider a case of stochastic one variable model given by: $\dot{x} = f(x) + g(x)\eta(t) + \xi(t)$ where $\eta(t)$ and $\xi(t)$ are independent Gaussian white noise processes with zero mean and variances σ_η^2 and σ_ξ^2. The Fokker-Planck equation for this system can be shown to be:

$$\frac{\partial P(x,t)}{\partial t} = -\frac{\partial}{\partial x}\Big[f(x)P(x,t)\Big] + \frac{1}{2}\frac{\partial^2}{\partial x^2}\Big[(\sigma_\xi^2 + \sigma_\eta^2 g(x)^2)P(x,t)\Big]. \tag{2.20}$$

The effective potential for this system can be obtained by:

$$U_e(x) = -\int_{x_0}^{x} \frac{f(y)}{\sigma_\eta^2 g(y)^2 + \sigma_\xi^2} + \log(\sigma_\eta^2 g(y)^2 + \sigma_\xi^2)|_{x_0}^{x} \tag{2.21}$$

The stationary probability density (solution of time independent Fokker Planck equation) is then given by $P_{st}(x) = N' \exp(-2U_e(x))$ where N' is the normalization factor.

The potential for the reduced equation with $\sigma_w = 0$ is shown in Fig 2.7(a). Clearly, the potential is asymmetric and we expect a tail at small values of B that can serve as an indicator of regime shift. When $\sigma_w > 0$, the effect of multiplicative noise term begins to affect the shape of the potential. In contrast to fluctuations arising from the additive noise term, the multiplicative noise term has lower amplitude for smaller values of B and it increases in strength as B increases (Fig. 2.7(b)). Thus, $\sigma_w \eta_w(t) g(B)$ contributes to fluctuations with an asymmetric tail towards larger values of B. The resulting fluctuations in the vegetation biomass with both the additive and multiplicative noise terms is nearly symmetric leading to a reduced (or nearly zero) skewness in the time series distribution. This explains the failure of skewness in predicting a regime shift when the fluctuations in the rainfall term are included.

The Fig. 2.7(c-e) shows the effective potential for the full equation Eq (2.19) (calculated using Eq. 2.21) for different values of σ_w. Clearly, the extent of asymmetry in the presence of fluctuations in rainfall is substantially reduced as σ_w is increased. This is consistent with the observed behavior of skewness with increase in σ_w, displayed in Fig. A.2(c).

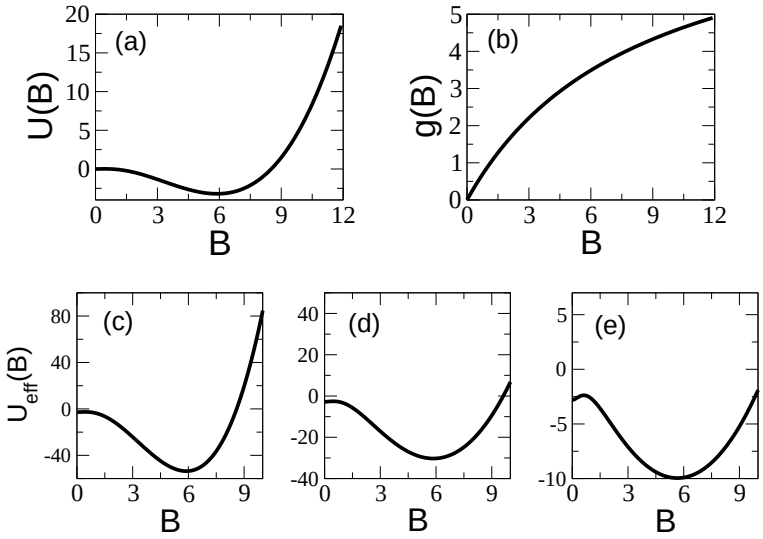

Figure 2.7: Analyzing the failure of skewness as an early warning signal when σ_w increases leading to a regime shift. In all the plots below $R = 1.5$, $\sigma_B = 0.25$ and rest of the parameters are: $\rho = 1.0, \alpha = 1.0, \lambda = 0.12, B_c = 10, B_0 = 1$. (a) Effective potential when the fluctuations in the rainfall rate are absent (*i.e.* $\sigma_w = 0$). (b) The function which modulates the strength of the multiplicative noise. (c)-(e): Effective potential when the fluctuations in the rainfall are present and increasing (from left to right): $\sigma_w = 0.01, 0.10$ and $\sigma_w = 0.25$.

Finally, we make a technical remark on the quasi-static approximation. Eliminating a degree of freedom (*i.e*, the variable w) by a the quasi-static approximation leads to a renormalized strength and correlations (*i.e*, frequency dependence) of the noise term $\tilde{\eta_w}$. We are tacitly assuming that the noise η_w in the dynamics of w is not white and more specifically, the time scale of fluctuations in rainfall is larger than the typical equilibrium

time for soil-water interaction processes. Since the time scale on which the vegetation biomass dynamics occurs is much longer than that of soil water or rain water fluctuations, a white noise structure (and hence no frequency dependence) for $\tilde{\eta_w}$ is justified. We take for simplicity $\tilde{\sigma_w} = \sigma_w$ to perform effective potential calculations for Eq. 2.18 since our focus is the calculation of the trends in the asymmetry and average skewness.

2.4 Two variable parameterized lake model

In this section, we consider a parameterized lake eutrophication model and mimic a plausible scenario of field measurements. We show that a trend of increasing skewness can be detected well in advance of a regime shift despite constraints of sparse data availability. Our results allow us to make useful observations and provide insights on the analysis of real data sets.

The model is a slightly modified version of [93]):

$$\frac{dP}{dt} = l - (s+h)P + rMR(P) + \sigma_r \eta_r(t) rMR(P) + \sigma_l \eta_l(t) \tag{2.22}$$

$$\frac{dM}{dt} = sP - bM - rMR(P) - \sigma_r \eta_r(t) rMR(P) \tag{2.23}$$

This system of equations describes the dynamics of coupled variables of water phosphorus concentration, P, and the sediment phosphorus, M. Here l is the nutrient loading rate to the lake, s is the sedimentation loss rate, h is the outflow rate, r is the recycling coefficient and b is the permanent burial rate of phosphorus in sediments. The function $R(P)$ is the nonlinear recycling function where P_0 is the value of phosphorus concentration at which the recycling is half its maximum rate and q is the so-called Hill coefficient. In addition, there are two Gaussian white noise terms in this model: an additive noise term η_l that corresponds to fluctuations in the phosphorus loading to the lake and a multiplicative noise term $\eta_r rMR(P)$ that models the fluctuating recycling of sediment phosphorus due

to stochastic events such as those driven by wind in summer [104]. Note that this system of equations does not satisfy Eq. 2.16 and hence we can not define an effective potential.

Appendix A.3 contains the bifurcation diagram and the results for the skewness. Here, we consider a scenario in which the mean nutrient inputs increase as a function of time which can occur with economic growth. We perform a 'dynamic simulation' to see if we can observe a trend of increasing skewness under such conditions. In our numerical calculations the mean nutrient loading is increased from 0.5 to 1.28 $gm^{-2}y^{-1}$ in 40 years time with constant increments every year and kept constant thereafter. We compute a simple moving average skewness from the data obtained by numerical simulation for the previous five years.

The results of the model calculations are presented in Fig 2.8 a and b. The phosphorus concentration data indicates that a regime shift occurred around year 45. Moving average skewness shows an increasing trend starting from year 34 and by the beginning of year 40 the trend is unmistakable (around 100% increase) and hence, this can serve as an early warning signal nearly five years in advance. We added a practical constraint of limited data sets by comparing the results of a dense data set (100 water phosphorus measurements per year) with those for a sparse data set of 33 measurements per year. We find that thinning the data set had negligible effect on the trend of changing skewness, thus providing confidence in its utility as an early warning signal. We note that for a specific set of parameters values (nutrient loading taken to be constant at $1gm^{-2}y^{-1}$ with the initial conditions $P_0 = 1gm^{-2}$ and $M_0 = 800gm^{-2}$), the skewness failed to detect a regime shift in nearly 30% of the cases.

More importantly, these model calculations suggest that skewness can fluctuate for short time periods and then relax to the background value; such behavior, observable far from a regime shift, should not be misinterpreted as signaling an impending transition. However,

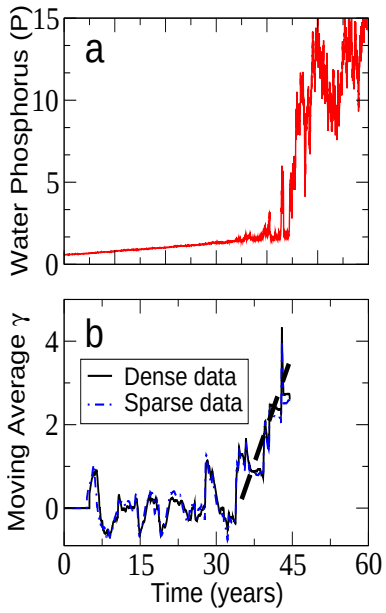

Figure 2.8: The figures show that changes in the skewness (denoted by γ) can be detected well in advance for a model system which mimics a field measurement scenario. These results are obtained by numerical simulation for the lake model when the nutrient inputs are increased as a function of time towards the eutrophication threshold as described in the text. The initial conditions for simulation are $P(t=0) = 0.58gm^{-2}$ & $M(t=0) = 410gm^{-2}$ and a time step of $dt = 0.01$. The moving average skewness has been calculated from data for the previous five years. The dense and the sparse data sets correspond to 100 and 33 measurements of lake water phosphorus concentration (P) per year respectively. Rest of the parameters are:$s = 0.7y^{-1}, h = 0.15y^{-1}, b = 0.001y^{-1}, P_0 = 2.4gm^{-2}, q = 8, \sigma_l = 0.01, \sigma_r = 0.01$

significant changes on a time scale larger than the background fluctuation time scale act as reliable early warning signals of an impending regime shift.

2.5 Analysis of Sahara data

We consider a well-dated record of terrigenous sediment deposition at Ocean Drilling Program Site 658C off Cap Blanc, Mauritania which indicates an abrupt termination of

North African (Sahara region) humid periods resulting in collapse of vegetation and desertification [1]. See Appendix A.4 for the analysis of the complete Sahara data set from 25000 years before present (BP) to the present. An abrupt change in the sediment concentration corresponding to the most recent regime shift in Sahara is found around year 5500 BP as shown in Fig. 2.9a. Our interest is to determine whether skewness of the data showed any reliable trends prior to the regime shift. We note that the data are relatively sparse and have errors both in the determination of the time and the sediment. Nevertheless, in an effort to illustrate the difficulties encountered in the prediction of regime shifts from available data we have performed a simple analysis of the data. The moving average skewness (calculated for the previous 10 data points) up to the year of the shift is shown in Fig. 2.9b. An increasing trend of moving skewness is clearly identifiable and occurred around 1000 years prior to the collapse. However we need to establish that this change is statistically significant in order to interpret it as an early warning signal. To do so we perform a simple diagnostic test based on the idea that an AR(1) process defined by $x(t+1) = \beta x(t) + \sigma\eta(t)$ (where $\eta(t)$ is a Gaussian white noise) acts as a null model for measuring changes in skewness. This is reasonable because an AR(1) process follows from a linear analysis around the fixed point and therefore, yields zero (long-time average) skewness. For finite sized time series, the moving skewness of an AR(1) process can therefore act as a reference to measure changes in skewness near a bifurcation.

We fit the data prior to the regime shift to the AR(1) process to obtain coefficients β and σ to be 0.59 and 1.51 units respectively. We then generated 100 time series each of length comparable to the real data (66 data points) and computed the moving skewness. In a typical simulation we find, unfortunately, that the changes in skewness are comparable to those in the Sahara data set. Hence we are unable to conclude that the changes in skewness

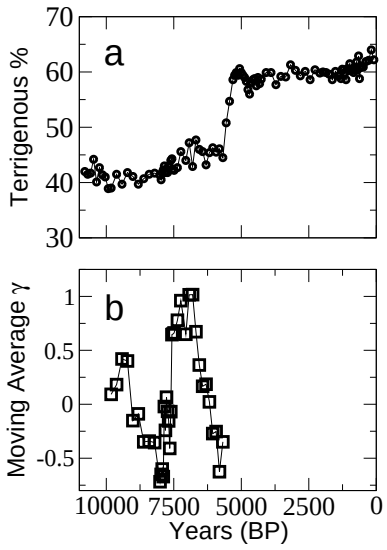

Figure 2.9: Analysis of terrigenous sediment data indicating climatic shift in Sahara (a) Time series of terrigenous sediment percentage record from Site 658C off Cap Blanc, Mauritania. Circles represent data while connecting line is meant to guide the eye. Note the regime shift which occurred around 5500 years before the present day (BP). (b) The moving average skewness: for any given time, skewness is calculated from the previous 10 data points. Squares represent computed skewness values with the connecting line meant to guide the eye.

observed in the Sahara data set arise from the proximity to a regime shift. These results, however, do not mean that the indices of regime shifts will always fail, but indicate the limitations involved in applying to an extremely sparse data set such as this one. As we show in the Appendix A.4, with a finer resolution data such as the Phosphorus concentration data available from Sandusky Bay [2] one can calculate changes in skewness more reliably. We further note that we have not considered a variety of statistical data analysis issues such as missing data, effects of seasonality, obtaining confidence intervals and detrending the data. One may also need to consider a dynamic AR(1) model in which parameters β and σ are time-varying.

2.6 Discussion

Our analysis of simple ecological models shows that changes in the asymmetry, quantified by changes in the skewness of the time series data, can be a generic indicator of an impending regime shift. We have shown that the skewness of the time series data increases as we approach a regime shift in one-variable and more complex ecological models. Although we have illustrated the case of skewness increasing from zero to non-zero values, in general, changing skewness (from non-zero skewness to even larger skewness, etc.) can serve as an indicator of regime shifts. The origin of asymmetry lies in the contribution of nonlinear terms to the dynamics of the system and hence changing skewness may be referred to as a 'nonlinear indicator' of regime shift; in contrast variance, recovery time and reddened power spectra can be derived by a linear analysis, and constitute 'linear indicators' of regime shift. In the following paragraphs, we discuss some of the simplifying assumptions of our model calculations and make suggestions for future research.

An important assumption in our calculations is that the stochastic dynamics of the model systems are a complete representation of the ecological data. Real ecological data are prone to multiple sources of errors including external and observational errors in addition to the uncertainty involved in identifying and modeling the dynamical processes. One possible pitfall is that the observed changes in asymmetry in the time series do not necessarily imply proximity to a regime shift since it may not be due to intrinsic dynamics but due to asymmetry in the exogenous noise, for example. Technically, this means that modeling all the uncertainties and errors by a simple Gaussian white noise is an oversimplification. This problem has to be addressed on a case by case basis by various statistical methods: If data are available for the noisy external variable that drives the system (such as nutrient input and rainfall data), we can remove associated trends from the time series of the state

variable. It has been shown that one can successfully separate true variance from other sources of noise by using dynamical linear modeling techniques of time series data [93] and such a calculation, at least in principle, can be extended to extract true skewness as well. More generally, the problem of detecting regime shifts as well as distinguishing environmental fluctuations from the true dynamics of the system is an issue of immense practical importance and has also been addressed by other techniques [105, 92, 106, 107, 108, 109, 110].

Next, we discuss the implications of choice of Ito calculus in solving stochastic differential equations and how the results may in general to differ if one chooses an alternative rule, namely the Stratonovich calculus. An equation of the form $\dot{x} = f(x) + g(x)\eta(t)$ when $g(x) \neq$ a constant, is meaningful only if we attach an interpretation rule to evaluate the multiplicative noise term. This is due to the random nature of $\eta(t)$ which can be thought of as a sequence of extremely short interval pulses. Such a pulse induces a jump in $\dot{x}$ which in turn leads to a jump in x. Hence a question arises as to what value of x should be used to evaluate the stochastic equation at time t which will in turn determine the value of the jump. In Ito calculus, we assign a value of x which is just prior to the jump. On the other hand, Stratanovich convention assigns a value of x which is an average value of the state variable before and after the jump. The results can be different depending on the choice of the calculus one uses. This is easily seen by the Fokker-Planck equation for the Stratanovich calculus:

$$\frac{\partial P(x,t)}{\partial t} = -\frac{\partial}{\partial x} f(x)P + \frac{1}{2}\frac{\partial}{\partial x} g(x)\frac{\partial}{\partial x} g(x)P \tag{2.24}$$

$$= -\frac{\partial}{\partial x}\Big[f(x) + \frac{1}{2}g(x)g'(x)\Big]P + \frac{1}{2}\frac{\partial^2}{\partial x^2} g(x)^2 P \tag{2.25}$$

Eq 2.25 shows the contrast between Ito and Stratanovich rules of calculus in the drift term for the "same" stochastic equation. Note that such a discrepancy does not arise when

$g(x)$ is not a function of the state variable or obviously, when there is no stochastic term. The Ito calculus we have employed is relatively easier to implement numerically. This rule is ecologically relevant because the state of an ecological system at time $t + \Delta t$ is determined by the state at time t and an access to the 'future' values of state variable is not meaningful in ecological systems. We have compared effective potential obtained by these two interpretations for the May's model with multiplicative noise term (in the grazing parameter, c). We find that the qualitative nature of the effective potential is independent of the choice of interpretation used in the rage $V \in [0.1, 12]$. Hence the results of skewness will continue to hold for the Stratonovich scheme of interpretation as well. Such an effective potential calculation is not possible for the lake model where noise in recycling led to a multiplicative noise term. However, it is possible to make some speculation based on the following heuristic arguments. Eq. 2.25 and a Fokker-Planck equation for the two variable lake model suggest that the derivative term will play an important role in deciding how the two rules of calculus differ in their results. The recycling function $R(P)$ is a sigmoidal function that has zero value for its derivative when the system is in either of the stable states. But recycling is strongly nonlinear for intermediate values of Phosphorus concentration and hence can be important for calculations involving the transition between two stable states. Our focus is on the characteristics of the transient state prior to the occurrence of a transition. Hence we can expect that the specific rule of calculus we chose is unlikely to affect the results we have presented in this chapter. Numerical simulations, however, are needed to confirm these speculations.

Future research work on the theoretical analysis of skewness under non-stationary conditions, the statistical issues of estimation and errors and developing simple methods to

extract true skewness from an error-prone data are needed which make this indicator further useful for practical applications. Other indices of nonlinearities such as S-maps and anisotropic variances in the time-1 return map [111] can also be explored as measures of changing asymmetry. Another area for future investigations is the study of early warning signals in spatially explicit models of regime shift and elucidating the relative merits of different indicators.

CHAPTER 3

LEADING INDICATORS OF REGIME SHIFTS IN SPATIAL ECOLOGICAL SYSTEMS

In developing an early warning signal for abrupt regime shifts in ecosystems in the previous chapter, we have ignored the spatial fluctuations. In this chapter, we propose that increase in the variance and changes in the skewness of the spatial probability distribution, i.e., of a *spatial snapshot* of the relevant ecological variable can be leading indicators of catastrophic regime shifts.

In section 3.1, we show how our proposal of the spatial variance is motivated from the behavior of equal time correlation function near the critical point of a second-order phase transition. In section 3.2, we show analytical and numerical results of increasing spatial variance and spatial skewness in a reaction diffusion model of vegetation collapse. We present the results on how the mean-field bifurcation diagram as well as the results on indicators are affected by the strength of spatial interactions. We show that an increasing spatial variance in conjunction with a reversal in the initial changing trend of spatial skewness is an unambiguous indicator of an impending ecological regime shift in the model system. This warning signal appears sufficiently early to initiate conservation strategies. In section 3.3, it is shown that the results of spatial variance and skewness are independent of details of dispersal kernels such as Gaussian, fat-tailed and heavily fat-tailed.

3.1 Near the critical point of second order phase transition

Studies on second order phase transition in physical systems show that quantities such as correlation length and susceptibility diverge at the critical point and the system exhibits universal properties independent of the details of the system under consideration. We take a leaf out of these studies and apply it to spatially extended ecological model systems to devise leading indicators of impending regime shifts. In this section, we present calculations for the correlation function near the critical point and connect it to our proposal of spatial variance as an indicator.

Consider the Landau free-energy functional as a function of the coarse-grained scalar order parameter $\phi(x,t)$:

$$\mathcal{F}[\phi] = \int d^d x [\frac{D}{2}|\nabla\phi|^2 + U(\phi)] \tag{3.1}$$

where $U(\phi) = \frac{\alpha}{2}\phi^2 + \beta\phi^4$ is a symmetric potential and $\beta > 0$. As $\alpha \to 0+$, the system undergoes a disorder-order phase transition. The equation for the time evolution of the order parameter is given by:

$$\frac{\partial\phi}{\partial t} = -\frac{\delta\mathcal{F}}{\delta\phi} + \eta(x,t) = -U'(\phi) + D\nabla^2\phi + \eta(x,t) \tag{3.2}$$

$$\approx -\alpha\phi(x,t) + D\nabla^2\phi + \eta(x,t) \qquad \text{up to linear order} \tag{3.3}$$

where $\eta(x,t)$ is a Gaussian white noise whose variance σ^2 is proportional to the temperature. In Landau's theory, the coefficient α is phenomenologically taken to be $\alpha = \alpha_0(T - T_c)$ where T_c is the critical temperature, $\alpha_0 > 0, T > T_c$. In our calculations, we study the equal time correlation function $C(r, \tau = 0) = \langle\phi(x + r, t + \tau)\phi(x,t)\rangle|_{\tau=0}$ as $\alpha \to 0$.

To obtain that quantity, we first calculate the spectral function defined by $S(q,\omega) = \int\int C(r,\tau)e^{i(qr-\omega\tau)}drd\tau$. Take the spatial and temporal fourier transforms of Eq. 3.2 by setting $\phi(x,t) = \int \exp(i\omega t - iqx)\tilde{\phi}(q,\omega)\frac{dq}{2\pi}\frac{d\omega}{2\pi}$ and $\eta(x,t) = \int \exp(i\omega t - iqx)\tilde{\eta}(q,\omega)\frac{dq}{2\pi}\frac{d\omega}{2\pi}$ to

obtain:

$$\tilde{\phi}(q,\omega) = \frac{\tilde{\eta}(q,\omega)}{i\omega + \alpha + Dq^2} \tag{3.4}$$

The spatio-temporal power spectrum is given by:

$$S(q,\omega) = \langle |\tilde{\phi}(q,\omega)|^2 \rangle = \frac{\sigma^2}{\omega^2 + (\alpha + Dq^2)^2} \tag{3.5}$$

The steady state spatial power spectra can then be obtained as:

$$S(q) = \int_{-\infty}^{\infty} \langle |\tilde{\phi}(q,\omega)|^2 \rangle \frac{d\omega}{2\pi} = \frac{\sigma^2}{2(\alpha + Dq^2)} \tag{3.6}$$

Now the equal time correlation function is easily obtained for one spatial dimension by:

$$C(r, \tau = 0) = \int_{-\infty}^{\infty} S(q) e^{-iqr} \frac{dq}{2\pi} = \frac{\sigma^2 \xi}{4D} e^{-|r|/\xi} \tag{3.7}$$

where $\xi = \sqrt{D/\alpha}$ is the correlation length. A quantity that is often measured in the context of magnetic materials is the susceptibility $\chi = 2\int_0^{\infty} C(r, \tau = 0) dr = \sigma^2 \xi/(2D)$.

As we approach the critical point by $\alpha \to 0$, the correlation length $\xi \to \infty$ and therefore the correlation function as well as the susceptibility diverge. We draw attention to the fact that the equal time and equal space correlation function $C(r = 0, \tau = 0) = \sigma^2 \xi/(4D)$ is nothing but the spatio-temporal variance of an extended system. If the system size is sufficiently large we may expect that spatial variance, a quantity easily measured in an ecological system (for example through satellite imagery), to show qualitatively similar behavior. These divergences are hallmarks of second order phase transitions where the order parameter changes continuously near a critical point. However, the abrupt transitions of interest in ecology are best modeled by the first order phase transitions where, unfortunately, no such divergences occur. Nevertheless, we show that the signatures of 'apparent divergence' can be found in the ecological systems of interest to us under a 'transient approximation'.

3.2 Indicators of transitions in diffusion model

We retain the one variable model of vegetation collapse in semi-arid ecosystems studied in previous chapter [8, 96]:

$$\frac{dV(t)}{dt} = rV\left(1 - \frac{V}{V_c}\right) - c\frac{V^2}{V^2 + V_0^2} \tag{3.8}$$

where V is the logistically growing population with growth rate r and carrying capacity V_c under a mean-grazing-rate which can reach the maximum value of c. This model has been applied to study variety of ecological systems such as exploitation of fish communities [98], vegetation in a semi-arid ecosystem [96], spruce budworm dynamics [8, 99] and harvesting of macrophytes [100], but typically in a non-spatial context. We recall that the deterministic non-spatial model exhibits a bistable region with coexisting high density and low density vegetated states. For $c > c^* = 26$, the system collapses from a densely vegetated state to a low-density state (see Fig 3.1).

We now include stochasticity and spatial interactions in the model. The fluctuations arising from variations in grazing population density, denoted by $\eta_c(x,t)$, is modeled by a spatially and temporally uncorrelated Gaussian noise with variance σ_c^2. Since $\eta_c(x,t)$ is a Gaussian, the grazing rate $c + \eta_c(x,t)$ can fluctuate to negative values which is not ecologically meaningful. In general, a cutoff can be imposed. However, for the relatively small values of σ_c/c we have chosen, we do not obtain a negative grazing rate in any of our simulations. We assume the simplest form of spatial interactions through random diffusive dispersal of seeds leading to:

$$\frac{\partial V(x,t)}{\partial t} = rV(1 - \frac{V}{V_c}) - (c + \eta_c(x,t))\frac{V^2}{V^2 + V_0^2} + D\nabla^2 V(x,t) \tag{3.9}$$

where D is the diffusion constant. In order for us to be able to exploit the features of critical fluctuations of second order transition, we need to go sufficiently close to the bifurcation

$\alpha \to 0$. However, from the studies of nonequilibrium phase transitions, we know that this model exhibits first order phase transitions where the bifurcation diagram does not show bistability and no divergences of the kind found in the previous section can be applicable. But this result is true only in the thermodynamic limit and the metastable state has lifetimes substantially large so as to be able to go sufficiently close to the bifurcation of the mean field model (where $\alpha \to 0$). We justify these claims in the next few sections.

3.2.1 Bifurcation diagram with space and noise

First, we show that the bifurcation structure remains qualitatively similar to the mean-field model results in the presence of spatial and stochastic fluctuations for the timescales of ecological interest. In order to do so, we define a 'transient bifurcation diagram' that holds true on a specified time scale of observation and show that its qualitative nature is same as that for the mean-field model through numerical simulations. The lifetime of the metastable state depends on various factors including the level of the noise, the initial conditions, and other factors including the size of the system. Thus, depending on its lifetime the metastable state can be stable on the time scale of observation. Therefore, the range of grazing parameters over which we find coexisting stable states depend on the specific numerical "experiment". We consider two definitions below.

Homogeneous initial conditions: First, we perform our simulations with spatially homogenous initial conditions (IC). For a given value of the grazing parameter c, we chose one of the stable equilibria suggested by the mean-field model as the IC. We then let the system evolve according to Eq. 3.9 for 1000 time units. The spatial average of $V(x,t)$ at $t = 1000$ units defines the stable state of the spatially extended system.

The results of such a bifurcation diagram for different values of diffusion constant is shown in Fig 3.1 along with the mean-field bifurcation diagram. When $D = 0$, we are effectively simulating a large number of mean-field models with noise. The resulting bifurcation diagram shows considerably reduced region of bistability, consistent with the results of our recent work on nonspatial bistable models with noise [95]. If the observation time were shorter or the strength of the noise were smaller, the region of bistability will be increased. For a fixed strength of noise, when we increase the strength of the diffusive coupling the region of bistability increases. This result is easy to understand intuitively because the effect of diffusion is to smoothen and reduce the fluctuations. This effect of the diffusive coupling is also reflected in the results shown in a later section 3.2.3.

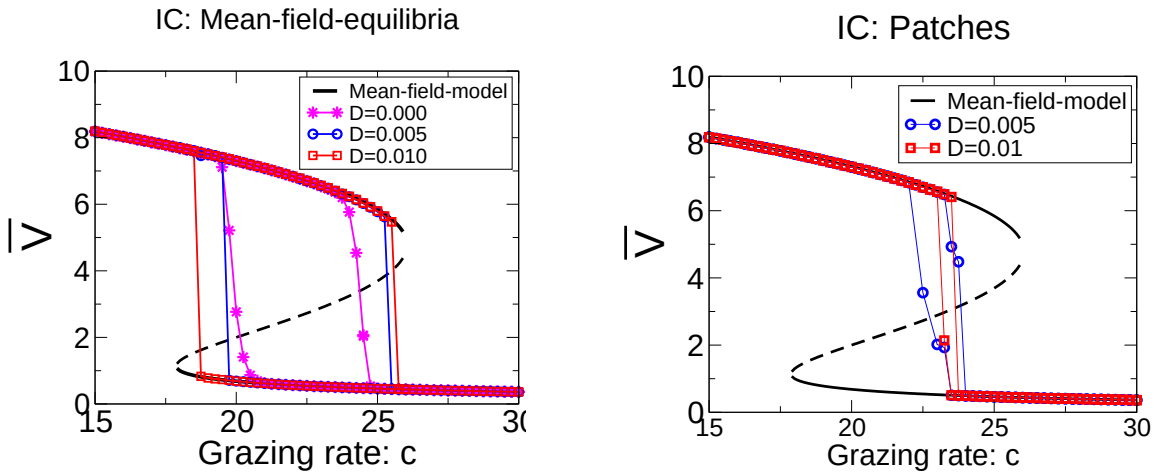

(a) (b)

Figure 3.1: The 'transient' bifurcation diagram for the May's model with space and noise. (a) This plot shows that the qualitative nature of the bifurcation is not affected by the spatial and stochastic fluctuations (b) This plot illustrates that if we wait sufficiently long, the bifurcation diagram shows characteristics of phase diagram of a first order phase transition.

Patchy initial conditions: We perform numerical simulations to obtain the long time behavior of the bifurcation diagram. The motivation for these calculations arises from the studies on first order phase transitions where we expect no hysteresis in the thermodynamic equilibrium. We address the question whether our spatial model with multiplicative noise also fails to exhibit hysteresis if we wait sufficiently long.

In order to answer this, we did numerical simulations on a two dimensional lattice with 128×128 lattice with the following initial conditions: 64×64 patch of the one of the stable state was embedded in the alternative stable state, for a given grazing rate c. We then let the system evolve according to Eq. 3.9 up to 4000 time units and the spatial mean at this time is chosen as the stable state of the ecosystem. The choice of initial condition ensures that we have avoided the exponentially long times required for the patches to be generated spontaneously by noise fluctuations in simulations of the type performed for obtaining Fig. 3.1(a). Results in Fig. 3.1(b) clearly show that the region of bistability is reduced in comparison to the short time simulations. This is an indicative of the fact that if one were to perform even longer time simulations, the region of bistability and hence the hysteresis will completely vanish leading to a first order transition in the limit of system size going to infinity. These calculations exemplify our statements about the transient nature of the bifurcation diagrams discussed earlier.

3.2.2 Mean field approximation (MFA) to obtain behavior of indicators

In this section, we establish that changes in spatial variance and skewness occur as we move close to the threshold of vegetation collapse. We do so by an analytical calculation based on the mean-field approximation of the spatial model developed by Van den Broeck et al along with the local equilibrium or transient approximation on the stability of the

fixed point [112]. Both these approximations do not hold as we approach the bifurcation point and hence in order to check the extent of validity of these results, we compare with the results of numerical simulations.

Continuing with the simpler notation for analytical calculations, we consider the following spatial model:

$$\frac{\partial v}{\partial t} = f(v) + g(v)\eta(x,t) + D\nabla^2 v \tag{3.10}$$

For a spatial model the state variable is a continuous function of the spatial coordinates: $v(x)$. If we discretize the space into N cells each of linear size Δx whose position is denoted by the discrete subscript i, we have the evolution equation for $v_i(t)$ in d-dimensions:

$$\frac{dv_i}{dt} = f(v_i) + g(v_i)\eta_i(t) + \frac{D}{\Delta x^2}\sum_{j\in n(i)}(v_j - v_i) \tag{3.11}$$

where $n(i)$ represents the nearest neighbors of site i. The discretized noise has the correlation structure given by $\langle \eta_i(t)\eta_j(t')\rangle = (\sigma^2/\Delta x^d)\delta(t-t')$. We denote the variance by $\sigma_d^2 = \sigma^2/\Delta x^d$. In the continuum limit $N \to \infty$. We then need to solve a system of infinite number of variables or infinite degrees of freedom coupled to each other.

We are interested in evaluating various moments of v and they can be obtained if we can find an 'effective potential' for this system of equations. To do so, we write the Fokker-Planck equation for the probability density of all the variables, $P(\{v_i\},t)$:

$$\frac{\partial P(\{v_i\},t)}{\partial t} = \sum_i \frac{\partial}{\partial v_i}[-f(v_i) + \frac{D}{\Delta x^2}\sum_{j\in n(i)}(v_j - v_i) + \frac{\sigma_d^2}{2}\frac{\partial}{\partial v_i}g(v_i)^2]P(\{v_i\},t) \tag{3.12}$$

Since we are interested in local moments we integrate the above equation over all variables other than a particular v_i. Using the boundary condition that $P(v_i = \pm\infty, t) = 0$ for all i, we obtain:

$$\frac{\partial P(v_i,t)}{\partial t} = \frac{\partial}{\partial v_i}[-f(v_i) + \frac{D}{\Delta x^2}\sum_{j\in n(i)}(E(v_j|v_i) - v_i) + \frac{\sigma_d^2}{2}\frac{\partial}{\partial v_i}g(v_i)^2]P(v_i,t) \tag{3.13}$$

Note that $P(v_i, t)$ is the marginal distribution since all other variables have been integrated out from the joint distribution and $E(v_j|v_i) = \int dv_j v_j P(v_j|v_i)$ is a conditional expectation value.

Mean field approximation (MFA): The above equation for the probability distribution of v_i couples all the variables due to the occurrence of the conditional expectation value and remains analytically intractable. The mean-field approximation is based on the key approximation making $E(v_j|v_i)$ independent of v_j. It amounts to assuming that the dynamics of the patch i is determined as if it is embedded in an "effective medium" that is homogeneous. Therefore, we have $E(v_j|v_i) = E(v_i) = E(v)$ independent of j. The unknown quantity $E(v_i)$ is determined self-consistently given $P(v_i)$ which depends on $E(v_i)$. The self-consistent mean-field equation is:

$$E(v) = \int v\, P_{mft}(v, E(v))dv \tag{3.14}$$

$$\text{where} \qquad P_{mft}(v) = \frac{1}{\mathcal{N}} \exp\Big[\frac{2}{\sigma_d^2}\int_{v_0}^{v} du \frac{f(u) - \sigma_d^2 g(u)g'(u) - \frac{zD}{(\Delta x^2)}(E(v) - u)}{g(u)^2}\Big] \tag{3.15}$$

$\mathcal{N}$ is the normalization constant and z is the number of nearest neighbors.

Local equilibrium or transient approximation: We make a simple approximation to evaluate the stationary probability distribution without having to solve the self-consistent equations 3.14 and 3.15. We assume that the local stability of equilibrium state (i.e. the stable fixed point of the deterministic nonspatial model) is not affected by the spatial interactions on the time and spatial scales of ecological interest. This is supported by results of previous section that such a local equilibrium or transient approximation holds as long as we are not too close to the threshold determined by the deterministic nonspatial model (see Fig 3.1(a)).

Within this approximation we set $E(v) = v^*(c)$ where $v^*(c)$ is obtained by solving $f(v^*; c) = 0$. The effective potential, defined as $P_{mft}(v) = 1/\mathcal{N} e^{-2U_{mfa}(V;c)/\sigma_d^2}$, can thus be written as:

$$U_{mfa}(V;c) = -\int_{V_0}^{V} du \frac{f(u) - \sigma_d^2 g(u) g'(u) - \frac{zD}{(\Delta x)^2}(v^*(c) - u)}{g(u)^2} \tag{3.16}$$

The results of calculation of effective potential for May's model with diffusion and noise

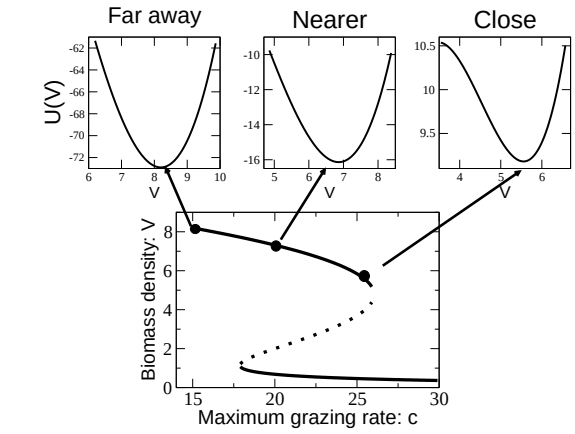

(a)

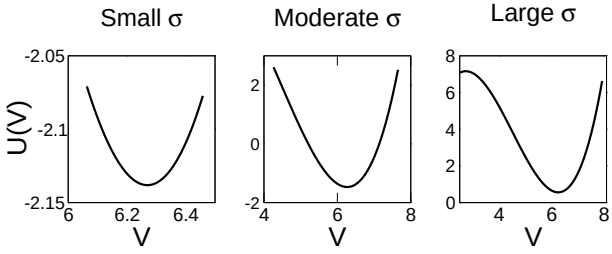

(b)

Figure 3.2: The panels of figures show how the asymmetry in the potential in the landscape picture evolves in the different pathways to regime shifts for a spatially explicit model with diffusion. This is strikingly similar to the ones obtained for the nonspatial model with noise (see Fig. 2.2 in chapter 2)

in the grazing term is shown in Fig 3.2. The qualitative features of the effective potential are strikingly similar to the ones obtained for the nonspatial model with noise (see Fig 2.2 in chapter 2).

We then calculate the moments corresponding to spatial mean, variance and skewness of the effective probability distribution $P_{mfa}(V;c) = 1/\mathcal{N}e^{-2U_{mfa}(V;c)/\sigma_d^2}$ by performing appropriate integrations in the region $R = (x_l, x_r)$ around the stable fixed point v^* such that $v_l = v^* - 2\sigma_d$ and v_r is determined by solving the equation $U_{mfa}(v_r;c) = U_{mfa}(v_l;c)$.

The results are shown along with those of numerical simulations on a two dimensional lattice in Fig 3.3. To numerically solve the Eq. 3.9, we use the fully explicit forward-time, centered-space differencing scheme on a two-dimensional spatial grid of 128×128 squares with periodic boundary conditions, using MATLAB and C++ [113]. For a fixed value of grazing rate c, we let the system evolve up to 100 time units. As the system evolves in time, we take a snapshot of the spatial pattern at regular time intervals and evaluate spatial variance and spatial skewness at each of those individual time steps. The temporal average for 100 time units is plotted. Fig. 3.3 shows that the numerics and the analytical calculations agree qualitatively. They also agree semi-quantitatively when the grazing rate is not too close to the threshold. This is expected because the mean field calculations ignore the spatial fluctuations which dominate the dynamics near a transition leading to increasing discrepancy near the bifurcation point.

3.2.3 Dependence of the results on the strength of spatial interactions

In this section, we study the implications of the strength of spatial interactions on the spatial indicators. The strength of spatial interactions can vary significantly for several reasons. Obvious scenarios include when the ecological systems under consideration are

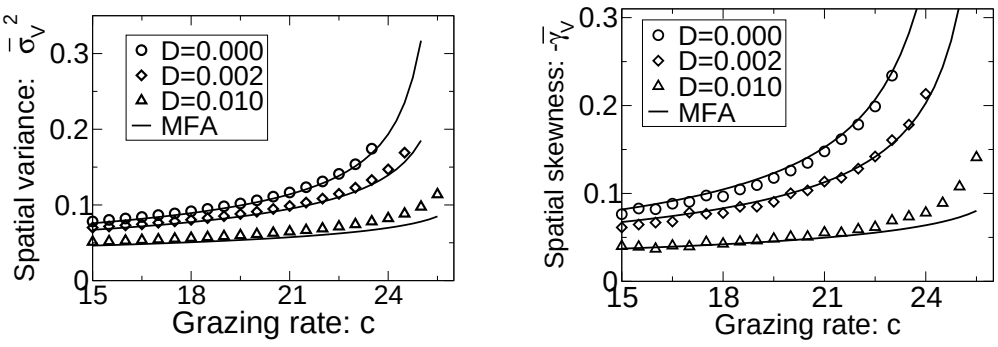

(a) (b)

Figure 3.3: The rising spatial variance and skewness as the threshold of vegetation collapse is approached in model of Eq 3.9. Parameter values are: $r = 10, K = 10, V_c = 1.0, \sigma_d = 1.0, dx = 0.1, dt = 0.001$. The thick line corresponds to analytical result obtained from the mean field approximation.

different or the same ecological system from different geographical regions are considered. It can also arise through a subtler way of "coarse-graining" approximation that a field ecologist (or a modeler) employs while taking and/or analyzing the spatial data. For example, the interactions between two patches of vegetation can be significantly different depending on their dimensions: for e.g., $1m \times 1m, 10m \times 10m$ or $100m \times 100m$.

We treat the diffusion constant D to be a measure of the strength of spatial interaction. As the diffusion constant increases, the patches interact relatively strongly with nearby patches. Fig. 3.3 show that as the strength of the spatial interactions increase, the absolute value of the indicator decreases. However, Fig. 3.4 show that the scaled values of both the variance and the skewness roughly increase at least by a factor of two before the catastrophic vegetation collapse occur.

As we saw in Fig 3.2, the MFA provides us with an effective potential landscape picture for the fully spatial system. We can calculate how effective potential changes as the strength

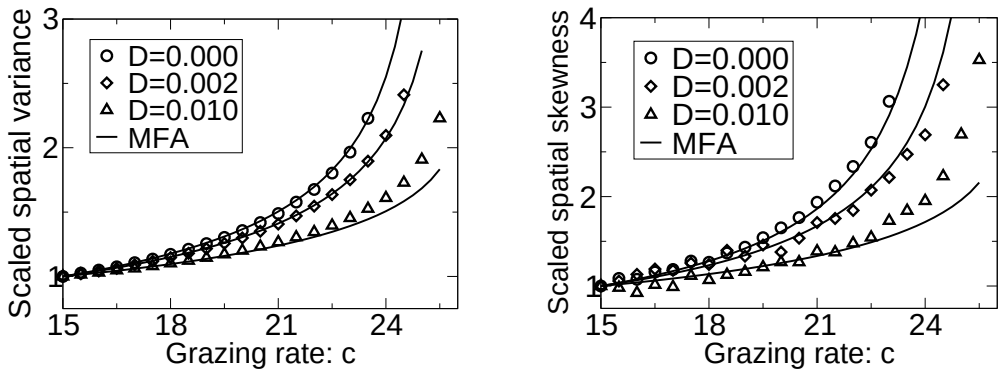

(a) (b)

Figure 3.4: Same as Fig 3.3, but scaled by their respective values at $c = 15$.

of diffusive coupling D increases (see Fig. 3.4): we observe that the local curvature is getting larger (thus reduced variance) and potential is more symmetric (thus reduced skewness) as D increases. This can be intuitively understood by recalling that the basic nature of diffusion is to smoothen the spatial fluctuations. A stronger spatial coupling would hence lead to reduced amplitude of fluctuations (i.e. reduced variance). A reduced fluctuation in turn has the implication that asymmetric part of the effective landscape not fully explored, thus leading to reduced skewness as well.

The results of a single time calculation, a quantity which a field ecologist is most likely to measure, exhibit qualitatively similar behavior. However, the temporal average shown here provides a smooth curve which allowed us to make better comparison with the results obtained for different spatial interactions and with the analytical calculations. See appendix B.1 to see how indicators can vary with time even for fixed grazing if the system is close to the threshold.

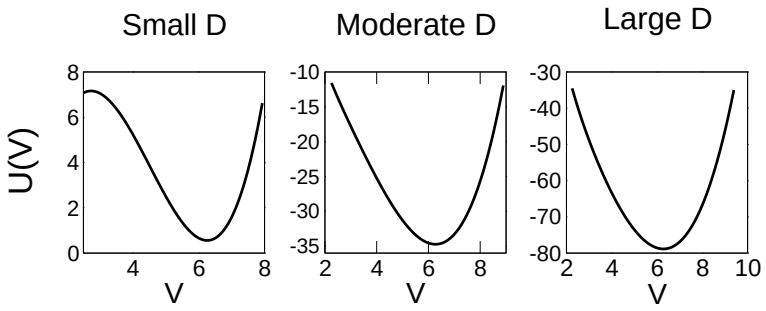

Figure 3.5: Effective potential for the spatially explicit model obtained using the mean-field approximation. The potential is shown around the vegetated fixed point as the diffusion constant increases.

3.2.4 Detection and prevention of an impending regime shift in a numerical experiment

In this section, we show that spatial indicators can be used to detect an impending vegetation collapse even with limited availability of spatial and temporal data by simulating a scenario that is likely to occur in field. We show that a joint monitoring of spatial variance and skewness can be helpful in obtaining an unambiguous measure of an impending catastrophic transition. Furthermore, the warning occurs sufficiently in advance that management practices can be initiated to prevent the undesirable collapse of vegetation.

We have chosen $dx = 0.1$ and $dt = 0.001$ for the simulation of diffusion model (same values were used for results shown in previous section too). We interpret each square grid of the two dimensional lattice to be of the area $100m^2$ and one unit to step to be 1 year. In these units, the time step of integration corresponds to approximately 1/3 of a day for Eq. 3.9. The values of diffusion constants used in this study which range from $D = 0.001$ to 0.1 units correspond approximately to the range $0.03m^2day^{-1}$ to $3m^2day^{-1}$ which covers the typical values of plant dispersal coefficients used in the previous studies [114]. However, we

are coarse graining the system on scales such that the spatial patterns observed in semi-arid regions are not important.

We consider a scenario in which the grazing rate c is increasing with time, a widely observed consequence of enhanced human influence on ecosystems. We begin with a high density vegetated state with the mean grazing rate $c = 21$ which undergoes a discrete increment of 0.1 units (approximately 0.5%) every year. The evolution of spatial patterns is depicted in Fig. 3.9(a). The ecosystem continues in the high vegetation state, albeit slowly declining in its density till the year 46. Within next six years the vegetation undergoes a dramatic collapse to a low density state. During this interval of abrupt collapse, a number of tiny low density patches emerge which are clearly identifiable if the complete spatial data is available at 48th year. These patches grow bigger in size with time and they coalesce with nearby patches leading to rapid decline in vegetated areas.

The abrupt nature of collapse is readily captured in the plot of spatial mean, $\bar{V}$ in Fig 3.9b(i) and the spatial indicators in Fig 3.9b(ii-iii), exhibit substantial changes during the period of transition. The key issue is the ability to predict proximity to a transition and hence the question of interest is whether these indicators show observable changes prior to the obvious collapse shown either by the drop in the spatial mean $\bar{V}$ or the visual observation of patches. In order to answer this question, we have plotted a magnified version of spatial mean, variance and skewness in an adjoining plot from year 40 to 56 (Fig 3.9b(iv-vi)). The spatial mean is decreasing slightly with time up to year 46 and a very small number of patches are visible. On the other hand, the spatial variance has increased by nearly 300% and the skewness has changed from zero to one by this time, therefore offering us two potential early warning signals of an impending transition when the spatial mean does not display a clear sign of the collapse.

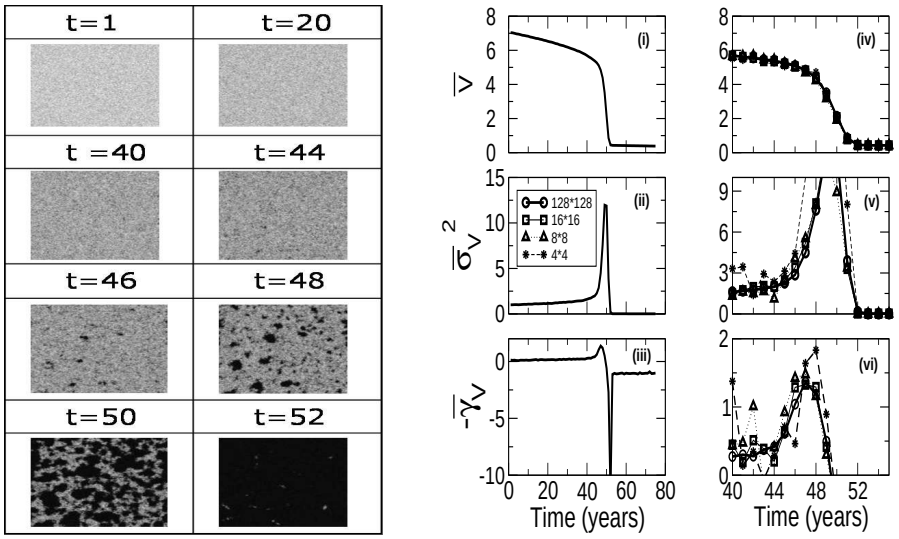

(a) (b)

Figure 3.6: Temporal evolution of the system on a two dimensional lattice with (Eq. 3.9) for a situation simulating increasing grazing rate (of 0.1 units every year) observed in the field. Parameter values are as in earlier figures. (a) Temporal evolution of spatial patterns while the grazing rate increases towards the threshold. The brighter color corresponds to higher vegetation densities. (b) Spatial mean, variance and skewness as a function of time.

Next, we argue that a joint monitoring of spatial variance and skewness can be used deduce an impending transition unambiguously. Results in Fig 3.9b show that spatial skewness peaks at year 47 even as the spatial variance continues to increase and the spatial mean shows quick decline beginning year 48. We suggest that a peak in skewness when observed with a continued increase in variance can constitute an additional signature of an imminent catastrophic vegetation collapse. We performed additional simulations to check if this sign occurs sufficiently early to be utilized for the prevention of the regime shift by beginning to reduce the grazing activity from year 48 The results for different conservation strategies are shown in Fig 3.7. These sample simulations suggest the plausibility of a

maintaining ecosystem in the highly vegetated state if the reduction rate in the grazing activity are beyond a certain threshold.

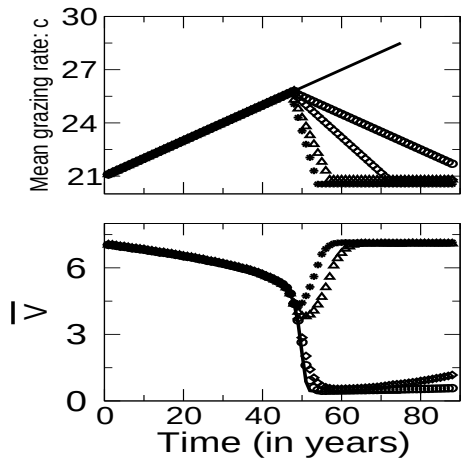

Figure 3.7: This plot demonstrates the plausibility of preventing a catastrophic vegetation collapse. Thick line is "business as usual" with an increase of 0.1 units/yr. For the rest, the reduction in grazing rate is initiated an year after the peak of skewness is observed and they are as follows: circles 0.1 units/yr, diamonds 0.2 units/yr, triangles 0.5 units/yr and stars 0.75 units/yr until they decrease to 21 units/yr.

For ecosystems such as vegetation a high resolution data may be available due to satellite images [115, 116], but it is not difficult to imagine systems such as lakes having only a few ground data collecting stations. To mimic such a scenario, we utilized only a part of the data available from simulation and evaluated the indicators based on sparse data. More specifically, we looked at data collected at grid points separated by 8 sites (hence, a total of 16×16 data points), 16 sites (8×8) and 32 sites (4×4). It is striking that the temporal trends of indicators largely remain unaffected even for as small a data set as 8×8, but at further lower resolutions they may not be statistically significant and this may depend on the diffusion constant (see appendix B.2).

3.2.5 Semianalytic arguments to show peaking of skewness in a bistable model

In this section, we discuss the generality of the result for May's model that skewness shows a peak while the variance is still rising as we approach the bifurcation point. We argue that this feature is not restricted to the specific model by studying the following generic bistable effective potential often used to study phase transitions in physical systems [117, 118]:

$$U(M;h) = M^2(M-1)(M+1) + hM\,. \tag{3.17}$$

When $h = 0$, the potential has two equal minima at $M = \pm 1$ and as h is increased we

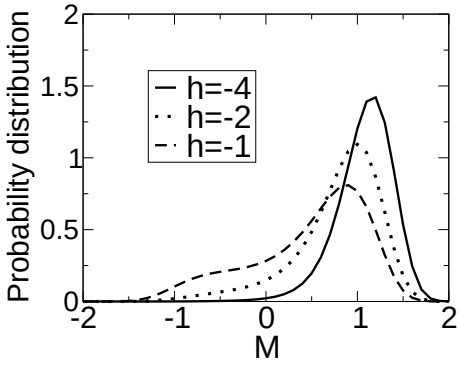

Figure 3.8: The probability distribution for different values of the control parameter value h.

have one stable and one metastable minimum. We study the probability density given by $P(M;h) = (1/\mathcal{N})e^{-U(M;h)}$. As the control parameter h increases from negative values towards 0, the probability density in Fig 3.8 shows a behavior qualitatively similar to that of time evolution of spatial probability density of the vegetation for the dynamic simulations we have performed. If h is varying slowly, within an adiabatic approximation we can treat

the parameter h itself to play the role of time whereas the $P(M;h)$ can be viewed as the instantaneous spatial probability distribution.

For this probability distribution, we evaluate the mean, variance and skewness as a function of the parameter h and show the results in Fig 3.9(i-iii). It is clear from the figure that the peak in skewness occurs even as the variance is increasing and prior to the transition in the state of M.

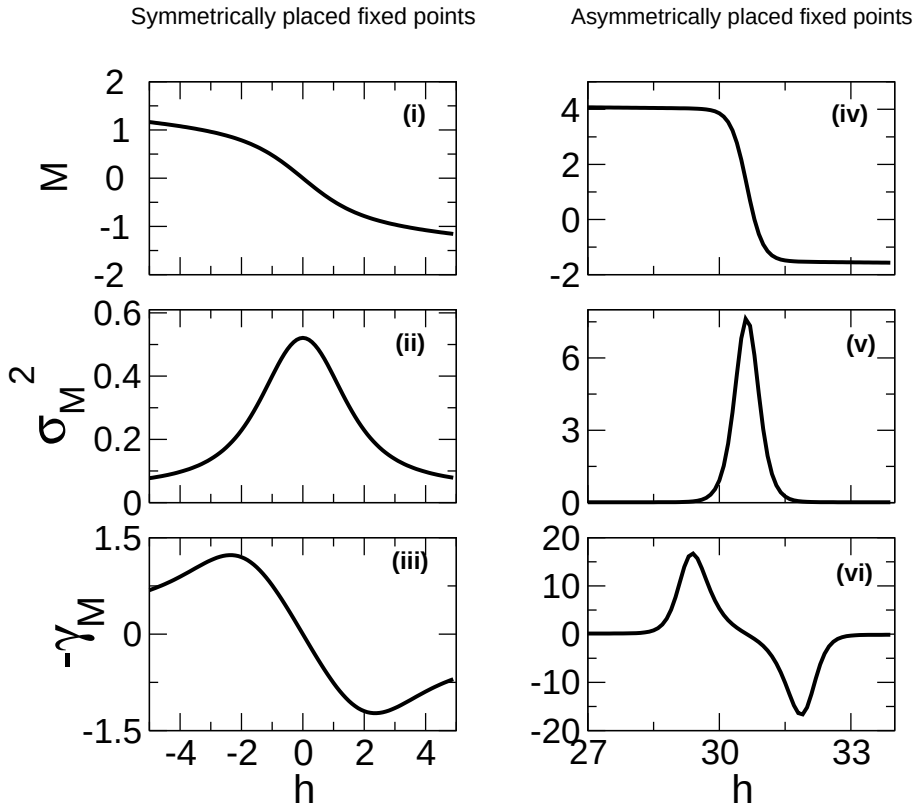

Figure 3.9: Variation of mean, variance and skewness. (i-iii) correspond to the potential function of Eq. 3.17 whereas (iv-vi) correspond to Eq 3.18.

For the bistable potential of Eq 3.17, the two stable states (of $M_s^* \approx +1$ or -1) are nearly symmetrically disposed around the unstable fixed point ($M_u^* = 0$). Next, we choose

a slightly modified bistable potential which resembles the scenario corresponding to May's vegetation model where the two stable states are asymmetrically placed around the unstable fixed point:

$$U(M;h) = M^2(M-6)(M+1) + hM \tag{3.18}$$

The results for the mean, variance and skewness of the probability distribution as the parameter h is varied are shown in Fig 3.9(iv-vi). Clearly, the transition is more abrupt and the skewness peaks much earlier even as the variance continues to increase and the collapse is just about to begin. In these calculations the only important criterion used in the constructing the potential was that it has to be bistable. Thus we believe that our suggestion to study correlations between two indicators can be applicable to different ecological systems.

3.3 Indicators in stochastic partial integro-differential model

Diffusion approximation for the seed dispersal, or more generally the spatial interaction kernel is often considered an oversimplification of representing the complex processes involved in the ecological systems. Several empirical and theoretical studies demonstrate the inadequacy of short ranged dispersal in determining the dynamics of populations, communities and ecosystems [119, 120, 121, 122, 123]. Therefore, we include the spatial interactions arising from the dispersal of seeds from the position y to x through different dispersal kernels $k(x,y)$ in a continuous one dimensional space. The resulting spatially explicit model is a stochastic partial integro-differential equation:

$$\frac{\partial V(x,t)}{\partial t} = rV\left(1-\frac{V}{V_c}\right) - (c+\eta(x,t))\frac{V^2}{V^2+V_0^2} + \int_\Omega k(x,y)[V(y,t)-V(x,t)]dy \tag{3.19}$$

where the prefactor of the kernel term contains a time scale which we have set to unity. The spatial interactions determine how the vegetation interacts with the surroundings and

spreads in space. We assume that the spatial habitat is homogeneous, the interactions are isotropic and depend only on the relative distance between the plant (at x) and the spatial region of interest (at y), *i.e.* $k(x,y) = k(|y-x|)$. We refer to $k(y)$ as the dispersal kernel and this is analogous to the dispersal kernel that is usually referred to in spatially explicit models of population dynamics based on integro-difference equations, for e.g. see [119]. The kernel $k(y)$ in our model has units of 1/length.

We assume that the kernel is always nonnegative and $\int_\Omega k(y)dy = 1$ where Ω is the spatial region over which the dispersal occurs: this normalization condition implies that the seed from the parent tree falls within the spatial region Ω. With these characteristics of the kernel, the spatial interaction term in Eq 3.19 leads to an increase in the growth rate when the local vegetation density is lower than the neighbors or a decrease in the growth rate if the local density is higher. In other words, the spatial kernels of the form assumed tend to make the vegetation density uniform.

3.3.1 Mean field approximation (MFA)

The calculations of mean-field approximation shown for the diffusion approximation can be easily extended to the case of a kernel. We have shown that the self-consistent equations for the mean-field approximation are:

$$E(v) = \int v\, P_{mft}(v, E(v))dv \tag{3.20}$$

$$\text{where} \qquad P_{mft}(v) = \frac{1}{\mathcal{N}} \exp\Big[\frac{2}{\sigma_d^2}\int_{v_0}^{v} du \frac{f(u) - \sigma_d^2 g(u)g'(u) - (1-k_0)(E(v)-u)}{g(u)^2}\Big] \tag{3.21}$$

where $k_0 = k(0)(\Delta x)^d$, $\mathcal{N}$ is the normalization constant and we have used the condition for the kernel $\sum_{j\in\Omega} k_{ij}(\Delta x)^d = 1$. The expression for the steady state probability was found by setting $\frac{\partial P(v_i,t)}{\partial t} = 0$ in Eq 3.13.

In the continuum limit, $\Delta x \to 0$ and hence $k_0 = 0$. A striking feature of this result is that the expression for the steady state density is independent of the spatial kernel within MFA. The effective potential can then be defined by:

$$U_{mfa}(V;c) = -\int_{V_0}^{V} du \frac{f(u) - \sigma_d^2 g(u) g'(u) - (v^*(c) - u)}{g(u)^2} \tag{3.22}$$

For the purpose of numerical simulations, we explicitly consider four dispersal kernels that have been commonly employed to study population dynamics and studies of invasive species. They are Gaussian, exponential, fat-tailed and heavily fat-tailed Cauchy or Lorentzian function [119]. A general feature of these kernels is that the effect of nearby neighbors is greater than that of the distant ones; but they differ in their characteristics in the tails *i.e.,* the range over which the seed dispersal occurs.

Table 3.1: Redistribution kernels and their properties

Name	k(x)	Moments	$\tilde{k}(s)$ (Generating function)
Gaussian	$\frac{1}{\sqrt{2\pi\sigma^2}} e^{-\frac{x^2}{2\sigma^2}}$	$k_2 = \sigma^2$, $k_4 = 3\sigma^4$	$e^{\frac{\sigma^2 s^2}{2}}$
Exponential	$\frac{1}{2\theta} e^{-\lvert x\rvert/\theta}$	$k_2 = 2\theta^2$, $k_4 = 24\theta^4$	$(1-\theta^2 s^2)^{-1}$
Fat tailed	$\frac{1}{4\alpha} e^{-\sqrt{\lvert x\rvert/\alpha}}$	$k_2 = 5!\alpha^2$, $k_4 = 9!\alpha^4$	Does not exist
Heavily fat-tailed	$\frac{1}{\pi}\frac{\beta}{\beta^2+x^2}$	Does not exist	Does not exist

3.3.2 Semianalytic arguments for spatial indicators

Before we move onto discussing results of numerical simulations, we show the power spectra, $S(q,\omega)$, which can be calculated for the case of generic kernel as we did for the

diffusion model. The steady state spatial power spectrum can then be obtained as:

$$S(q) \equiv \int_{-\infty}^{\infty} \langle |\tilde{v}(q,\omega)|^2 \rangle \frac{d\omega}{2\pi} = \frac{\sigma^2/2}{\alpha + (1 - K(q))} \tag{3.23}$$

As the system approaches bifurcation, *i.e.* α decreases in magnitude and therefore the denominator of the spectral function decreases for all values of the wave vector q. In particular, spatial fluctuations on large length scales given by $S(q = 0) = \sigma^2/(2\alpha)$ increases when the system approaches the threshold of a regime shift. Moreover, the spatio-temporal variance $\sigma_V^2 = \int S(q)dq$ which includes contributions from all q, increases as α decreases in magnitude.

Next we turn our attention to spatial skewness for which we need to include the nonlinear terms in analyzing the dynamics of perturbation from the equilibrium to obtain:

$$\frac{\partial v(x,t)}{\partial t} = -\alpha v(x,t) + \beta v^2(x,t) + \int_{\Omega} k(y-x)[v(y,t) - v(x,t)]dy + \eta(x,t) \tag{3.24}$$

where $\beta = f''(V^*, c)/2! > 0$. Using Fourier analysis as shown above in the linear problem the is difficult. Here we spatially discretize this system, write a Fokker-Planck equation and obtain the 'effective potential' uisng the mean-field and local equilibrium approximations described in Appendices C and D, but with an additive noise (i.e., $g(u) = 1$). The resulting expression for the effective potential is:

$$U_{mfa}(v) = \frac{\alpha + 1}{2} v^2 - \frac{\beta}{3} v^2 \tag{3.25}$$

This potential goes to negative infinity and hence in the spirit of the local equilibrium approximation we are interested only in the interval $(-v_m, v_m)$ where $v_m = (\alpha + 1)/\beta$. We can then calculate the moments (spatial mean, variance and skewness) of the effective probability distribution $P_{mfa}(V; c) = 1/\mathcal{N} e^{-2U_{mfa}(V;c)/\sigma_d^2}$ by performing integrations around the stable fixed point v^* such that $v_l = v^* - 2\sigma_d > -v_m$ and v_r is determined by solving the

equation $U_{mfa}(v_r; c) = U_{mfa}(v_l; c)$. As we approach the bifurcation $\alpha \to 0$ and the cubic nonlinear term dominates the potential leading to an increasing magnitude of the skewness.

3.3.3 Numerical calculations and comparison with results of MFA

The spatially extended system of Eq 3.19 under different dispersal kernels is solved numerically on a one dimensional lattice of size $N = 16384$ with periodic boundary conditions. We employ Ito calculus and the equation is discretized using an Euler forward time scheme which is first order accurate in time when averaged over many realizations or $\sqrt{dt}$ accurate for a single simulation. The spatial discretization used to calculate the dispersal integral follows differencing scheme which is first order accurate. The time required for the computation can grow proportional to N^2 owing to the dispersal term which is an integral over the complete spatial domain and hence, the method is computationally expensive. The computation cost of evaluation of this term is reduced by the following approximation. We evaluate a cutoff distance such that 95% of the dispersal occurs within this range and renormalize the kernel to unity. We then perform the integration of dispersal term only within this range from the source tree. Introducing this cutoff improves the computational efficiency tremendously since the time required for the computation now grows linearly with lattice size. Comparison with analytical results confirms that such a cut-off approximation doesn't affect the qualitative nature of the results obtained.

For each simulation, the value of grazing rate c is held constant. As the system evolves in time, we take a snapshot of the spatial pattern at regular time intervals and evaluate spatial variance and spatial skewness at each of those individual time steps. The average of those indicators is then calculated in one dimension and shown for different kernels as

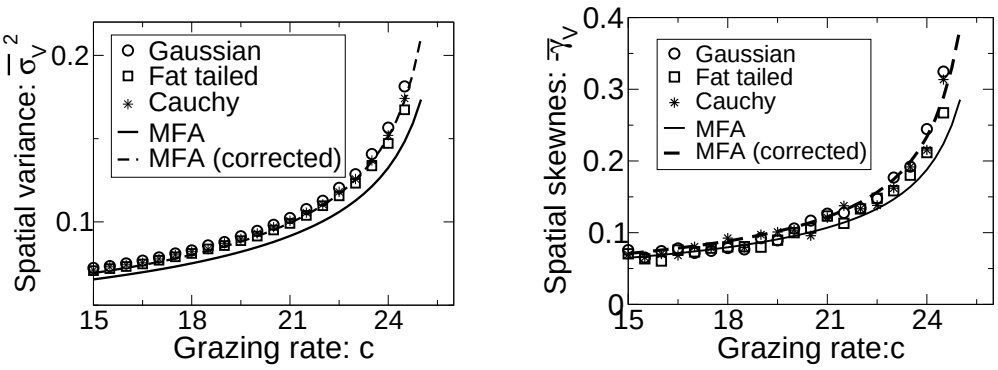

(a) (b)

Figure 3.10: Results of spatial indicators for integro-differential model. Comparison between results of mean field approximation and the numerical simulations of Eq 3.19

a function of grazing rate in Fig 3.10. Both the spatial variance and the spatial skewness increase as the grazing rate approaches the threshold at $c^* = 26$.

The results are of numerical simulations are clearly independent of the details of the kernel used, in agreement with the prediction of MFA and holds true independent of dimension. More specifically, the results of this analytical approximation obtained for spatial indicators shown in Fig 3.10(a-b) (thick line) are in semi-quantitative agreement with the results of numerical simulations in one dimension. Small deviations (of the order of 10%) found between results of the different kernels and from the mean-field conclusions are due to discretization of the space in the numerical simulations. This correction which depends on the kernel under study can be included in the mean-field-analysis which further improves the match between analytical and numerical results (up to 2%: dotted line in Fig 3.10(a-b)).

3.4 Discussion

The study of spatially explicit models to study regime shifts is important because the dynamics of the transition from the metastable state to the stable state depends on the spatial degrees of freedom [117, 118]. For example, the mechanism of nucleation of a droplet or patch of the other phase in an initially homogeneous phased and its subsequent growth leading to the transition is absent in an aspatial model [124, 125]. Our study of a spatially explicit model of a bistable ecological system has shown that an increase in spatial variance and the spatial skewness in the snapshot of the ecological system are leading indicators of impending regime shifts. Although spatial coupling tends to make the spatial distribution of the variable more homogeneous and hence, narrower, we show that scaled spatial variances and skewness are clearly observable and can serve as leading indicators of regime shift. We showed that a novel feature that an observation of an increasing spatial variance together the reversal in the initial changing trend (i.e., a peak) in the spatial skewness is a nonrelative measure of proximity to an impending catastrophic regime shift. We comment on various features of spatial indicators along with their limitations below.

Catastrophic transitions occur in wide array of aquatic, terrestrial, region climatic as well as complex socio-economic systems [9, 57]. It is obvious that the scale of interactions can vary significantly between, and even within any of these complex systems. The spread of nutrients or algae in lake is driven by local mixing (diffusion) for short time scales; but a complex hydrodynamics or an unexpected storm can lead to an occasional longer ranged mixing. Empirical data on animals and seeds indicate that their dispersal can be strongly leptokurtic, i.e., the concentration of dispersal at the source and the tails is larger than what a Gaussian dispersal with comparable mean and variance would predict [119, 120, 121]. Theoretical studies show that even infrequent long range dispersal

can disproportionately influence the structure of the population, community and ecosystems [119, 122, 123]. Clearly, a reaction diffusion equation would be an oversimplification to model the spatial processes of such systems. For the purpose of detecting an impending regime shift, we have shown that spatial indicators proposed in this paper are insensitive to the details of the specific dispersal kernel and thus they can be applied to wide range of spatial ecological systems where abrupt flips between alternative stable states can occur.

We argue that, in comparison to nonspatial indicators [93, 126] the spatial indicators can provide a more reliable warning signal of a regime shift even for substantially shorter time scales of observation. We note that the values of non-spatial indicators such as variance and skewness, calculated as moving averages, reflect the state of the system over the entire interval over which the moving average was calculated. This can potentially underestimate the actual proximity to a threshold. On the other hand, to evaluate the spatial indicators, we look at the instantaneous spatial pattern that provides a more accurate measure of the state of the system at that time.

Next, for the calculations corresponding to Fig 3.6, we find that the nonspatial indicators cannot provide an early warning signal in more than 65% of the simulations even at higher temporal resolution (10 times) of data collection. When we slowed down the rate of approach to the threshold by a factor of ten and reduced the external noise fluctuations by a factor of two, the results were better with at least one of the indicators exhibiting early warning in 50% of the cases. However, we never observed any clear peaking of moving average skewness along with increasing variance as suggested by the study of the spatially extended data. Since all ecological systems are spatially extended and the nonspatial indicators can be referred to as 'one point indicators' since they take measurements at only one spatial point (Appendix B.3). On the other hand, calculations of mean escape time to

an alternative state show that the nonspatial models, often used by a ecosystem modelers, can lead to transitions more frequently. Our numerical simulations (Appendix B.3) and the mean-field approximation of the spatial model show that the spatial fluctuations are reduced due to smoothing effects of a kernel and hence one should use a renormalized value for the external fluctuations when modeling an ecosystem without space.

Spatial variance is considered an important quantity to understand ecological patterns [127, 128] and has been measured in the contexts such as populations and abundance of species [129, 130, 131]. Availability of remotely sensed data for semi-arid vegetation systems provides an excellent candidate ecosystem to test the aspects of measurability and applicability of indicators suggested in our work [116, 115, 132]. However, few cautionary remarks regarding the application of these indicators are needed. In our calculations we have always plotted the negative of skewness which increases as we approach the proximity of the threshold. More generally, it is the change in skewness from zero to negative, negative to positive and so on) which needs to be interpreted as an early warning signal [126]. There are several sources of errors associated with the ecological variable as well as measurement of ecological data. Limited spatial data availability can render the evaluations of indicators inaccurate. We refer reader to recently published literature on issues related to real field applications of indicators([93, 94, 126, 133]; also Appendix B.2). We wish to emphasize that monitoring multiple indicators of regime shift in any field applications can lead to greater confidence in our results.

We have made several simplifying assumptions in our model calculations. We have made semianalytic arguments that suggest that the main features we have observed continue to hold provided the qualitative features of bifurcation diagram of the nonspatial model calculated using an effective potential approximation remain unaltered. We have checked

that this holds true for our model if we include noise in the growth rate r. The possibility of spatially and temporally correlated noise in grazing rates may have to be considered. One way of including this is by altering the coarse-graining length and time scales and the scales of observation. This warrants further study with specific assumptions on the correlations. Next, we have ignored the spatial heterogeneity which can be very important depending on the scale of interest [39, 56, 134, 135]. Studies on phase transition from liquid to solid/crystalline phase of ice in the physics literature show that heterogeneity plays a key catalytic role in initiating the nucleation: a step in which the first crystal of ice forms triggering a process of relatively quick transition thereafter [117, 118]. Analogous situations can occur in ecological systems and the potential of direct observation of growth of bare patches, for example, as a candidate for early warning signal in such scenarios needs further investigation. Many variable models with space can nontrivially alter the stability of spatially uniform state leading to spatial patterns and they can be used as fingerprints of an impending regime shift as suggested from studies of models on vegetation patterns of semi-arid ecosystems [12, 13, 115]. Applicability of the simple indicators suggested in this study in such scenarios needs further study.

CHAPTER 4

SELF-ORGANIZATION AND PRODUCTIVITY IN SEMI-ARID ECOSYSTEMS: IMPLICATIONS OF SEASONALITY IN RAINFALL

4.1 Motivation

Seasonality, despite being an obvious and most significant source of external variability, has been studied only in selected few systems such as population dynamics and spread of infectious diseases, but only in nonspatial context [47, 100, 136, 137, 138, 139, 140, 141, 142, 143]. Vegetation in semi-arid regions is driven by a strongly *seasonal* rainfall. They show striking self-organizing patterns such as gaps, labyrinths, spots and bands. A picture from Google Earth is shown in Fig. 4.1. We had ignored these factors in previous chapters where the focus was on developing the indicators for regime shift. In this chapter, we turn our attention to the spatial and temporal scales in which the spatial patterns as well as the seasonality in the driving parameter are relevant. We begin by introducing a spatially extended model of pattern formation in these systems. This will be followed by a detailed study of impact of seasonality in rainfall on the ecosystem patterns and productivity. The main aim of this study is to understand the dynamics of the self-organizing ecosystems when driven by a seasonal parameter. The work is published in *Journal of Theoretical Biology* [144].

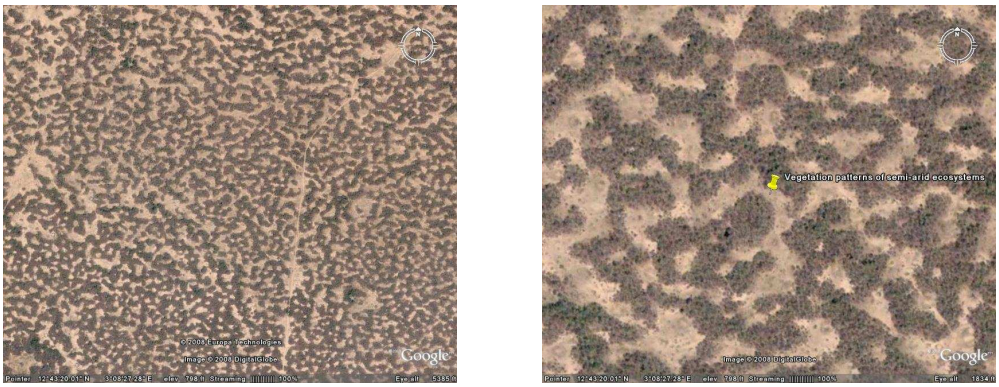

(a) (b)

Figure 4.1: Patterns of vegetation from Niger (Africa), $12^0 43'$N, $3^0 08'$E. Length scale corresponds to (a) 1 mile (b) 400m (East to West or North to South). Credit Google Earth. Accessed on March 17th 2008.

4.2 A model for pattern formation in semi-arid vegetation

A number of models have been developed which produce the observed patterns of vegetation in semi-arid regions. They are based on cellular automata, partial differential equations (one and multi variable models) and integro-differential equations [13, 114, 115, 145, 146, 147, 148, 149, 150, 151, 152, 153, 154]. Most of these studies agree on the key role played by the positive feedback between water and vegetation. However, they differ in details such as precise mechanism leading to positive feedback and how it is incorporated in mathematical models. For our study, we consider a model based on the partial differential equations which gives raise to regular spatial patterns for part of the parameter region based on Turing mechanism. More specifically, we adopt a model developed by Hillerislambers, et al [114, 155] which assumes that water infiltrates better into vegetated regions leading to a net flow of water towards them. The model describes the dynamics of three

coupled variables: the plant biomass, P, soil water, W, and surface water, O driven by uniform rainfall R throughout the year. The time evolution of our model is determined by the following partial differential equations:

$$\frac{\partial O}{\partial t} = R - \alpha O \frac{P + W_0 k_2}{P + k_2} + D_o \nabla^2 O \tag{4.1}$$

$$\frac{\partial W}{\partial t} = \alpha O \frac{P + W_0 k_2}{P + k_2} - g_{max} \frac{W}{W + k_1} P - r_w W + D_w \nabla^2 W \tag{4.2}$$

$$\frac{\partial P}{\partial t} = \left(c g_{max} \frac{W}{W + k_1} - d \right) P + D_p \nabla^2 P \tag{4.3}$$

A brief description of biophysical interpretation of various terms in the model is presented below. The surface water O increases according to the rainfall, R, and decreases due to (vertical) water infiltration that is an increasing but saturating function of the local plant density, P reaching a maximum value of α. The soil water W increases due to surface water infiltration and decreases due to uptake by plants (up to a maximum rate of g_{max}) and evaporation at a rate of r_w. The plants exhibit saturated growth from water intake (with a conversion factor c) and there is a simple decay due to mortality or herbivory (at a rate d). k_1 is value of soil water density at which the water uptake by plants is half maximum and k_2 is a plant density scale that determines how surface water infiltration increases with P. To perform a stability analysis, we rescale various parameters and obtain the non-dimensionalized version of the model:

$$\frac{c g_{max}}{\alpha} \frac{\partial O_s}{\partial \tau} = R_s - O_s \frac{P_s + W_0}{P_s + 1} + \nabla_s^2 O_s \tag{4.4}$$

$$\frac{\partial W_s}{\partial \tau} = O_s \frac{P_s + W_0}{P_s + 1} - \frac{W_s}{W_s + 1} k P_s - r W_s + D_{ws} \nabla_s^2 W_s \tag{4.5}$$

$$\frac{\partial P_s}{\partial \tau} = \left(\frac{W_s}{W_s + 1} - d_s \right) P_s + D_{ps} \nabla_s^2 P_s \tag{4.6}$$

where we have chosen $\tau = tcg_{max}$, $x_s = x\sqrt{D_o/\alpha}$, $P_s = P/k_2$, $W_s = W/k_1$, $O_s = O\alpha/(k_1 cg_{max})$, $R_s = R/(k_1 cg_{max})$, $k = k_2/(k_1 c)$, $r = r_w/(ck_1)$, $d_s = d/(cg_{gmax})$, $D_{ws} = D_w\alpha/(D_o cg_{max})$ and $D_{ps} = D_p\alpha/(D_o cg_{max})$.

The mean-field version of this model (i.e., with all the diffusion coefficients set to zero) has two equilibria. The bare state equilibrium is given by:

$$P_s^b = 0 \qquad W_s^b = R_s/r \qquad O_s^b = R_s/W_0. \tag{4.7}$$

The vegetated state equilibrium is given by:

$$P_s^v = \frac{R_s - rW_s^v}{kd_s} \qquad W_s^v = \frac{d_s}{1-d_s} \qquad O_s^v = R_s\frac{P_s^v + 1}{P_s^v + W_0} \tag{4.8}$$

Next, we perform a stability analysis of both mean-field and spatially extended models. Spatial analysis requires that we introduce a spatially heterogeneous perturbation and find out if the homogeneous state is unstable to any one such perturbation (also known as *Turing* analysis). We adopt a simpler notation of $\partial P(x,t)/\partial t = f^p(P,W,O) + D_{po}\nabla^2 P$ and so on. Small perturbation of the type $\delta O(x,t) = \delta O(t)e^{iqx}$, from the fixed point (upto linear order) obeys:

$$\frac{d}{dt}\begin{pmatrix} \delta O \\ \delta W \\ \delta P \end{pmatrix} = \begin{pmatrix} f_o^o - q^2 & f_w^o & f_p^o \\ f_o^w & f_w^w - D_{ws}q^2 & f_p^w \\ f_o^p & f_w^p & f_p^p - D_{ps}q^2 \end{pmatrix}\begin{pmatrix} \delta O \\ \delta W \\ \delta P \end{pmatrix} \tag{4.9}$$

$$= J_q \begin{pmatrix} \delta O \\ \delta W \\ \delta P \end{pmatrix} \tag{4.10}$$

where $f_o^o = \partial f^o(O,W,P)/\partial O$ and so on. We now make a quasi-static approximation which simplifies the problem: the surface water dynamics occurs on time scales much faster than soil water and plant growth dynamics. Hence, we set $\partial\delta O/\partial t = 0$ leading to:

$$\delta O = \frac{f_w^o \delta W + f_p^o \delta P}{q^2 - f_o^o} \tag{4.11}$$

Substituting this in Eq. 4.9 leads to:

$$\frac{d}{dt}\begin{pmatrix}\delta W\\ \delta P\end{pmatrix} = \begin{pmatrix}\frac{f_w^o}{q^2-f_o^o}f_o^w + f_w^w - D_{ws}q^2 & \frac{f_p^o}{q^2-f_o^o}f_o^w + f_p^w\\ \frac{f_w^o}{q^2-f_o^o}f_o^p + f_w^p & \frac{f_p^o}{q^2-f_o^o}f_o^p + f_p^p - D_{ps}q^2\end{pmatrix}\begin{pmatrix}\delta W\\ \delta P\end{pmatrix} \tag{4.12}$$

$$= J_q^{red}\begin{pmatrix}\delta W\\ \delta P\end{pmatrix} \tag{4.13}$$

With the quasi-static approximation, we have effectively reduced the system of three coupled variables to a two variable problem.

We now impose the stability conditions on this reduced system. For the stability of the mean-field or spatially homogeneous solutions, the eigenvalues of the Jacobian matrix $J(q=0)$ must be negative. This requires that $Tr[J^{red}(q=0)] < 0$, $Det[J^{red}(q=0)] > 0$ when evaluated at the stable fixed points. The resulting conditions for the bare state is:

$$\frac{W_s^b}{W_s^b+1} < d_s \qquad \frac{W_s^b}{W_s^b+1} < d_s + r \tag{4.14}$$

Clearly, the second condition is redundant. This condition simplifies to $R_s < rd_s/(1-d_s)$ for the stability of bare state. In other words, the bifurcation occurs at $R_{sc} = rd_s/(1-d_s)$ and for the parameters chosen in this work its 1 $mm\,d^{-1}$ (note that R_c is in the original unscaled units).

Our interest is in checking if this system has Turing instability, *i.e.,* if there exists a q vector such that either or both of the $Tr[J^{red}(q)] < 0$, $Det[J^{red}(q)] > 0$ is violated when evaluated at the fixed point. It is easy to check that the stability conditions hold given the Eq 4.14. In other words, the bare state is not unstable to any small spatially heterogeneous perturbations.

Similar calculations yield mean-field stability criteria for the vegetated state to be:

$$-\Big(r + k\frac{P_s^v}{(1+W_s^v)^2}\Big) < 0 \qquad d_s\frac{P_s^v}{(1+W_s^v)^2} > 0 \tag{4.15}$$

which are satisfied if $R_s > rW_s^v$ or $R > R_c = 1mm\,d^{-1}$. A similar analysis on the reduced Jacobian shows that the vegetated state is unstable to a q mode perturbation satisfying:

$$D(q^2) = D_{ps}q^2(kf_w^o + r + D_{ws}q^2) - (f_p^w + \frac{f_p^o}{q^2 - f_o^o}f_o^w)f_w^o < 0 \tag{4.16}$$

The expressions for various elements of the Jacobian matrices are provided in the Appendix C.1. We plot (not shown) the function $D(q^2)$ numerically and find that when $1 < R < 1.29$, there exists q modes for which the function $D(q^2)$ is negative, thus leading to Turing instability. This expression however, does not provide any useful insights on the ecological interpretation of the conditions required. However, we can device a simpler two variable model (for example, based on the two variable model presented in the Chapter 2) and we find that the Turing instability occurs when $D_p/D_w \ll 1$: i.e., the plant (seed) dispersal should occur on much smaller spatial scales (or larger time scales) compared to the motion of water.

Fig 4.2 shows the spatial patterns obtained from the model simulations along with the mean-field bifurcation diagram. As the rainfall reduces, one finds gaps, labyrinths and spotted vegetation patterns. In addition the figure reveals a striking feature: for $R < R_c = 1mm\,d^{-1}$ the spatial patterns continue to appear even though our analysis shows spatially homogeneous bare state is stable. These patterns are occur due to (non-Turing) nonlinear instabilities. Numerical numerical simulations show that small spatially heterogeneous perturbations on the bare state does not lead to patterns where as large perturbations for which nonlinear effects can be prominent often lead to spatial patterns as shown in the figure.

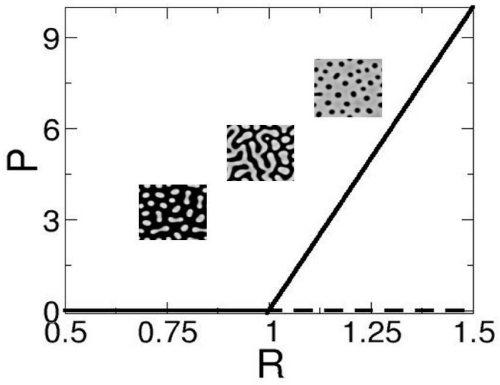

Figure 4.2: Bifurcation diagram for the model Eq 4.1 with:$c = 10, g_{max} = 0.05, k_1 = 5, k_2 = 5, r_w = 0.2, W_0 = 0.2, \alpha = 0.2, d = 0.25, D_p = 0.1, D_w = 0.1, D_o = 100, N = 256 \times 256$ and $dx = 1$. For spotted patterns, R=0.75. For Labyrinths, R=1.00. For gapped patterns, $R = 1.25$.

4.3 The modified model including adaptive nature of plants

In this section, we present a modified version of the above model with which we study the role of seasonality in rainfall on the spatial patterns and productivity. Typically, different models that produce these patterns assume that the rainfall is uniform throughout the year [114, 145, 146, 148, 149, 150]. If one introduces a dry season into this model, the low productivity leads to a bare state: any pre-existing vegetation pattern decays to a bare state rapidly within a time scale of a month (for the parameters used in their paper) of the start of the dry season; the vegetation is unable to recover even if the dry season is followed by a wet season with very good rainfall. Dry seasons in most arid regions last much longer than a month and nevertheless, the productivity is sufficient to yield vegetation patterns similar to those found in the models.

The key feature that we incorporate into the model is the seasonal variation of plant growth rates due to the adaptation of plants to the dry and wet seasons. In nature, as the seasons change, various physical factors affecting the vegetation growth can also be expected to change. For instance, in the dry season the rates of evaporation of surface and soil water are higher than in the wet season. This results in rapid loss of surface water and soil water available for plant growth. Physiology is found to play an important role in the context of aquatic vegetation having alternative stable attractors [47, 100]. In arid regions, it is well-known that xerophytes (plants adapted to arid conditions) exhibit water stress tolerance and display various adaptive features that enable them to survive the extended dry season. Morphological and physiological changes can occur down to the cellular level to adapt to the water stress. Primarily, during dry spells, plants exhibit a significantly decreased growth rate [156]. The plants can decrease the amount of transpiration by shedding or rolling of leaves [157, 158] and reducing the stomatal apertures that also serves to decrease carbon assimilation. In essence, therefore, the plants exhibit seasonal dormancy entering into an anabiotic state or becoming metabolically less active in the absence of water [156, 157, 158, 159]. These seasonal changes in the attributes of plants enable them to survive during the long spells of hot and dry seasons.

The modified model with the seasonal rainfall $R(t)$ is given by:

$$\frac{\partial O}{\partial t} = R(t) - \alpha O \frac{P + W_0 k_2}{P + k_2} + D_o \nabla^2 O \tag{4.17}$$

$$\frac{\partial W}{\partial t} = \alpha O \frac{P + W_0 k_2}{P + k_2} - g_{max} \frac{W}{W + k_1} P - r_w W + D_w \nabla^2 W \tag{4.18}$$

$$\frac{\partial P}{\partial t} = \frac{1}{\tau_p(W)} \left(c g_{max} \frac{W}{W + k_1} - d \right) P + D_p \nabla^2 P \tag{4.19}$$

$$\frac{1}{\tau_p(W)} = \frac{1}{4} \frac{W^2 + f k_3^2}{W^2 + k_3^2} \tag{4.20}$$

The key difference with the original model is the introduction of the adaptation term $\tau_p(W)$. This model with R constant in time and the coefficient $\tau_p(W)^{-1}$ set to unity, is the model studied by [114] and [155] (apart from the changes in the values in some of the parameters we have introduced). Note that we have now reverted back to the original unscaled system of equations.

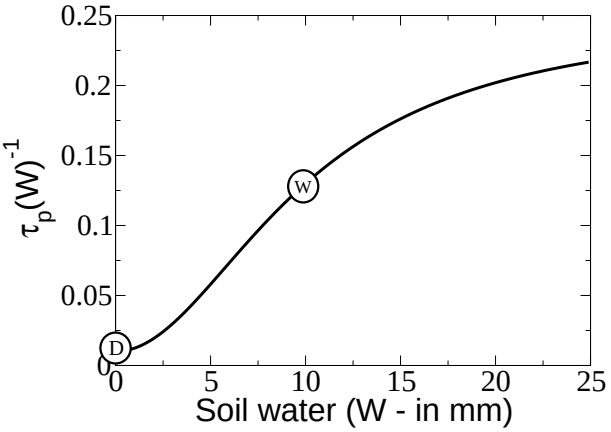

Figure 4.3: Soil water dependent or seasonal adaptation term $\tau_p(W)^{-1}$. This modulates the growth and decay of plants depending on soil water availability. The markers D and W indicate typical value of this adaptation term during dry and wet seasons, respectively.

We numerically study this model in the presence of seasonal rainfall, $R(t)$ chosen as follows: the total number of days in a year is fixed to be $N = 350$, the wet season is assumed to last N_w consecutive days with the rest of the $N - N_w$ days constituting the dry season in a year. The rainfall R is assumed to be constant during the entire wet season, and therefore, R is given by PPT/N_w during the wet season where PPT is the total annual precipitation and is zero during the dry season (R as a function of time is a square wave). We study the model both for the mean field version (with all the diffusion coefficients set to zero) and the spatially extended version, as a function of the total annual precipitation,

PPT and the number of wet days, N_w. Having a more realistic model of rainfall events, such as a Poisson process, is not expected to change the qualitative nature of our results. When intense rainfall events occur as N_w is decreased, we expect the amount of water that infiltrates the soil to be limited by runoff of the water from the region of interest. While this is a complex process we will model it as follows: the amount of water available for infiltration increases linearly with R up to a critical value R_{rc} and saturates at R_{rc} for larger values of R. We chose $R_{rc} = 10mm\,day^{-1}$ for the mean field model and $R_{rc} = 3.25mm\,day^{-1}$ for the spatially extended model.

We discuss the new soil-water dependent term $\tau_p(W)^{-1}$ in the equation for plant growth (Eqs. 4.19-4.20) It determines the time scale on which the *local* plant dynamics occurs. The key ecological consequence of the form of the function chosen is that the dynamics of the plant growth is considerably slower in the absence of soil water while normal growth rate occurs when there is good soil moisture (see Fig. 4.3). We note that this time scale affects both the growth rate and the mortality rate. The mortality term, represented by $-dP$ in Eq. 4.19, describes both natural mortality and plant loss due to herbivory; it is reasonable to modulate this term even in the case of herbivory since plants show seasonal adaptation to avoid grazing [156, 157]. Seasonal variations can also occur in other parameters such as the rate of evaporation of water. We neglect these in our study since their inclusion does not alter the basic qualitative conclusions that we present below.

Another difference in comparison to the original model of [155] is that we choose the parameters so that the critical value of R at which the mean-field bare state becomes unstable at a transcritical bifurcation occurs at $R_c = 2$; this corresponds to $350mm$ of rainfall if the rainy season lasts half an year (note that we have chosen the number of days in an year to be 350 for convenience). In addition, the plant diffusion constant, D_p, was

chosen to be smaller. We have checked that the qualitative conclusions we draw are not sensitive to the specific functional form of $\tau_p(W)$ that we have chosen as long as the key features are the same: for example, the value of $\tau_p^{-1}(W = 0)$ is small (0.01 for the results in this paper); this sets the scale for the slowing down of metabolic processes when there is no soil moisture. We have checked that a Gaussian functional form for $\tau_p(W)$ yields similar results to those for the form given above.

4.4 Methods

The mean field model (ordinary differential equations) was solved numerically using MATLAB; for the spatially extended case, the partial differential equations were solved numerically by a forward-time, centered-space differencing scheme on a two-dimensional spatial grid of 128×128 squares with periodic boundary conditions, using C++ and FORTRAN. Each square element of the grid corresponds to $1m^2$ area. The typical time step chosen was 10^{-3} of a day which satisfies the stability criterion [113]. The numerical solution was obtained with different initial conditions: (i) plant peaks ($P = 20$) at 10% of the randomly chosen grid elements; the initial values of surface and soil water were set to zero at all spatial elements to mimic the end of dry season (or the onset of wet season); and (ii) well-developed spatial patterns. The results are not sensitive to the initial conditions in most of the cases.

4.4.1 Discussion on convergence

The *fully explicit* scheme used for our calculations is first order accurate in time and second order accurate in space [113] and stable for the time discretization used. Nevertheless, we have performed additional calculations as a check on our results to confirm the convergence to the correct equilibrium solution. First, we used much finer spatial grids

with 256×256 and 512×512 square spatial elements where each element corresponds to $0.25m^2$ of area. Then the system was evolved on finer time steps of 2×10^{-4} of a day. The results of these finer spatial and temporal grid simulations are consistent with those of coarser simulations reported in this paper.

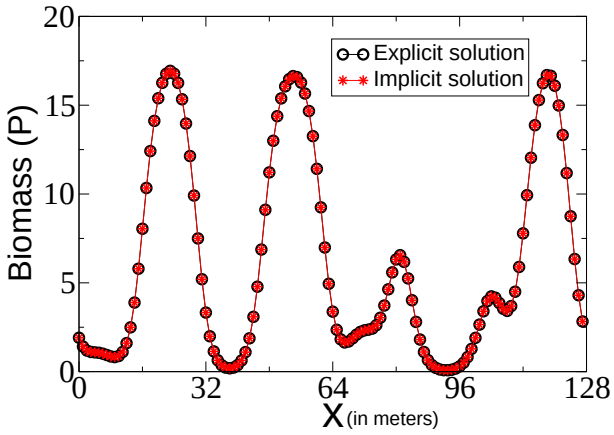

Figure 4.4: Comparison between simulations of pattern formation on a 1 dimensional lattice of 128 spatial grids by two different numerical integration schemes (i) Crank Nicolson implicit scheme and (ii) Fully explicit scheme. For this specific simulation, the rainfall was assumed to be uniform ($N_w = 350d$). The time step for implicit scheme was chosen to be 0.01 of a day where as that for the explicit scheme was chosen to be 0.0001 of a day. Similarly, the results for the seasonal rainfall case with $N_w = 150d$ obtained by different schemes of integration show excellent agreement with each other (within 0.1%). Parameters are: $c = 5, g_{max} = 0.1, k_1 = 5, k_2 = 5, r_w = 0.4, W_0 = 0.2, \alpha = 0.4, d = 0.25, D_p = 0.01, D_w = 0.1, D_o = 100, N = 256 \times 256$ and dx=1.

Second, we have performed calculations using the *Crank-Nicolson* implicit numerical integration scheme [160]. This method is second order accurate in space and time. Moreover, this scheme is unconditionally stable, i.e. the correct equilibrium solution is obtained for any time step Δt. However, for large Δt, the details of small time scale evolution from a given initial condition can be inaccurate. Performing this calculation in two dimensions

is computationally prohibitive: for each time step, we need to solve a set of $3N^2$ nonlinear coupled algebraic equations (approximately 50,000 equations for $N = 128$, i.e., a 128×128 spatial grid). Fortunately, the one-dimensional version of the model also exhibits qualitative features that are the same as those of the two-dimensional system. For instance, both of them show Turing patterns on the same length scales and as the rainfall increases the patterns occur in the order of bare, patchy and fully vegetated patterns. Therefore, as a computational compromise we have implemented the implicit scheme on a one-dimensional spatial lattice of 128 grid points with the grid spacing corresponding to 1m and a time step of one day. The resulting 3×128 coupled nonlinear equations were solved using a multi-root solver available from the GNU Scientific Library [160]. Comparison between sample equilibrium solutions obtained with the implicit scheme and the explicit scheme when the system was evolved from identical initial conditions show numerical agreement at the level of 0.1% (see Fig. 4.4). Based on the excellent agreement between the implicit and explicit calculations in the one-dimensional problem we believe that our numerical simulations in 2 dimensions space yield the correct equilibrium solution. In addition to the numerical checks it is worth emphasizing that the original set of partial differential equations have been shown to have a Turing instability leading to the patterns seen numerically; the length scale of the instability is consistent with the scale of the patterns observed numerically.

4.5 Results and Discussion

We present the results of the numerical solution of both the mean-field (non-spatial) and the spatially extended version of the model and discuss various implications of seasonality in rainfall. In the case of uniform rainfall ($N_w = 350$ and $N_d = 0$), we obtain the following sequence of patterns which are in agreement with those in the original model:

homogeneously vegetated, gapped, labyrinthine, spotted and homogeneously bare as the rainfall is decreased (see Fig. 4.5). We note also that in the limit when the soil and surface water levels are at their wet season levels, the behavior of our model is similar to that exhibited by the model of [155]. We begin with a description of how the self-organized patterns are affected with seasonality in rainfall. We then provide a detailed discussion of the implications of seasonal rainfall for productivity and the effect of the variation of the length of the wet season for the same annual precipitation. We compare our results with field data. We also discuss the implications due to year-to-year fluctuations in the number of wet days as might arise due to climatic changes and make comments on the limitations of our model.

4.5.1 Self-organized pattern formation

We discuss results for how the spatial self-organization of the vegetation system is affected when the resource necessary for growth, water, shows seasonal variations. We show the results for the patterns when we switch on seasonality in the rainfall with the length of the wet season set to be 150 days and keep the daily rainfall rate, R, uniform during the wet season. We look at the pattern development for different values of R. The temporal development of patterns during the wet season is similar to that produced by the model of [155]. However, the transients are different in detail because of the diffusive time scale and the slow increase in the plant growth rate. In contrast to the original model, the plants survive the dry season albeit with a reduced biomass density. Moreover, the same sequence of patterns is obtained as the total rainfall is reduced keeping the number of wet days the same. Thus, the model accomplishes the goal of maintaining the results for the patterns in the presence of seasonality. The mechanism for the stability of self-organized

patterns is the adaptive features of the plants encapsulated in $\tau_p^{-1}(W)$. The absence of soil moisture in dry season leads to substantial reduction in the metabolic activity of the plants and this results in a much slower decay of vegetation. Hence the vegetation survives the dry season with reduced density of biomass. These patterns, as a snapshot at the end of the rainy season, are shown in Fig 4.5 and in the Appendix C.2. Whereas the patterns reach a steady state (independent of time) for the models with no seasonality, here patterns obviously do not reach a steady state due to the presence of a time-dependent driving term, the rainfall R. The spatial patterns eventually reach a stable periodic state and oscillate with a period of 350 days (same as the period of the driving term R) asymptotically.

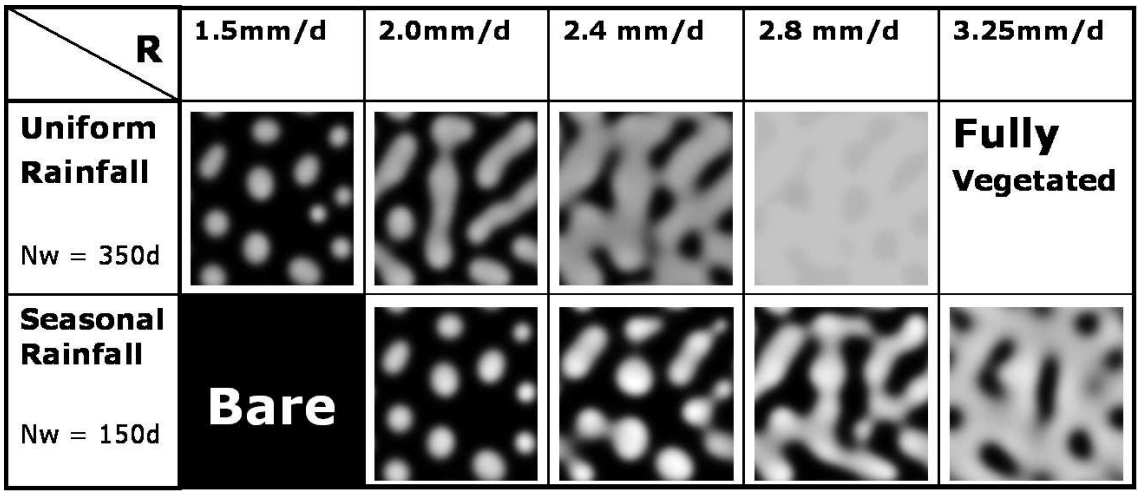

Figure 4.5: These figures show the vegetation patterns with and without seasonality in rainfall at the end of 6800 days. The equations 4.17-4.20 were numerically simulated starting with several plant patches on the grid, with soil and surface water set to zero everywhere. Periodic boundary conditions were chosen for all these cases. In this grey scaled picture, darker patch represents bareness whereas the brighter patch indicates presence of vegetation. The length scale of the spatial grid is $128m \times 128m$. Rest of the parameters are as given in Fig. 4.4.

4.5.2 Insufficiency of PPT in determining the system behavior

We present results for the behavior of the model, the productivity (biomass or area covered by vegetation) and the nature of the patterns, as we vary the parameters that characterize the seasonal rainfall. In the previous section, we have followed the evolution of the system as a function of R, the rainfall rate during the wet season given a fixed length for the wet season. We can, alternatively, study the behavior of our model as the number of rainy days, N_w, is varied. Altering R or N_w changes the total annual precipitation ($PPT = N_w\, R$). It is customary to use the mean annual precipitation (MAP) or PPT as the key variable [85]. This leads to the following interesting question: Is the total annual precipitation PPT alone sufficient to determine the system behavior? We have investigated this question systematically by keeping PPT fixed and varying the number of wet days N_w and the daily rainfall R such that $N_w R = PPT =$ constant. The results of the primary productivity calculations and the patterns formed suggest that the answer is no.

Mean-field model: We first present results for the model without spatial fluctuations by setting the diffusion constants to zero in Eqs 4.17-4.20. We compute the plant biomass density at the end of the rainy season and call this the productivity of the system. Since the model does not explicitly include competition (for example, a term such as $-d_1 P^2$ in the evolution equation for P), the value of the plant biomass continues to increase as R increases. We have therefore used the rescaled productivity, the plant biomass scaled by the saturation biomass. We calculate the productivity for a fixed annual precipitation ($PPT = 350mm$), but for different seasonal rainfall distributions with a cutoff in R due to runoff effects. The results are displayed in Fig. 4.6(a). The productivity remains at zero for small amounts of rainfall spread over a long wet season. As we decrease the number of days, the productivity increases and reaches a maximum. Further reduction in the rainy

days leads to intense rainfall showers resulting in heavy runoff and consequent decline in the productivity to zero. The length of the wet season for which there is maximum productivity shows nearly a linear dependance on the total annual precipitation.

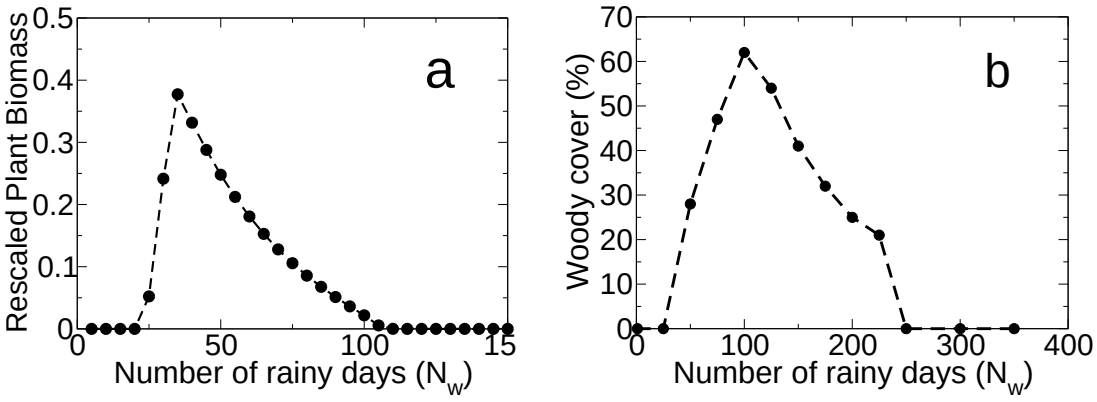

(a) (b)

Figure 4.6: Variation in the productivity of the system as a function of the number of rainy days (N_w) for a given annual precipitation (PPT). (a) The mean-field model productivity is the (rescaled) plant biomass density calculated at the end of 100^{th} rainy season ($t = 34800\,days$) starting with a nonzero plant density. Here, $R_{rc} = 10\,mm\,day^{-1}$, $P_{scaling} = 160\,g\,m^{-2}$ (b) The productivity in the spatial model computed as the percentage of land area covered by plants at the end of the 20^{th} rainy season ($t = 6800\,days$). Here, $R_{rc} = 3.25 mm\,day^{-1}$. For both the plots, we have set the total number of days in an year to be 350, $PPT = 350\,mm\,year^{-1}$ and all other parameters are as indicated in 4.4. The circles are the data points obtained from numerical simulations and the dotted line, obtained by linear interpolation between two consecutive data points, is meant to guide the eye.

Spatially extended model: We address the dependence of the mean-field conclusions when we include spatial fluctuations and the development of patterns. To do so, we solve Eqs. 4.17-4.20 numerically with nonzero diffusion coefficients. The percentage of land covered by plant biomass, an average measure of ecosystem productivity, is plotted as a function of number of rainy days for in Fig. 4.6(b). We emphasize that the behavior is

similar to that of the mean-field model even though we have used a different measure for the productivity. The productivity measure used here does not contain much information about the corresponding spatial patterns. This will be discussed in the next subsection.

Spatial patterns: We now ask the question as to how do the patterns change as the length of the wet season is varied for a given PPT? As Fig. 4.6 indicates, we get a bare pattern for $N_w = 350\,days$ and a vegetated patch when we decrease the number of days to $N_w = 150\,days$ while keeping PPT fixed at $350\,mm\,year^{-1}$. In fact, we find that for the range of parameters used, the same sequence of patterns that are observed for nonseasonal model occur as N_w and R are varied. As N_w decreases one goes from the bare state to a state with vegetated spots and then to the labyrinthine states and so on. However, decreasing N_w below a critical value (corresponding to productivity maximum in Fig. 4.6 (b)) leads to excessive runoff and hence, patterns now occur in the reverse order eventually leading to a bare pattern. This leads to the conclusion that we cannot determine the pattern formed from the value of the annual precipitation PPT alone or the mean daily rainfall R in the wet season alone. We need to have the knowledge of both R and PPT (or R and N_w or PPT and N_w). In other words, given the total annual precipitation or the average rainfall during the rainy season, the distribution of the rainfall (i.e. the number of wet/dry days) within the year is critical in determining the exact pattern formed.

4.5.3 Maximum productivity as a function of PPT

We have noted the dependence of the productivity on the distribution of the rainfall for a given annual precipitation in Fig. 4.6. From these data we have extracted the maximum productivity for a given annual precipitation, PPT, and studied its behavior as a function of PPT. A considerable amount of data for this quantity has been assembled from Savanna

grasslands in Africa [85]. Our results for the mean-field model are shown in Fig. 4.7(a). The behavior displays the same general features as the experimental data in a qualitative way. This is reasonable given that the experimental data are for the percentage area of woody cover and we have used a re-scaled productivity in a mean-field setting. We recall the occurrence of a transcritical bifurcation in the mean-field model without seasonality [114]. The fixed point corresponding to the bare state is stable for small values of PPT and exchanges stability with the fixed point corresponding to the vegetated state for larger values of PPT. This accounts for the basic behavior reported in [85] in a rudimentary way. The behavior in the seasonal model is more subtle since the maximum value of the productivity is being considered.

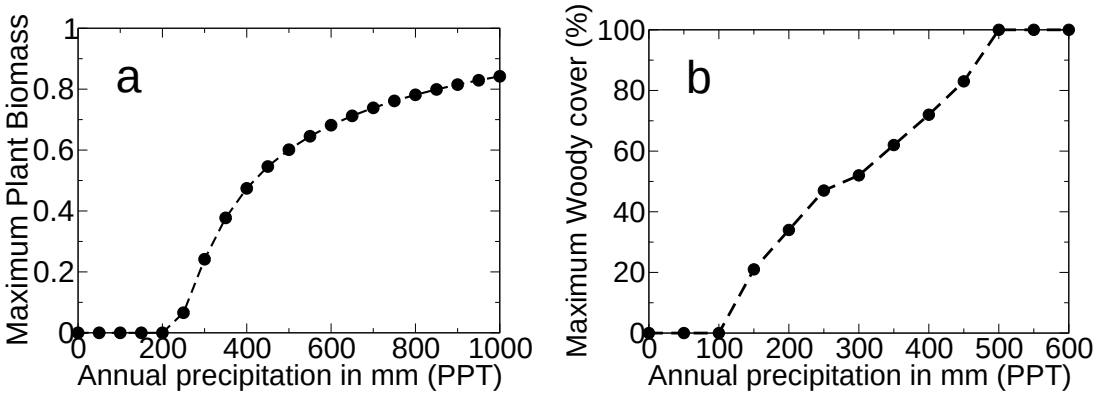

(a) (b)

Figure 4.7: The maximum productivity of the system as a function of the annual precipitation (PPT). For a given PPT, we calculate the productivity (as in Fig 4.6) as a function of N_w and extract the maximum value and display it as a function of PPT. (a) The mean-field results, where productivity is the (rescaled) plant biomass density. (b) The spatial model results, where the productivity is the percentage of land area covered by plants. For both the plots, all parameters are as of those in Fig 4.6.

The results for the spatially extended model are shown in Fig. 4.7(b). The maximum productivity, measured by the fraction of the vegetated area, is plotted as a function of the annual precipitation. The maximum value is obtained by varying the number of rainy days for a fixed PPT, as described earlier for the mean-field case. The results of numerical simulations indicate a nearly linear trend of woody cover as a function of PPT (from 100mm to 500mm). The general agreement of our model calculations with the results of [85] is extremely good. While the trends in the data are obtained even in a model without spatial extent and thus without patterns in the vegetation cover, the results for the spatially extended model show more satisfactory agreement with the field data.

We make a few additional remarks about productivity in the model with seasonality. An interesting consequence of our study is that for the same annual precipitation different levels of productivity are possible, as also is seen in the field observations. The variations can also occur for a variety of reasons and most certainly, due to soil heterogeneities such as clay vs sand. Our model shows that variations in the length of the rainy season can independently lead to a distribution of productivity. In other words, fluctuations in the number of wet days alone can be a major contributing factor to variations in the vegetation cover. Even though the patterns observed are attributed to self organization and not due to preexisting heterogeneity [132], soil heterogeneity may have a crucial role constraining the self-organization [161]. We note that such heterogeneity in soil characteristics corresponds to variations in some of the parameters in the model. Quantitative characterization of such heterogeneities is difficult. The parameters most likely to vary due to soil characteristics are α, the proportion of surface water available for infiltration, r_W, the rate of soil water loss due to drainage, evaporation, etc., and R_{rc}, the saturation value of the daily rainfall due to overflow. We have checked that the maximum productivity is relatively insensitive

to changes in α of the order of $\pm 10\%$. We find that the results are more sensitive to an independent variation of r_W only. However, as r_W decreases there is more soil water available after rainfall and therefore, for a given rate of infiltration more of the surface water will be lost due to overflow. Thus, if we increase or decrease r_W and R_{rc} together, our results are quantitatively unaltered. A careful comparison with the experimental data would need a better understanding of soil mechanics and hydrology.

Clearly, Fig. 4.6 indicate that for the same annual precipitation, seasonality enhances average biological productivity in arid ecosystems. By concentrating the rainfall for a shorter duration, we are able to produce patterns that would otherwise go bare. We recall that the productivity depends on the initial spatial distribution of plant biomass as noted even in the original model [155]: self-organized vegetation patterns can exist in highly arid regions where the homogeneous initial condition decays to a bare state. These results suggest that even temporal variations in the rainfall, in particular a seasonal distribution, can also lead to a higher plant cover.

4.5.4 Effect of perturbations on the behavior of the system

We discuss the robustness of the results obtained in the seasonal model: by this we mean whether the behavior of the system persists under different kinds of disturbances or perturbations. In an obvious sense the patterns produced by our seasonal model are considerably more robust with respect to temporal perturbations than those in the original model. For example, if the rainfall shows variability so that during the wet season there is a period of a few weeks with no rain then the vegetation pattern can survive and recover since we have built in adaptability. We have also checked the robustness of the patterns in the model with respect to a variety of other random perturbations in the rainfall amount R.

However, care must be exercised in making such comparisons because the conclusion can depend on what quantities are being varied. For example, if we vary the rainfall per day during the wet season, PPT will change and the non-seasonal model can be more robust.

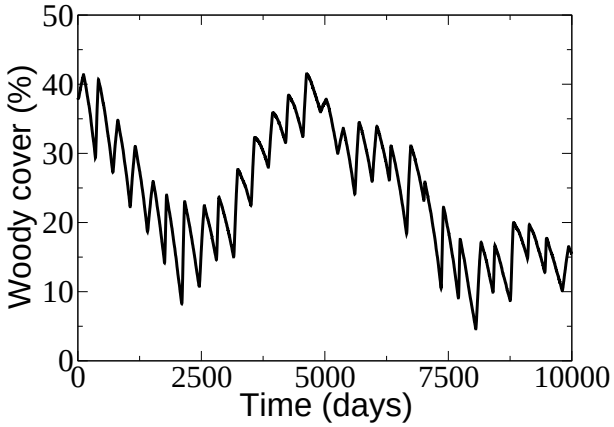

Figure 4.8: Productivity in the spatial model, i.e, fraction of area covered by plants, as a function of time in the scenario of increased variation in interannual rainfall fluctuations (N_w). We have chosen $PPT = 250\, mm\, year^{-1}$. The number of rainy days is generated according to uniform random number distribution with mean $\langle N_w \rangle = 75\, days$ and a variation of 75% around the mean.

We consider the following application of our model in the context of robustness and regime shifts: It is known that drylands exhibit large inter-annual variations in the number of rainy days and total annual precipitation [157]. Extreme climatic events such as extended droughts or large interannual rainfall fluctuations associated with El Nino Southern Oscillation phenomena play a critical role in shaping the arid and semiarid ecosystems [162]. Climate changes brought about by global warming can be expected to increase such fluctuations in N_w, as also extreme precipitation events [163]. As an example, we discuss results for the spatially extended model in which the number of rainy days vary annually, but keeping the PPT fixed at 250mm. The interannual variations of N_w are chosen to

be uncorrelated and with a uniform distribution between $m/4$ and $7m/4$, with $m = 75$ days. In other words, m is the mean number of rainy days and the variation of random number distribution is 75% around the mean. For illustrative purposes we have chosen the width of the distribution to be large. The consequent fluctuations in the productivity are large (see Fig. 4.8) and point to the possibility of irreversible regime shifts in those years when the productivity is small due to other environmental stressors. We note that the mean-field model shows similar results. However, these calculations cannot be used for prediction of such regime shifts, but are only meant to illustrate the plausible impact of increased interannual variations in rainfall induced by climatic changes. A recent mathematical modeling study shows that climatic fluctuations can enhance the resilience in a dryland ecosystem [164]. Thus, understanding the causes for such regime shifts is crucial for building predictive theories and better management of these resources. We wish to emphasize that the increased robustness of the plants due to their adaptability and more realistic description of biophysical processes (see below), apart from large scale feedback processes such as those between vegetation and water cycle [165, 166], in the models are necessary features that must be included if one wants to investigate regime shifts.

4.5.5 Limitations

We add a few cautionary remarks about the specific limitations of our seasonal model. Various mechanisms have been proposed to explain spatial patterns found in semi-arid ecosystems as discussed in the introduction. Our goal is to understand the implications of seasonality within a detailed calculation and we choose to do so in a model that is based on enhanced soil water infiltration [13]. As discussed earlier, the inclusion of the soil-water dependent time scale for plant growth improves the time behavior of the plant biomass

during the change of seasons. However, the present model is still not designed to capture the transient dynamics in detail, particularly at the onset of wet and dry seasons. This is due to the simplification of biophysical processes involved; for example, the surface and soil water flows which has been approximated to be a diffusion process. The diffusion constants in the terms that arise from Darcy's law can also depend on the degree of wetness. The vertical infiltration rate depends on whether the soil is wet or dry and thus this term depends directly on the water level W in addition to the dependence on P. A realistic model should include these complex flow processes. On the biological side, the adaptability of the vegetation assumed in the model must be modified to include a threshold effect so that there is mortality if the plant biomass level falls below a certain minimum, particularly during the dry season. These and other effects that affect transients and hence, determine the survival of the vegetation, must be included if one is to further our understanding of the disturbance and recovery aspects of vegetation on shorter time scales. For predictions on larger spatial scales, both intrinsic spatial heterogeneity and spatial variation in rainfall must be included [135]. Nevertheless, since our focus is on long term dynamics of vegetation pattern formation and productivity of the ecosystem, including the detailed description of realistic processes are unlikely to affect the qualitative nature of the results we have obtained, as we show below for one particular case.

We have investigated the effect of including a threshold in the biomass below which mortality occurs as follows. We retain the dynamics of the wet season as defined by Eqs. 4.17-4.20. However, the dry season is modeled by a discrete event: at the end of the dry season all the surface water is set to zero, all the soil water is set at $W_d = 1mm$ and plant densities less than a threshold ($P_{th} = 10g/m^2$) are set to zero and those above the threshold is reduced to fP where $f = 0.5$. We find that the qualitative features of

self-organization we have obtained for our model without a threshold hold for this model. For the ranges of values we have checked the results are not sensitive to the precise values of W_d, P_{th} and f. However, in our simulations we find that the threshold behavior in the survival of vegetation during the dry season increases the chances of a regime shift from a spotted to a homogeneously bare pattern.

4.6 Summary and Concluding remarks

In summary, we have studied the effect of seasonality in an ecosystem model that is resource-limited; specifically, we report results for a model of vegetation pattern formation in arid ecosystems with seasonality in the rainfall that determines productivity. We have devised a model with seasonality by including variations in the intrinsic characteristics of the ecosystem (plants, in our case) in response to external variations. The self-organization manifested in the various patterns survives long dry seasons due to the inclusion of natural metabolic adaptation of the plants. Our results lead to the conclusion that the vegetation patterns and the productivity can be significantly altered due to variations in the duration of the wet season even if the mean annual precipitation (PPT) remains constant. Indeed, different patterns can be obtained for the same PPT depending on the number of wet days; thus there is a subtle relation between seasonality and self-organization that is not easily predicted without an explicit calculation like the one we have done. This also leads us to observe that a simple characterization of a time-varying resource in an ecosystem using just the temporal average is insufficient. We also found that the maximum productivity for a given annual precipitation (obtained by varying the number of wet days) varies as a function of PPT possibly accounting for field observations. This reflects a general result

that large variations in the productivity can occur due to variations in the resource during the year keeping the annual total constant.

CHAPTER 5

SUMMARY AND FUTURE WORK

5.1 Summary

In this thesis, we have applied ideas and techniques from nonequilibrium statistical physics and have proposed leading indicators of proximity to a threshold of abrupt transition in ecological systems. We showed that when a time series data from a system is available, an unidirectional change in the skewness of time series distribution can be used as an early warning signal of a nearby transition. A novel feature of the proposed indicator is that its based on a nonlinear analysis of the (meta) stable fixed point and exploits large fluctuations ubiquitous to ecological systems.

When the spatially extended data is available, we proposed that the variance and skewness of the distribution obtained from the snap shot of a spatial pattern can be used as an early warning signal. The idea of spatial variance being an indicator was motivated by the studies on phase transitions which show that the correlation length and susceptibility diverge at the critical point. The proposed indicators, however, qualitatively differ from them. First, the diverging nature of correlation length and the derived quantities occur only in a second order phase transition where the order parameter varies continuously as the control parameter changes. Secondly, those quantities are obtained for steady state and in the thermodynamic limit. On the other hand, ecological systems of interest are those

which show discontinuous transitions or the first order phase transitions where no such divergences occur. In addition, we are calculating non-steady state properties of quantities such as variance and skewness. However, we showed that the non-steady state quantities show some of the features expected in a second order transition due to substantially long life times associated with the meta stable states. This feature was exploited in devising indicators of the transition.

We have studied the implications of temporal fluctuations in the driving parameter on a self-organizing ecosystem. More specifically, we studied the role of seasonal fluctuations in rainfall on the patterns of vegetation. We find that the sequence of patterns obtained with the seasonal forcing remains the same. However, with seasonal forcing the patterns are shifted towards higher values of daily rainfall.

We compared our results with field data in two cases. In chapter 2, we calculate the moving average skewness of Sahara climatic data which exhibits catastrophic transition from a vegetated to desert state around 5500 years ago. We find that the data is not sufficiently resolved and hence we were unable to find a trend in skewness prior to the regime shift. Second, in chapter 4, we compare the results of maximum vegetation cover with the recently published data from Savanna grasslands to a reasonably good agreement [85].

5.2 Future work

The non-diverging nature of indicators for our model systems suggests a limitation in their applicability. It is plausible that the transition to the alternative stable state occurs earlier than any changing trends in the indicators are detectable. Study is needed to obtain conditions when such effects can mask the utility of indicators in the model as well as real systems.

In most of our results on indicators of regime shifts, especially in the spatially extended systems, we have restricted ourselves to models where an effective potential could be defined. In multivariable models we often can not define such a potential and hence our intuition of a potential which helped device various indicators does not hold. Obtaining conditions for applicability of these results in such non-potential systems and devising new indicators forms an important direction for further study.

Ecological systems are patchy and heterogeneous in nature. They are governed by dynamics of a large number of coupled variables on spatially extended systems. In our spatial models, we coarse grained the system and observed it on a scale such that the patchiness and heterogeneity were not important. We have implicitly assumed that the coupled multivariable system can be approximated by a dynamics of a few variables, sometimes even ignoring the spatial degrees of freedom. In lieu of such simplifying approximations, several important questions are needed to be addressed to enhance our theoretical understanding as well as the practical application of early warning signals. Starting from microscopic scales where a number of key variables interact with each other and heterogeneity and patchiness can be important, can we obtain coarse grained equations of dynamics for a reduced number of variables relevant to devising indicators of regime shifts? Is there an optimal scale for coarse graining and are there universal features which can be applicable to different ecological systems? It will also be useful to take raw spatial data and analyze it at different scales of coarse grained approximations.

In well mixed systems where the spatial fluctuations are correlated on the time scales of measurements, the time series indicators such as variance, recovery time, spectral function and skewness can be useful indicators [90, 91, 92, 93, 94, 126]. For spatially extended systems with a number of kernels and diffusive coupling, spatial variance [167] and skewness

can be leading indicators. Based on the regular patterns of vegetation found in semi-arid regions, two indicators of catastrophic regime shifts have been suggested [148, 13, 153, 115, 116]. If the feedback is scale dependent (short range facilitation and long range inhibition), the regular spotted patterns appear prior to a catastrophic vegetation collapse [13]. On the other hand, if the positive feedback is a local effect and constraints are global, a deviation from the power law distribution of patches has been suggested as an indicator [115]. These studies hint that the scale and strength on which the feedback occurs may hold the key to devising early warning signals for impending regime shifts. Integrating these ideas to provide a framework based on the spatial scale and strength of interactions for developing indicators can be theoretically interesting and practically useful.

Last but not the least, field testing of the proposed indicators is the need of the hour. Ecological data are often difficult and expensive collect. Our results suggest that although we do need well resolved data, finer resolution does not always mean a better confidence in our results. The data must in fact be separated by the correlation time and length to be considered as independent measurements. Thus, a key question that needs to be addressed is how to obtain the relevant time and spatial scales of measurement in model and real ecological systems.

To conclude, this thesis addresses issues related to multistable ecological systems, a topic of critical importance in ecology. We show that the techniques of nonequilibrium statistical mechanics can be very useful in understanding the dynamics of these complex systems. We make important contributions to this field by devising early warning signals for catastrophic transitions in ecological systems.

APPENDIX A

SUPPORTING MATERIALS FOR CHANGING SKEWNESS: AN EARLY WARNING SIGNAL FOR REGIME SHIFTS IN ECOSYSTEMS

A.1 Results for the two-variable vegetation model

Here we report results of the two variable vegetation model which does not have the potential (see section 2.3). The rainfall rate, R, is a natural control parameter with a stable high density vegetation state at large values of R that collapses to a desert below a critical threshold. We include the stochastic fluctuations in the rainfall rate and an additive term in the dynamics of the biomass density B. The bifurcation diagram is shown in Fig A.1a.

The results of the simulation yield a time series for $\{B(t), w(t)\}$ that constitutes a sampling of the joint probability distribution for B and w. We looked at the time series of the biomass density B alone motivated by the fact that in a real ecological system data are restricted to a (small) subset of the relevant variables. With the available data from the simulations, we compute the skewness of marginal distribution of the biomass density B, i.e. the probability distribution of B averaged over all possible values of the coupled variable w since the latter evolves on a fast time scale (if on the other hand, the unobserved variables vary on a much slower scale than the interval of observation we would be measuring a conditional probability distribution). The results plotted in Fig. A.1b and c show that skewness rises as one approaches a regime shift either due to proximity to the threshold or enhanced external fluctuations. Thus we confirm the role of skewness as a warning signal in a more complex ecological model.

More results for the two-variable vegetation model described by are shown in Fig. A.2.

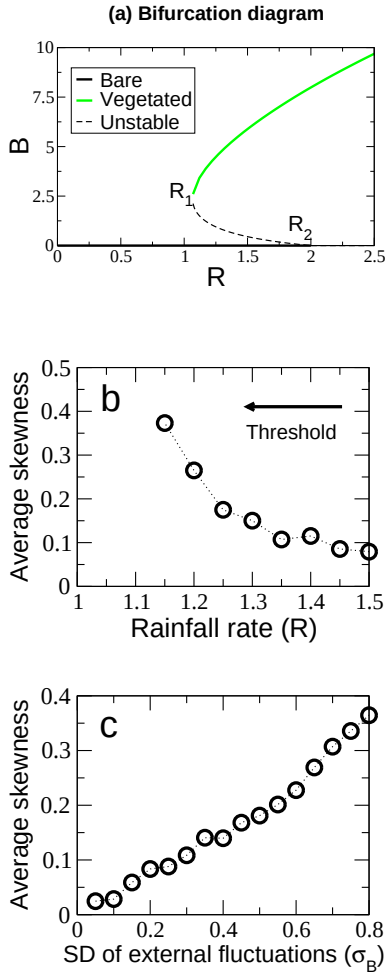

Figure A.1: (a) The bifurcation diagram as a function of the rainfall rate R. Here, $R_1 = 1.06$ and $R_2 = 2.0$. Increase in the skewness as the threshold to regime shift is approached in different ways for the two variable vegetation model. The open circles are the average value of skewness obtained by the numerical simulations. The dotted line is meant to guide the eye. Note that we have plotted the absolute value of the (average) skewness. (b) Approaching the threshold by reduction in rainfall rate with $\sigma_B = 0.25$ and $\sigma_w = 0.01$ (c) Increase in external fluctuations (σ_B) with $R = 1.5$ (far from threshold of vegetation collapse) and $\sigma_w = 0.01$.

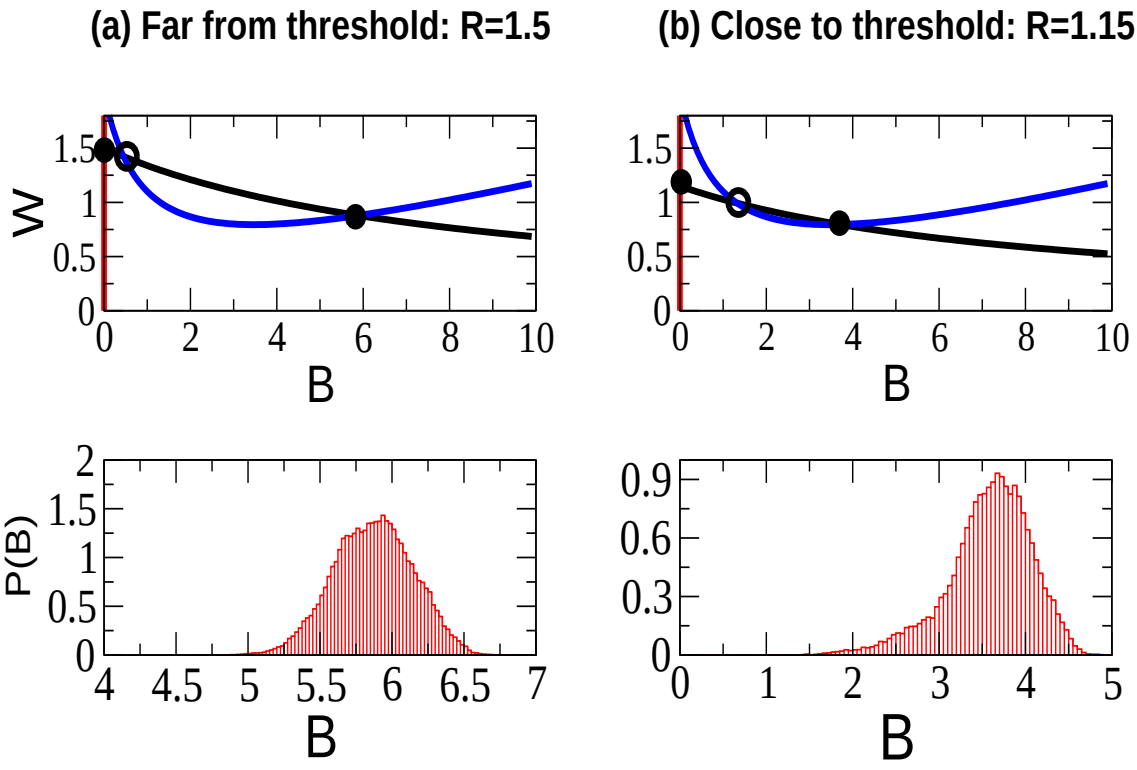

Figure A.2: More results of the two variable vegetation model (a) and (b): Nullclines (indicated by think lines) and fixed points (at the intersection of nullclines; stable fixed points are represented by full circles whereas the unstable fixed point is an open circle) are shown in the top row. The bottom row shows the time series distribution for a representative simulation.

.

A.2 Validity of asymmetric arguments for coupled multivariable models

As we discussed in chapter 2, for multivariable dynamical systems, an effective potential exists only under extremely restrictive conditions [88]. It is nevertheless possible to devise an intuitive understanding of how the asymmetry arises by considering the vector field that represents the "forces" that determine the dynamics of the coupled variables. This is explained in this appendix with the help of Fig A.3.

We consider the representation of the dynamics of the two-variable vegetation model in the phase plane defined by the two variables (w, B). The direction field (sometimes referred to as the velocity field) is a vector field that specifies the rate at which the two variables change as a function of time at each point in the phase plane. If the dynamics of the system is described by

$$\frac{dw}{dt} = f(w, B) \qquad \frac{dB}{dt} = g(w, B) \tag{A.1}$$

then the direction field at any point in the phase plane $\mathbf{x} = (w, B)$ is given by the vector $(f(\mathbf{x}), g(\mathbf{x}))$. This is represented in the diagram as follows: draw short segments of lines whose length is proportional the strength of the field (*i.e.* velocity) at that point. Additionally, arrows are used to indicate the direction of the local flow (not shown in our figure). With the help of this picture, one can visualize the evolution of the dynamical system.

In Fig. A.3, the two dotted lines represent the nullclines ($f = 0$ and $g = 0$) which are contours in the phase plane along which the rate of evolution of one of the variables vanishes. The intersection of nullclines is the stable vegetated fixed point. Fig. A.3(a) represents the case where the system is far from the bifurcation for the two-variable vegetation model.

Here, the direction field is nearly "symmetric": consider two points which are equidistant but diametrically opposite from the fixed point. At these two points the arrow lengths are nearly the same which means that the magnitude of velocities are the same. This leads the system to spend equal amount of time sampling small and large biomass values. The marginal distribution of the biomass density B (*i.e.* B averaged over all directions of movement along w) would thus be symmetric.

On the other hand, consider Fig. A.3(b) which represents the behavior close to the bifurcation. It clearly shows that strength of the field is asymmetric along at least one direction in phase place: consider a line which passes through the fixed point and passes through the region where the nullclines make a closed loop. When the system enters this closed loop region it spends relatively more time inside (smaller magnitude of the direction field as indicated by shorter segments) than compared to the diametrically opposite direction from the fixed point. This results in an asymmetric marginal distribution of B when averaged over all possible realizations of w.

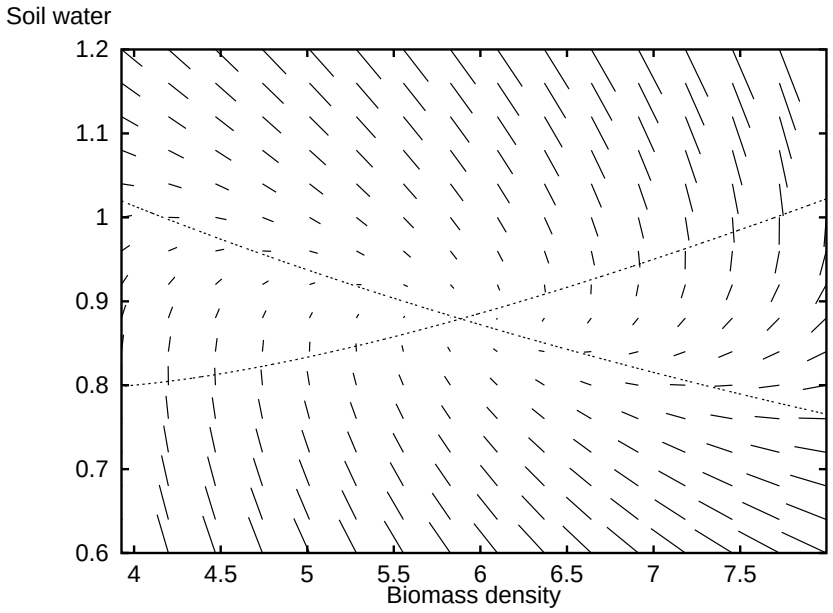

(a)

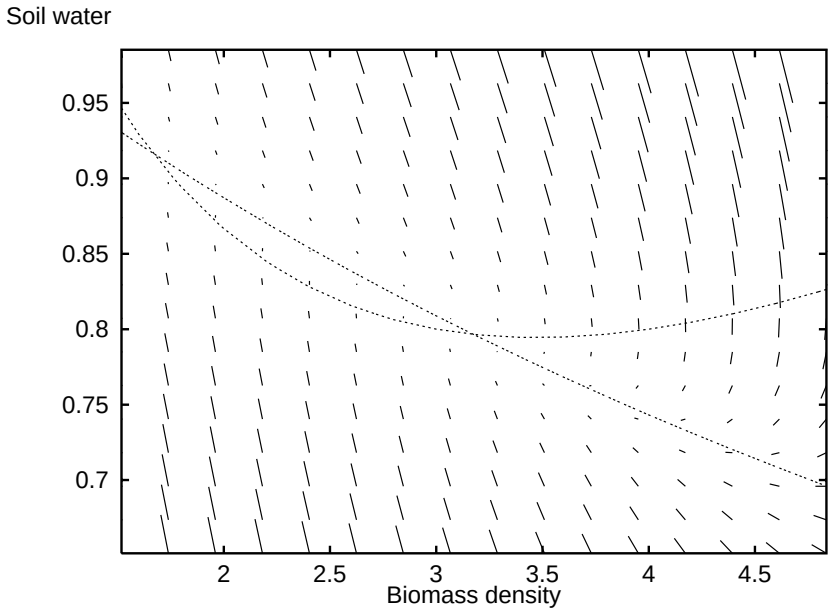

(b)

Figure A.3: Plots of the direction field for the two variable vegetation model. The dottel lines represent the nullclines of the system. The point of intersection of nullclines is the vegetated fixed point. The short segment of lines represent the strength of the direction field (*i.e.* velocity at any point n the phase plane. (a) Far from bifurcation: R=1.5 (b) Close to the bifurcation: R=1.10. The bifurcation occurs at R=1.06.

A.3 Results for the parameterized lake model

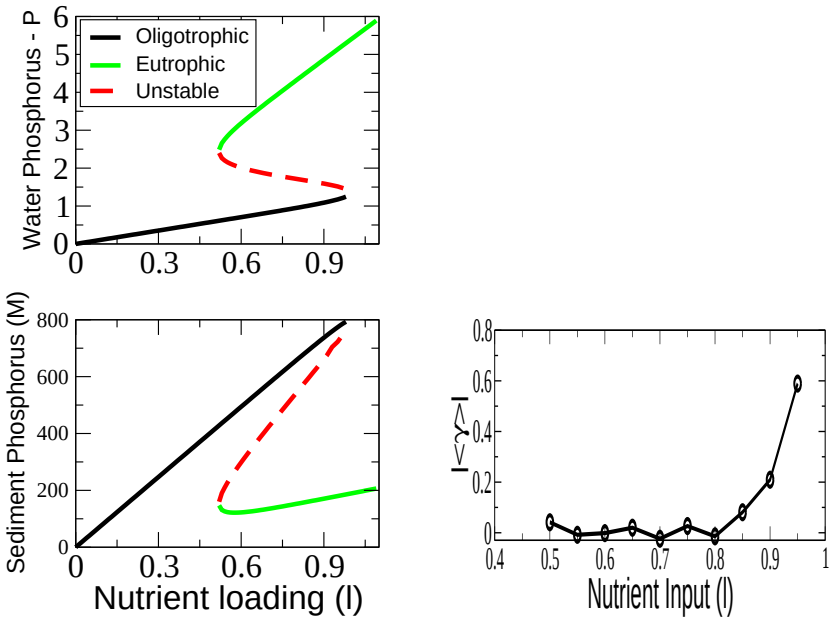

(a) (b)

Figure A.4: Results for the parameterized lake eutrophication model (see chapter 2, section 2.4) (a) The bifurcation diagram for Lake eutrophication model as a function of nutrient loading. The thick lines represent the stable oligotrophic and eutrophic states whereas the broken lines represent the unstable state. The two bifurcation points correspond to $l \approx 0.5$ and $l \approx 0.95$. (b) Absolute value of the average skewness of lake model as obtained by numerical simulations, as we approach the threshold due to increased nutrient loading. Calculation of skewness are performed for 500 time units and then averaged over 200 such simulations.

A.4 Analysis of real data sets

In this section we calculate skewness for two data sets: the Sahara climatic shift data available from 25000 before present (BP) to present [1] and a 10 year data of very good resolution from 1997 to 2006 for total phosphorus concentration taken at the Sandusky Bay where the Sandusky river drains into Lake Erie [2]. We also compute variance for the Sahara data set.

Sahara data set: During the past 25000 years, the Sahara has witnessed three large scale regime shifts which have been very well documented by the terrigenous sediment data [1]: the first around 14800 years BP, second at 12300 years BP and the most recent one being at 5500 years BP. The full data are shown in Fig. A.5(a) which we have divided into four different intervals for the analysis of indicators. For the regime shift at 14800 yrs BP, the data immediately prior to the shift is unavailable and hence does not form a suitable candidate for testing the indicators. The data prior to the second regime shift at 12300 yrs BP are too few (interval (ii) in Figure) to perform any reliable analysis. There is no regime shift in interval (iv) yet and hence again this data cannot be directly used for testing the indicators (it can serve as a reference, however). Thus the main text showed the average moving skewness only for the data preceding the most recent regime shift (interval (iii)). However, it is an useful and instructive exercise to look at the average fluctuation of skewness in the entire data set. In addition, we have also studied variance - another recently proposed indicator of regime shift [93] - and checked its behavior for this data set. Evaluating two other important indicators, recovery time and spectra, usually require longer time series and hence we did not compute them. Moreover the (linear) indicators variance, recovery time and spectra all arise from the same underlying mechanism.

A visual inspection of the variance and skewness clearly suggests that both these indicators show fluctuations comparable in magnitude to those found in interval (iii) even in other parts of the data set. Hence we are unable to conclude whether fluctuations that occur in interval (iii) of the Figure can be attributed to proximity to the regime shift which eventually occurred at 5500 yrs BP. This conclusion for the behavior of the skewness is also consistent with the results from a simulation AR(1) model (for parameters obtained from original data fitting an AR(1) process: see maintext) where the fluctuations of this order were commonplace for 10 point moving skewness.

However we would like to mention important caveats with regards to comparing indicators across different parts of time series separated by very long time intervals. In nature various parameters that determine the dynamics of system do not remain constant and hence comparison of variance/skewness between different time intervals (or even within an interval) need to take this into account. For example, not only can the mean value of the driving parameters vary but also the strength of their fluctuations around the mean value may vary. In such instances true value of indicator will be difficult to extract (see [93] for a model system where it was possible to extract true variance when the data for driving parameter is approximately known). Furthermore, we can expect that the error associated with obtaining the age as well as the composition of sediment is likely to increase as we go back in time. Hence the data in interval (i) is more prone to error than the one in interval (iii) implying that a direct comparison of skewness (as well as variance) fluctuations in different intervals may not be appropriate. Also note that relatively large skewness observed in interval (iv) dies out quickly. A detailed comparative analysis of moving skewness and variance incorporating standard statistical techniques for model systems as well as data

sets such as this can be an important direction of future research.

Lake loading data: We have analyzed a 10 year data set (1997 to 2006) of total phosphorus concentration taken at the Sandusky Bay where the Sandusky river drains into Lake Erie. The primary purpose of this specific data collection is to obtain detailed data on pollutant loading patterns to Lake Erie and not for regime shift investigations at the site of data collection [2]. However, our goal is to demonstrate that skewness calculations can be done with data obtained from routine monitoring if the data is sufficiently resolved. The total phosphorus data is plotted in Fig A.6a and results for the moving skewness is shown in Figs. A.6b. Relatively large changes in skewness are observed for this time series. To check if this changes in skewness are statistically significant, we perform the diagnostic test presented in the main text where we compare the skewness of real data to a data set generated from an AR(1) process. To parameterize the AR(1) model, we chose the total phosphorus concentration data from 09/07/1998 to 01/17/1999: a total of 131 data points and these data do not show substantial asymmetry and hence can act as a reference or null model . We find $\beta = 0.185$ and $\sigma = 0.028$ units. An AR(1) model with these model parameter values is simulated and in a typical simulation we find that the moving average skewness of 100 previous data points fluctuates within the range of $(-0.75, 0.75)$. Clearly the skewness observed in real data is much larger (upto 4) indicating that early warning signal such as skewness can be reliably calculated using long and finely resolved data sets. Results for moving averages calculated for lengths of 75 and 50 data points show qualitatively similar results, but the width of fluctuation for the moving skewness increases as we reduce the window of averaging. Clearly, for 10 data points on which the Sahara data was averaged, the window is large and hence we were unable to make reasonable predictions

for the impending regime shift. We expect that conclusions based on standard statistical significance tests will confirm these inferences based on simple heuristic analysis.

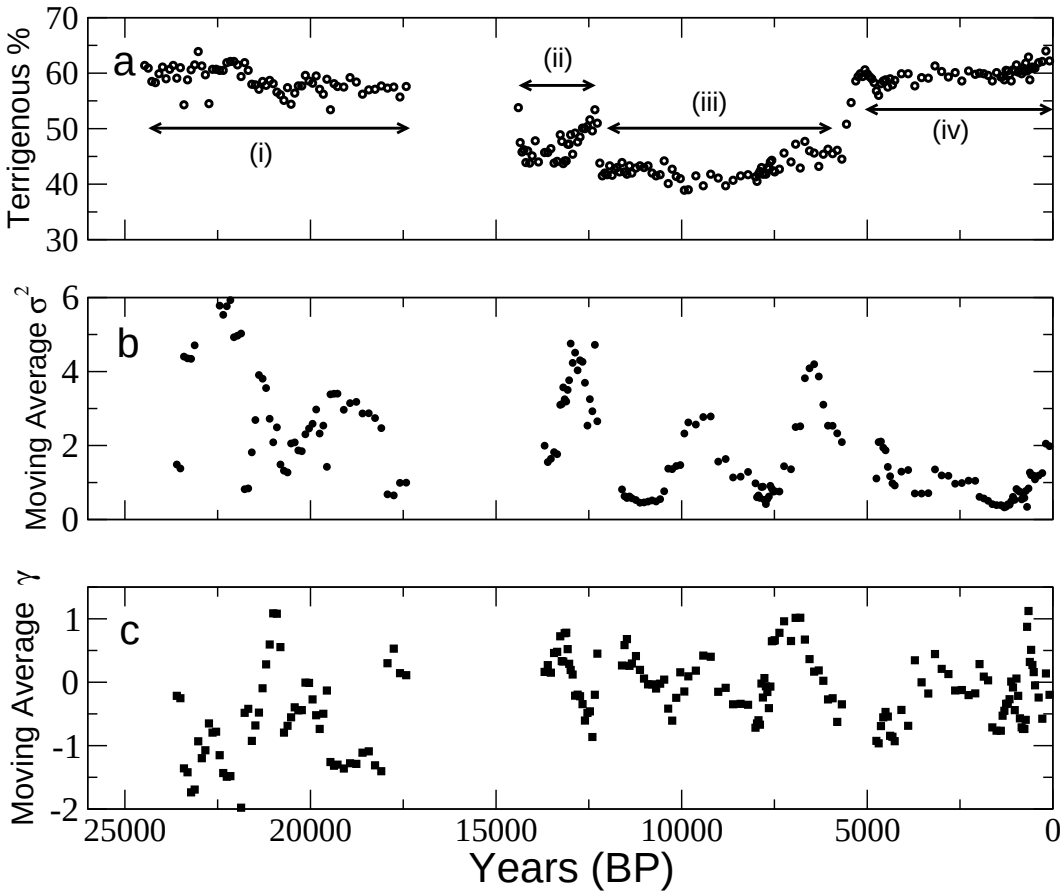

Figure A.5: Analysis of terrigenous sediment data indicating climatic shift in Sahara (a) Time series of terrigenous sediment percentage record from Site 658C off Cap Blanc, Mauritania [1]. Circles represent data while connecting line is meant to guide the eye. BP stands for 'before present'. (b) The moving average variance: for any given time, variance is calculated from the previous 10 data points. (c) The moving average skewness: for any given time, skewness is calculated from the previous 10 data points.

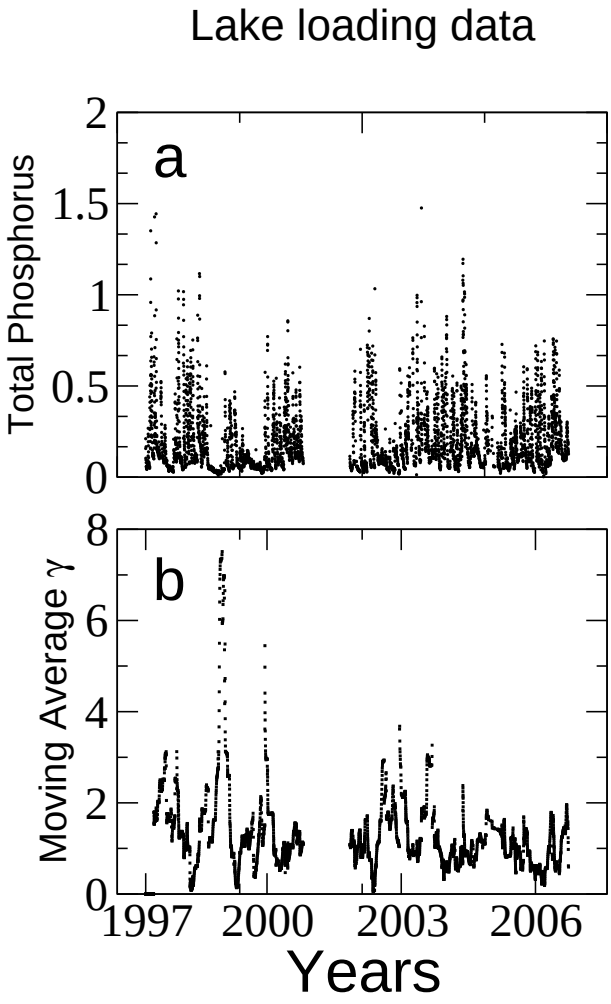

Figure A.6: Analysis of total phosphorous concentration data obtained at one station (Sandusky Bay) in Lake Erie [2] (a) The time series of the data from 1997 to 2006 in units of mg/litre. (b) The moving average skewness, calculated from the preceding 100 data points.

APPENDIX B

SUPPORTING MATERIAL FOR SPATIAL INDICATOR CHAPTER

B.1 Time dependence of indicators for fixed grazing

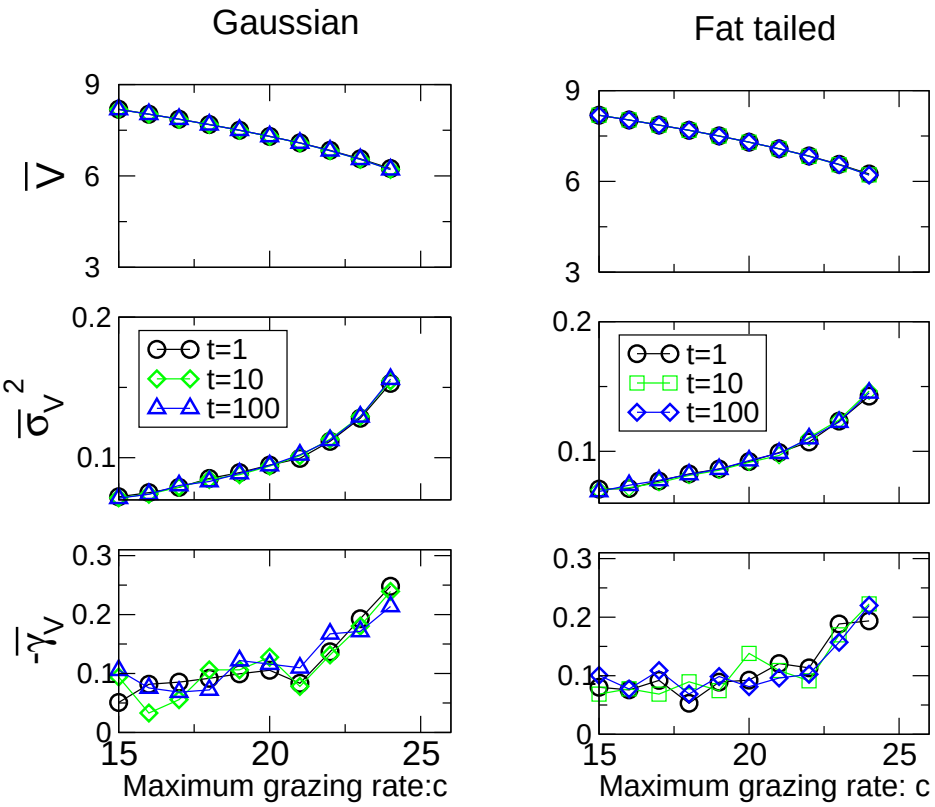

(a) (b)

Figure B.1: Spatial mean, variance and skewness for different kernels. (a) Gaussian Kernel: Parameters are: $dx = 0.1, dt = 0.1, N = 16384, \sigma = 0.1, \sigma_c = 1.0$. (b) Fat tailed kernel: $\theta = 0.1$ and all other parameter values are same as the previous plot.

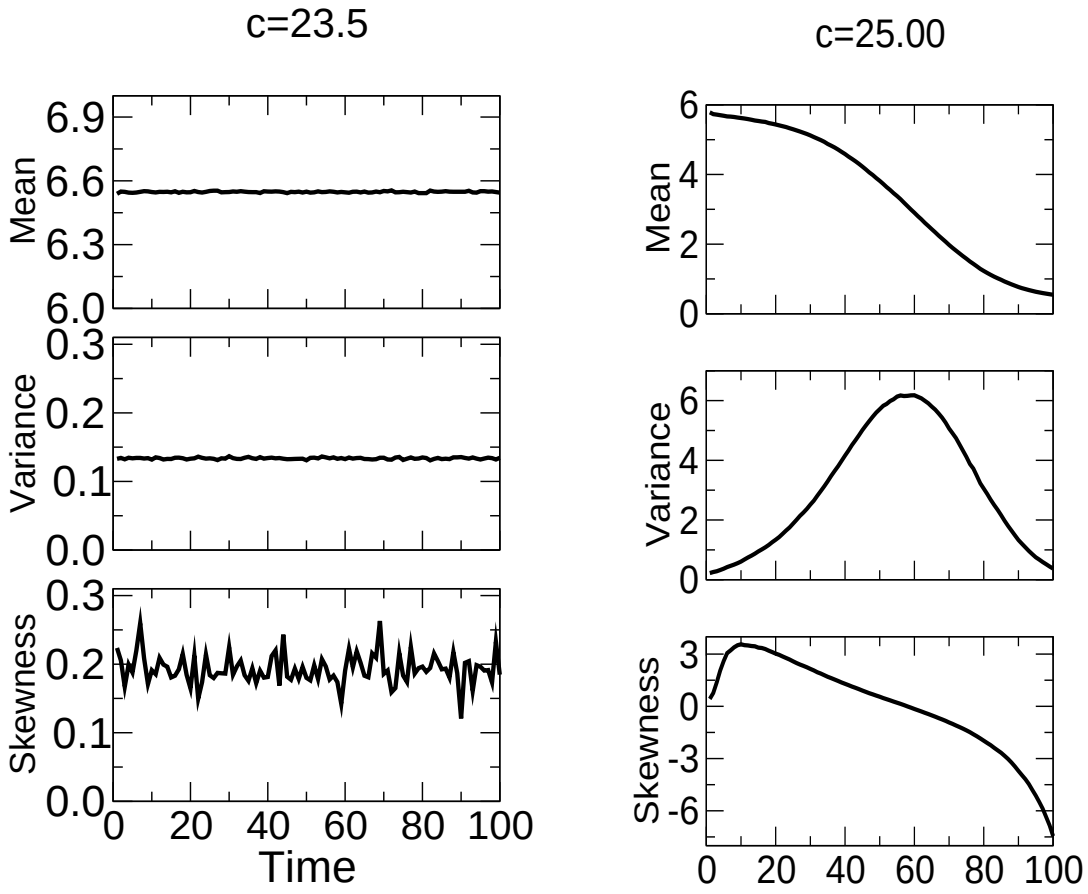

(a) (b)

Figure B.2: To study the temporal dependence of mean, variance and skewness for far from and close to bifurcation for spatial model with diffusion. Parameter values: $N = 128 \times 128, dx = 0.1, dt = 0.001, D = 0.001, r = 10, K = 10, \sigma_c = 4.0$. As (b) clearly indicates, even if the grazing parameter is a constant and has not yet crossed the mean-field threshold for collapse, various moments show a time dependence and the system ultimately collapse to a low density vegetated state.

B.2 Results of dynamic grazing simulations

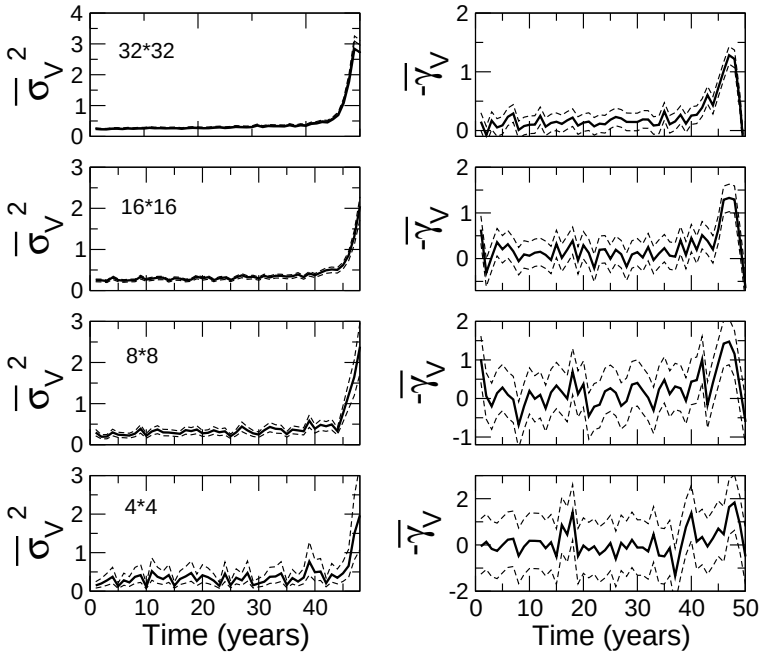

Figure B.3: Spatial variance and skewness with 95% CI for $D = 0.01$. The full results are shown in Chapter 3, Fig. 3.6. We assume that the data points thus obtained form independent set of random numbers. The error bars for the skewness are obtained by $\gamma_{actual} \pm 1.96 * sde$ where sde is the standard error given by $sde = \sqrt{6/N}$ where N is the total number of data points available for the calculation [3]. For this specific simulation, we find that changes in variance and skewness can be reliably detected for data collection at 16×16 or more spatial points.

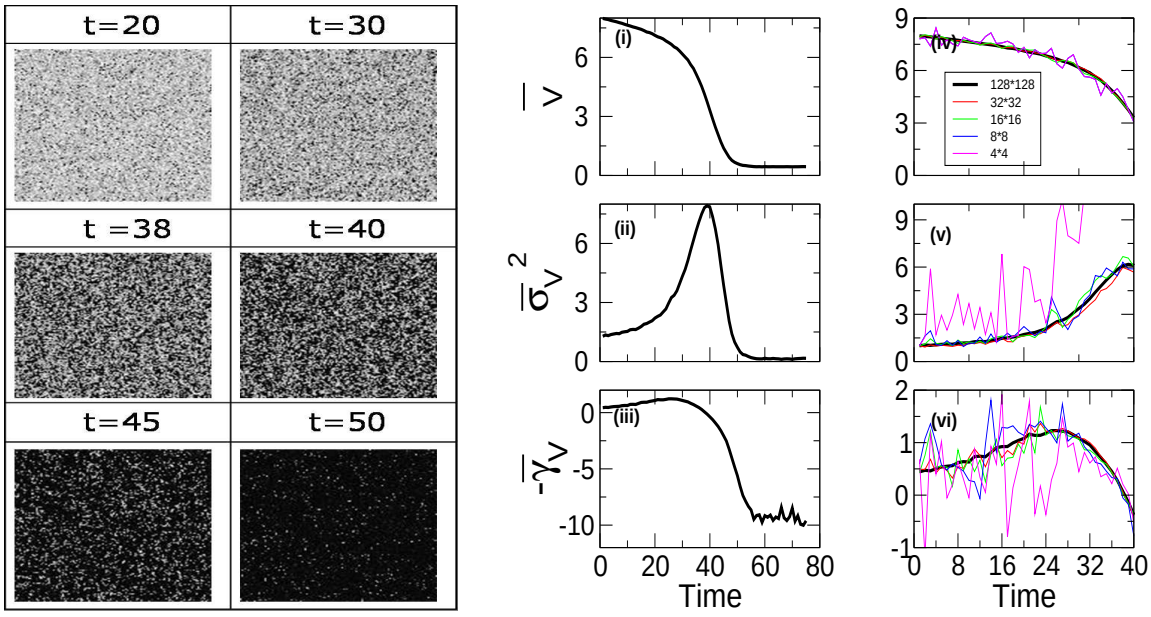

(a) (b)

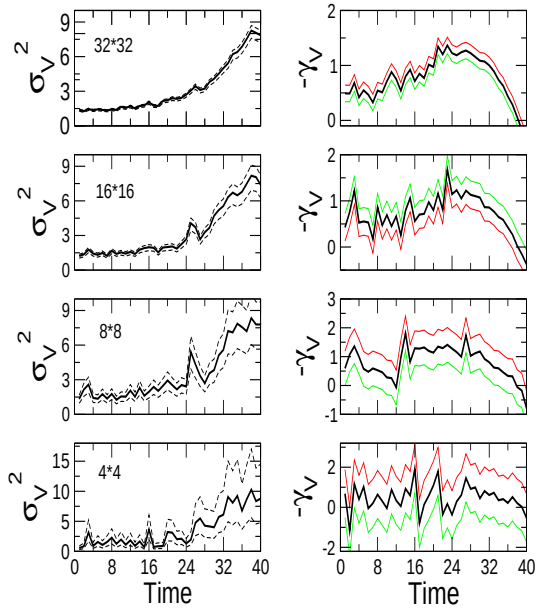

(c)

Figure B.4: Results of dynamic simulation with D=0.001. Parameters are: $r = 10, K = 10, V_0 = 1, \sigma_c = 4.0, c(t = 0) = 15.0$. The grazing rate is incremented discretely by 0.2 units every year until it reaches 26 and is kept constant thereafter. (a) Full spatial patterns. (b) Moments as a function time, with right panel zoomed in just prior to the transition. (c) Variance and skewness with 95% CI.

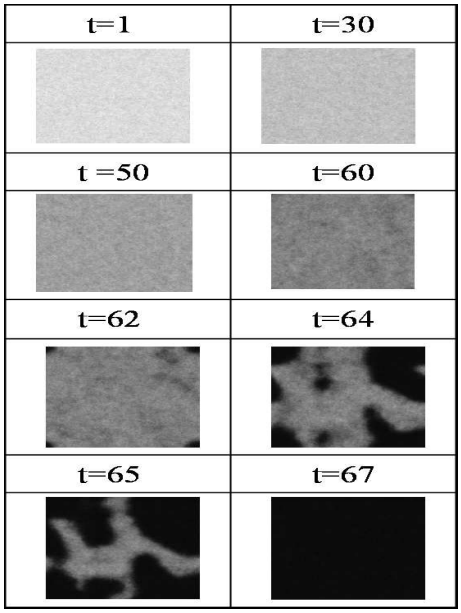

(a)

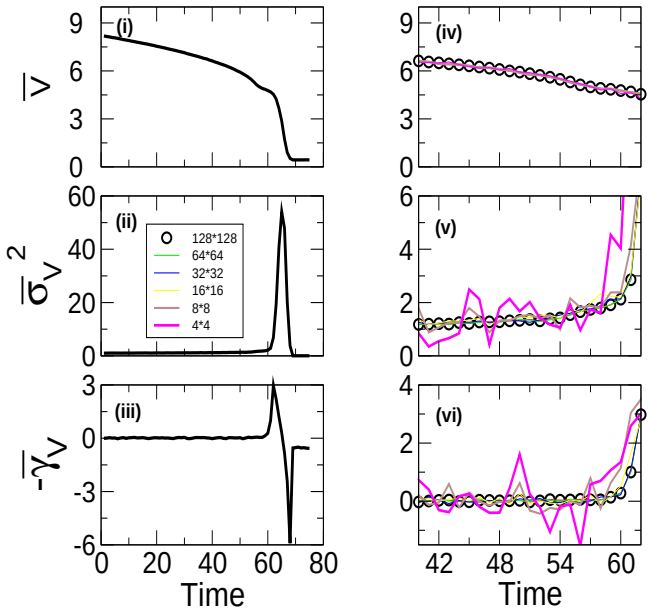

(b)

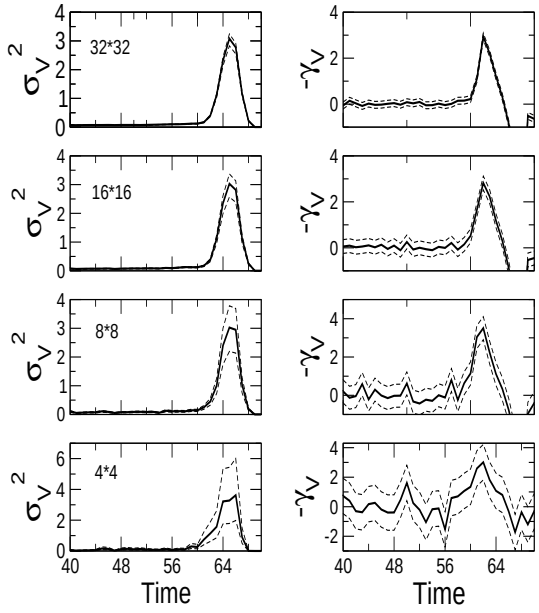

(c)

Figure B.5: Same as Fig B.4, except for $D = 0.1, \sigma_c = 2.0$. Unlike previous cases, we find that changes in variance and skewness can be reliably detected for fewer data collection points (at 8×8 or more).

B.3 One point indicators

In this Appendix we report results for data collected at a single grid point: for each mean grazing rate c, we run the simulation for the full spatial model. The variance and skewness are evaluated from the time series data for 2000 time units and a further averaging over 100 realizations. The time interval corresponds to 2000 years and the results demonstrate that at least in some situations this is an unrealistic procedure. The numerical simulations are not shown if the system starts collapsing to the alternative state within the time period of simulation (*i.e.*, 2000 time units). The results for the mean variance and the magnitude of mean skewness are shown in Fig. B.6.

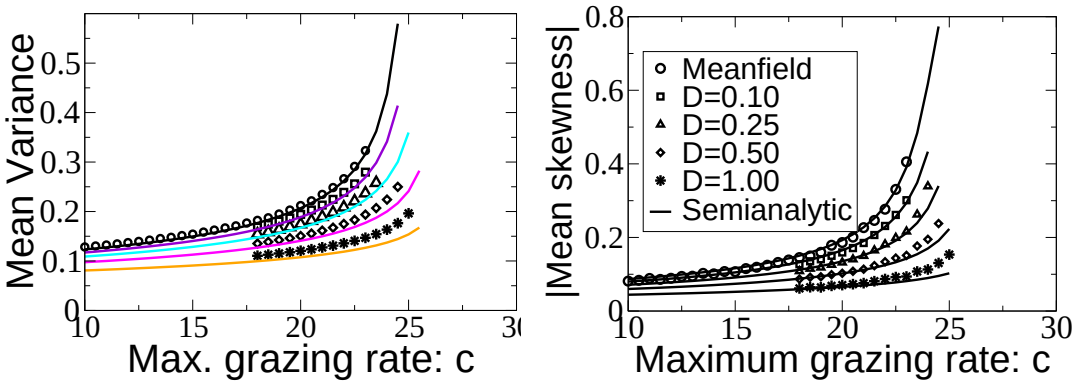

(a) (b)

Figure B.6: One point indicators (variance and skewness) with diffusion.

As the system approaches the threshold c^*, both the mean variance and the (magnitude of) mean skewness increase for different strengths of spatial interaction determined by the diffusion constant D. The results of numerical simulations match fairly well with those of analytical calculations based on a mean field approximation of the full spatial system. Hence

the non-spatial indicators developed under the assumption of a well-mixed system can serve as an early warning signal for the full spatial system with local diffusive interactions. We expect that these results will continue to hold even for other dispersal kernels discussed in the paper, including the heavily fat tailed Cauchy kernel.

APPENDIX C

SUPPORTING MATERIAL FOR SELF-ORGANIZATION CHAPTER

C.1 Jacobian matrix elements

Recall that the three functions are given by:

$$f^o = R_s - O_s \frac{P_s + W_0}{P_s + 1} \tag{C.1}$$

$$f^w = O_s \frac{P_s + W_0}{P_s + 1} - \frac{W_s}{W_s + 1} k P_s - r W_s \tag{C.2}$$

$$f^p = \left(\frac{W_s}{W_s + 1} - d_s \right) P_s \tag{C.3}$$

The matrix elements for a fixed point P^*, W^* and O^*.

$$f^o_o = -f^w_o \qquad f^o_w = 0 \qquad f^o_p = O^* \frac{W_0 - 1}{(1 + P^*)^2} \tag{C.4}$$

$$f^w_o = \frac{P^* + W_0}{1 + P^*} \qquad f^w_w = -r - k f^p_w \qquad f^w_p = -\frac{W^*}{W^* + 1} k - f^o_p \tag{C.5}$$

$$f^p_o = 0 \qquad f^p_w = \frac{P^*}{(1 + W^*)^2} \qquad f^p_p = \frac{W^*}{W^* + 1} - d_s \tag{C.6}$$

Bare state: Many of the expressions can be simplified and we obtain:

$$f^o_o = -W_0 \qquad f^o_w = 0 \qquad f^o_p = O^b_s (W_0 - 1) \tag{C.7}$$

$$f^w_o = W_0 \qquad f^w_w = -r \qquad f^w_p = -\frac{W^b_s}{W^b_s + 1} k - O^b_s (W_0 - 1) \tag{C.8}$$

$$f^p_o = 0 \qquad f^p_w = 0 \qquad f^p_p = \frac{W^b_s}{1 + W^b_s} - d_s \tag{C.9}$$

We also evaluate the elements of the reduced Jacobian matrix. They are denoted by a_{ij}.

$$a_{ww} = -r - q^2 D_{ws}\,, \quad a_{wp} = -\frac{W^b_s}{W^b_s + 1} k - O^b_s (W_0 - 1) + \frac{O^b_s (W_0 - 1)}{W_0 + q^2} W_0 \tag{C.10}$$

$$a_{pw} = 0 \qquad a_{pp} = \frac{W^b_s}{1 + W^b_s} - d_s - q^2 D_{ps} \tag{C.11}$$

Vegetated state: Many of the expressions can be simplified and we obtain:

$$f^o_o = -f^w_o \qquad f^o_w = 0 \qquad f^o_p = O^* \frac{W_0 - 1}{(1 + P^*)^2} \tag{C.12}$$

$$f^w_o = \frac{P^* + W_0}{1 + P^*} \qquad f^w_w = -r - k f^p_w \qquad f^w_p = -d_s k - f^o_p \tag{C.13}$$

$$f^p_o = 0 \qquad f^p_w = \frac{P^*}{(1 + W^*)^2} \qquad f^p_p = 0 \tag{C.14}$$

We now evaluate the elements reduced Jacobian matrix for the vegetated state:

$$a_{ww} = -r - k\frac{P^*}{(1+W^*)^2} - D_{ws}q^2 \quad a_{wp} = -d_s k - \frac{f_p^o}{f_o^o - q^2} f_o^w \tag{C.15}$$

$$a_{pw} = \frac{P^*}{(1+W^*)^2} \qquad a_{pp} = -q^2 D_{ps} \tag{C.16}$$

C.2 Patterns plotted with scale and in color

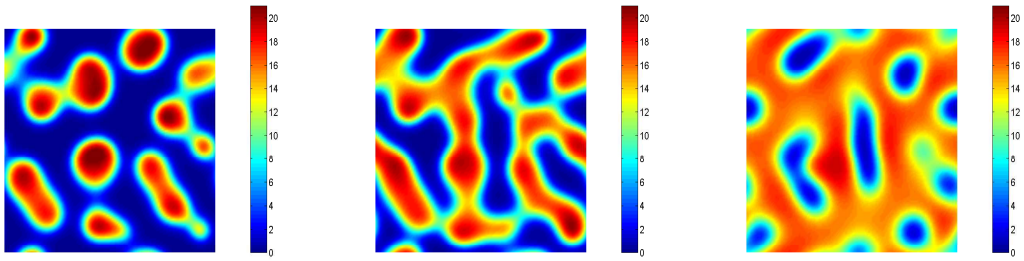

(a) (b) (c)

Figure C.1: These figures show the state of the vegetation patterns at the end of 20^{th} rainy season (t=6800 days). The equations (1-3) were numerically simulated using fully explicit scheme on a $128m \times 128m$ spatial grid starting with plant peaks (P=20) at 10% of the grids, with soil and surface water set to zero everywhere. Periodic boundary conditions were chosen for all these cases. The animation showing how the pattern varies with seasonality is available as online. The length of the rainy season was set to $N_w = 150$ days. All other parameter values are as indicated earlier. (a) Spotted pattern at $R = 2.4\,mm\,d^{-1}$. (b) Labyrinthine pattern at $R = 2.8\,mm\,d^{-1}$ and (c) Gap pattern at $R = 3.25\,mm\,d^{-1}$.

BIBLIOGRAPHY

[1] P. deMenocal, J. Ortiz, T. Guilderson, J. Adkins, M. Sarnthein, L. Baker, and M. Yarusinsky, "Abrupt onset and termination of the african humid period: rapid climate responses to gradual insolation forcing," *Quarterly Science Reviews* **19** (2000) 347–361.

[2] Heidelberg-College, "National center for water quality research, ohio tributary loading program," *Website: http://wql-data.heidelberg.edu/* (2006) Accessed Oct 2006.

[3] B. Tabachnick and L. S. Fidell, *Using multivariate statistics*. Allyn and Bacon, Boston, MA, 2001.

[4] S. Newey, T. Willebrand, D. T. Haydon, F. Dahl, N. J. Aebischer, A. A. Smith, and S. J. Thirgood, "Do mountain hare populations cycle?," *Oikos* **116** (2007) 1547–1557.

[5] K. Higgins, A. Hastings, J. N. Sarvela, and L. W. Botsford, "Stochastic Dynamics and Deterministic Skeletons: Population Behavior of Dungeness Crab," *Science* **276** (1997), no. 5317, 1431–1435.

[6] R. F. Costantino, R. A. Desharnais, J. M. Cushing, and B. Dennis, "Chaotic Dynamics in an Insect Population," *Science* **275** (1997), no. 5298, 389–391.

[7] E. Beninc, J. Huisman, R. Heerkloss, K. D. Jhnk, P. Branco, E. H. V. Nes, M. Scheffer, and S. P. Ellner, "Chaos in a long-term experiment with a plankton community," *Nature* **451** (2008) 822–825.

[8] R. M. May, "Thresholds and breakpoints in ecosystems with a multiplicity of stable states," *Nature* **269** (1977) 471–477.

[9] M. Scheffer, S. R. Carpenter, J. A. Foley, C. Folke, and B. Walker, "Catastrophic shifts in ecosystems," *Nature* **413** (2001) 591–596.

[10] A. Schroder, L. Persson, and A. M. D. Roos, "Direct experimental evidence for alternative stable states: a review," *Oikos* **110** (2005) 3–19.

[11] C. Taylor and A. Hastings, "Allee effects in biological invasions," *Ecology Letters* **8** (2005) 895–908.

[12] J. Murray, *Mathematical Biology*. Springer, Heidelberg, Germany, 2nd ed., 1993.

[13] M. Rietkerk, S. C. Dekker, P. C. de Ruiter, and J. van de Koppel, "Self-organized patchiness and catastrophic regime shifts in ecosystems," *Science* **305** (2004) 1926–1929.

[14] J. van de Koppel, D. van der Wal, J. P. Bakker, and P. M. J. Herman, "Self-Organization and Vegetation Collapse in Salt Marsh Ecosystems," *American Naturalist* **165** (2005) E1–E12.

[15] J. Van de Koppel, A. Altieri, B. Silliman, J. Bruno, and M. Bertness, "Scale-dependent interactions and community structure on cobble beaches," *Ecology Letters* **9** (2006) 45–50.

[16] S. Levin, "The Problem of Pattern and Scale in Ecology: The Robert H. MacArthur Award Lecture," *Ecology* **73** (1992) 1943–1967.

[17] R. May, "Simple mathematical models with very complicated dynamics," *Nature* **261** (1976) 459–467.

[18] A. J. Lodka, *Elements of Physical Biology*. Williams and Wilkins, Baltimore, MD, 1925.

[19] V. Volterra, "Variazioni e fluttazioni del numero d'individui in specie animale conviventi," *Mem R Accad Nazionale del Lincei* **2** (1926) 31–113.

[20] V. Volterra, "Fluctuations in the abundance of a species considered mathematically," *Nature* **118** (1926), no. 558-60,.

[21] R. MacArthur, "Fluctuations of Animal Populations and a Measure of Community Stability," *Ecology* **36** (1955) 533–536.

[22] R. MacArthur, "Population Ecology of Some Warblers of Northeastern Coniferous Forests," *Ecology* **39** (1958) 599–619.

[23] R. MacArthur, *Geographical Ecology: Patterns in the Distribution of Species*. Princeton University Press, Princeton, NJ, 1984.

[24] R. MacArthur and E. Wilson, *The Theory of Island Biogeography*. Princeton University Press, Princeton, NJ, 2001.

[25] R. Lewontin, "The meaning of stability.," *Brookhaven Symp Biol* **22** (1969) 13–24.

[26] J. Sutherland, "Multiple Stable Points in Natural Communities," *The American Naturalist* **108** (1974), no. 964, 859–873.

[27] A. Hastings, C. Hom, S. Ellner, P. Turchin, and H. Godfray, "Chaos in Ecology: Is Mother Nature a Strange Attractor?," *Annual Review of Ecology and Systematics* **24** (1993) 1–33.

[28] S. Levin, "Ecosystems and the Biosphere as Complex Adaptive Systems," *Ecosystems* **1** (1998), no. 5, 431–436.

[29] H. Andrewartha and L. Birch, *The Distribution and Abundance of Animals*. University of Chicago Press, Chicago, IL, 1954.

[30] C. Huffaker, "Experimental studies on predation: dispersion factors and predator-prey oscillations," *Hilgardia* **27** (1958), no. 14, 343–383.

[31] S. Levin, "Dispersion and Population Interactions," *The American Naturalist* **108** (1974) 207–228.

[32] R. Paine and S. Levin, "Intertidal Landscapes: Disturbance and the Dynamics of Pattern," *Ecological Monographs* **51** (1981) 145–178.

[33] C. Neuhauser, "Mathematical challenges in spatial ecology," *Notices of the American Mathematical Society* **48** (2001) 1304–1314.

[34] J. A. Wiens, "Spatial Scaling in Ecology," *Functional Ecology* **3** (1989), no. 4, 385–397.

[35] S. Chandrasekhar, "Stochastic Problems in Physics and Astronomy," *Reviews of Modern Physics* **15** (1943), no. 1, 1–89.

[36] S. Weinberg, *The First Three Minutes: A Modern View of the Origin of the Universe*. Basic Books, 1993.

[37] S. Ma, *Statistical Mechanics*. World Scientific, 1985.

[38] Wikipedia, "Community (ecology) — wikipedia, the free encyclopedia," 2007. [Online; accessed 9-March-2008].

[39] J. Connell and W. Sousa, "On the Evidence Needed to Judge Ecological Stability or Persistence," *The American Naturalist* **121** (1983), no. 6, 789–824.

[40] S. Hare and N. Mantua, "Empirical evidence for North Pacific regime shifts in 1977 and 1989," *Progress in Oceanography* **47** (2000), no. 2-4, 103–145.

[41] I. Blindow, G. Andersson, A. Hargeby, and S. Johansson, "Long-term pattern of alternative stable states in two shallow eutrophic lakes.," *Freshwater biology. Oxford* **30** (1993), no. 1, 159–167.

[42] C. Schelske and P. Brezonik, "Can Lake Apopka be restored," *Restoration of Aquatic Ecosystems (Maurizi, S. et al., eds)* (1992) 393–398.

[43] L. Bengtsson and T. Hellström, "Wild-induced resuspension in a small shallow lake," *Hydrobiologia* **241** (1992), no. 3, 163–172.

[44] S. Engel and S. Nichols, "Aquatic macrophyte growth in a turbid windswept lake," *Journal of Freshwater Ecology* **9** (1994), no. 2, 97–109.

[45] S. Carpenter, D. Ludwig, and W. Brock, "Management of Eutrophication for Lakes Subject to Potentially Irreversible Change," *Ecological Applications* **9** (1999), no. 3, 751–771.

[46] M. Meijer, *Biomanipulation in the Netherlands: 15 years of experience*. Wageningen University, Wageningen, 2000.

[47] M. Scheffer, A. H. Bakema, and F. G. Wortelboer, "Megaplant: a simulation model of the dynamics of submerged plants," *Aquatic Botany* **45** (1993) 341–356.

[48] M. Coe and G. Bonan, "Feedbacks between climate and surface water in northern Africa during the middle Holocene," *Journal of Geophysical Research* **102** (1997), no. D10, 11087–11102.

[49] J. Kutzbach, G. Bonan, J. Foley, and S. Harrison, "Vegetation and soil feedbacks on the response of the African monsoon to orbital forcing in the early to middle Holocene," *Nature* **384** (1996), no. 6610, 623–626.

[50] A. Broström, M. Coe, S. Harrison, R. Gallimore, J. Kutzbach, J. Foley, I. Prentice, and P. Behling, "Land surface feedbacks and palaeomonsoons in northern Africa," *Geophysical Research Letters* **25** (1998), no. 19, 3615–3618.

[51] A. Berger and M. Loutre, "Insolation values for the climate of the last 10,000,000 years," *Quaternary Science Reviews* **10** (1991), no. 4, 297–317.

[52] P. DEMENOCAL and D. RIND, "Sensitivity of Asian and African climate to variations in seasonal insolation, glacial ice cover, sea surface temperature, and Asian orography," *Journal of Geophysical Research* **98** (1993), no. D4, 7265–7287.

[53] W. Prell and J. Kutzbach, "Monsoon variability over the past 150, 000 years," *Journal of Geophysical Research* **92** (1987), no. D7, 8411–8425.

[54] M. Claussen, C. Kubatzki, V. Brovkin, A. Ganopolski, P. Hoelzmann, and H. Pachur, "Simulation of an abrupt change in Saharan vegetation in the mid-Holocene," *Geophysical Research Letters* **26** (1999), no. 14, 2037–2040.

[55] M. Gladwell, *The Tipping Point: How Little Things Can Make a Big Difference*. Back Bay, 2000.

[56] M. Scheffer and S. R. Carpenter, "Catastrophic regime shifts in ecosystems: linking theory and observation," *TRENDS in Ecology and Evolution* **18** (2003) 648–656.

[57] W. Brock, "Tipping points, abrupt opinion changes, and punctuated policy change," in *Punctuated equilibrium and the Dynamics of US Environmental Policy*, R. P. Repetto, ed. 2006.

[58] C. Simenstad, J. Estes, and K. Kenyon, "Aleuts, Sea Otters, and Alternate Stable-State Communities," *Science* **200** (1978), no. 4340, 403–411.

[59] J. Steele, "Regime shifts in fisheries management," *Fisheries Research* **25** (1996), no. 1, 19–23.

[60] P. Petraitis and S. Dudgeon, "Detection of alternative stable states in marine communities," *Journal of Experimental Marine Biology and Ecology* **300** (2004), no. 1-2, 343–371.

[61] C. Walters and S. Martell, *Fisheries Ecology and Management*. Princeton University Press, Princeton, NJ, 2004.

[62] K. Cottenie, N. Nuytten, E. Michels, and L. De Meester, "Zooplankton community structure and environmental conditions in a set of interconnected ponds," *Hydrobiologia* **442** (2001), no. 1, 339–350.

[63] J. M. Chase, "Experimental evidence for alternative stable equilibria in a benthic pond food web," *Ecology Letters* **6** (2003) 733–741.

[64] B. McCune and T. Allen, "Will similar forests develop on similar sites?," *Canadian Journal of Botany* **63** (1985), no. 3, 367–376.

[65] D. Lawrence, P. DOdorico, L. Diekmann, M. DeLonge, R. Das, and J. Eaton, "Ecological feedbacks following deforestation create the potential for a catastrophic ecosystem shift in tropical dry forest.," *Proceedings of National Academy of Sciences, USA* **104** (2007) 20696–20701.

[66] C. Dent, "Multiple states in river and lake ecosystems," *Philosophical Transactions: Biological Sciences* **357** (2002), no. 1421, 635–645.

[67] N. Knowlton, "Thresholds and Multiple Stable States in Coral Reef Community Dynamics," *Integrative and Comparative Biology* **32** (1992), no. 6, 674.

[68] T. Done, "Phase shifts in coral reef communities and their ecological significance," *Hydrobiologia* **247** (1991), no. 1, 121–132.

[69] T. Hughes, "Catastrophes, Phase Shifts, and Large-Scale Degradation of a Caribbean Coral Reef," *Science* **265** (1994), no. 5178, 1547–1551.

[70] L. McCook, "Macroalgae, nutrients and phase shifts on coral reefs: scientific issues and management consequences for the Great Barrier Reef," *Coral Reefs* **18** (1999), no. 4, 357–367.

[71] P. D'Odorico and A. Porporato, "Preferential states in soil moisture and climate dynamics," *Proceedings of the National Academy of Sciences* **101** (2004), no. 24, 8848–8851.

[72] G. T. Narisma, J. A. Foley, R. Licker, and N. Ramankutty, "Abrupt changes in rainfall during the twentieth century," *Geophysical Research Letters* **34** (2007) L06710.

[73] G. M. Daskalov, A. N. Grishin, S. Rodionov, and V. Mihneva, "Trophic cascades triggered by overfishing reveal possible mechanisms of ecosystem regime shifts," *Proceedings of National Academy of Sciences* **104** (2007) 10518–10523.

[74] E. Mccauley, R. M. Nisbe, W. W. Murdoch, A. M. de Roos, and W. S. C. Gurney, "Large-amplitude cycles of Daphnia and its algal prey in enriched environments," *Nature* **402** (1999), no. 6762, 653–656.

[75] W. Nelson, E. McCauley, and F. J. Wrona, "Multiple dynamics in a single predator-prey system: experimental effects of food quality," *Proceedings: Biological Sciences* **268** (2001), no. 1473, 1223–1230.

[76] J. Drake, "Community-Assembly Mechanics and the Structure of an Experimental Species Ensemble," *The American Naturalist* **137** (1991), no. 1, 1–26.

[77] S. Sait, W. Liu, D. Thompson, H. Godfray, and M. Begon, "Invasion sequence affects predator-prey dynamics in a multi-species interaction.," *Nature* **405** (2000), no. 6785, 448–50.

[78] M. Scheffer, S. Szabo, A. Gragnani, E. van Nes, S. Rinaldi, N. Kautsky, J. Norberg, R. Roijackers, and R. Franken, "Floating plant dominance as a stable state," *Proc Natl Acad Sci US A* **100** (2003), no. 7, 4040–4045.

[79] J. Price and P. Morin, "Colonization history determines alternate community states in a food web of intraguild predators," *Ecology* **85** (2004).

[80] G. Harrison, "Multiple stable equilibria in a predator-prey system," *Bulletin of Mathematical Biology* **48** (1986), no. 2, 137–148.

[81] J. van de Koppel, M. Rietkerk, and F. J. Weissing, "Catastrophic vegetation shifts and soil degradation in terrestrial grazing systems," *Trends in Ecology and Evolution* **12** (1997) 352–356.

[82] M. Rietkerk and J. van de Koppel, "Alternate stable states and threshold effects in semi-arid grazing systems," *Oikos* **79** (1997) 69–76.

[83] M. Rietkerk, F. van den Bosch, and J. van de Koppel, "Site-specific properties and irreversible vegetation changes in semi-arid grazing systems," *Oikos* **80** (1997) 241–252.

[84] M. Genkai-Kato, "Macrophyte refuges, prey behaviour and trophic interactions: consequences for lake water clarity," *Ecology Letters* **10** (2007), no. 2, 105–114.

[85] M. Sankaran, N. P. Hanan, R. J. Scholes, J. Ratnam, D. J. Augustine, B. S. Cade, J. Gignoux, S. I. Higgins, X. L. Roux, F. Ludwig, J. Ardo, F. Banyikwa, A. Bronn, G. Bucini, K. K. Caylor, M. B. Coughenour, A. Diouf, W. Ekaya, C. J. Feral, E. C. February, P. G. H. Frost, P. Hiernaux, H. Hrabar, K. L. Metzger, H. H. T. Prins, S. Ringrose, W. Sea, J. Tews, J. Worden, and N. Zambatis, "Determinants of woody cover in african savannas," *Nature* **438** (2005) 846–849.

[86] S. Strogatz, *Nonlinear Dynamics and Chaos*. WestView Press, U.S.A., 1994.

[87] G. Uhlenbeck and L. Ornstein, "On the Theory of the Brownian Motion," *Physical Review* **36** (1930) 823–841.

[88] C. W. Gardiner, *Handbook of stochastic methods for Physics, Chemistry and the Natural Sciences.* Springler-Verlag, 3rd edition ed., 2003.

[89] W. Horsthemke and R. Lefever, *Noise-Induced Transitions*. Springer-Verlag, New York, NY, 1984.

[90] C. Wissel, "A universal law of the characteristic return time near thresholds," *Oecologia* **65** (1984), no. 1, 101–107.

[91] T. Kleinen, H. Held, and G. Petschel-Held, "The potential role of spectral properties in detecting thresholds in the Earth system: application to the thermohaline circulation," *Ocean Dynamics* **53** (2003), no. 2, 53–63.

[92] H. Held and T. Kleinen, "Detection of climate system bifurcations by degenerate fingerprinting," *Geophysical Research Letters* **31** (2004), no. 23, L020972.

[93] S. R. Carpenter and W. A. Brock, "Rising variance: a leading indicator of ecological transition.," *Ecology Letters* **9** (2006) 308–315.

[94] E. H. van Nes and M. Scheffer, "Slow recovery from perurbations as a generic indicator of a nearby catastrophic regime shift," *American Naturalist* **169** (2007) 738–747.

[95] V. Guttal and C. Jayaprakash, "Impact of noise on bistable ecological systems," *Ecological Modelling* **201** (2007) 420–428.

[96] I. Noy-Meir, "Stabilty of grazing systems: An application of predator-prey graphs," *Journal of Ecology* **63** (1975) 459–482.

[97] S. R. Carpenter, "Eutrophication of aquatic ecosystems: Bistability and soil phosphorus," *Proceedings of the National Academy of Sciences* **102** (2005) 10002–10005.

[98] J. H. Steele and E. W. Henderson, "Modelling long-term fluctuations in fish stocks," *Science* **224** (1984) 985–987.

[99] D. Ludwig, D. D. Jones, and C. S. Holling, "Qualitative analysis of insect outbreak systems: the spruce budworm and forest," *Journal of Animal Ecology* **47** (1978) 315–332.

[100] E. van Nes, M. Scheffer, M. van den Berg, and H. Coops, "Dominance of charophytes in eutrophic shallow lakes– when should we expect it to be an alternative stable state?," *Aquatic Botany* **72** (2002), no. 3, 275–296.

[101] J. van de Koppel, M. Rietkerk, and F. J. Weissing, "Catastrophic vegetation shifts and soil degradation in terrestrial grazing systems," *Trends in Ecology and Evolution* **12** (1997) 352–356.

[102] H. Risken, *The Fokker-Planck Equation: Methods of solution and applications.* Springer-Verlag, 1984.

[103] K. L. Drury, "Shot noise perturbations and mean first passage times between stable states," *Theoretical Population Biology* **72** (2007), no. 1, 153–166.

[104] P. A. Soranno, S. R. Carpenter, and R. C. Lathrop, "Internal phosphorus loading in lake mandota: response to external loads and weather," *Can. J. Fish. Aquat. Sci.* **54** (1997) 1883–1893.

[105] A. Ives, "Measuring Resilience in Stochastic Systems," *Ecological Monographs* **65** (1995), no. 2, 217–233.

[106] N. Mantua, "Methods for detecting regime shifts in large marine ecosystems: a review with approaches applied to North Pacific data," *Progress in Oceanography* **60** (2004), no. 2-4,.

[107] S. Rodionov, "A sequential algorithm for testing climate regime shifts," *Geophysical Research Letters* **31** (2004), no. 9, L09204.

[108] C. Hsieh, S. Glaser, A. Lucas, and G. Sugihara, "Distinguishing random environmental fluctuations from ecological catastrophes for the North Pacific Ocean," *Nature* **435** (2005), no. 7040, 336–340.

[109] A. Mayer, C. Pawlowski, and H. Cabezas, "Fisher Information and dynamic regime changes in ecological systems," *Ecological Modelling* **195** (2006), no. 1, 72–82.

[110] S. Rodionov, "Use of prewhitening in climate regime shift detection," *Geophysical Research Letters* **33** (2006), no. 12, L12707.

[111] G. Sugihara, M. Casdagli, E. Habjan, D. Hess, P. Dixon, and G. Holland, "Residual delay maps unveil global patterns of atmospheric nonlinearity and produce improved local forecasts," *Proceedings of the National Academy of Sciences of the United States of America* **96** (1999), no. 25, 14210.

[112] C. Van den Broeck, J. M. R. Parrondo, and R. Toral, "Noise-induced nonequilibrium phase transition," *Phys. Rev. Lett.* **73** (Dec, 1994) 3395–3398.

[113] W. H. Press, S. A. Teukolsky, W. T. Vetterling, and B. P. Flannery, *Numerical recipes C++*. Cambridge university press, UK, 2nd edition ed., 2002.

[114] R. HilleRisLambers, M. Rietkerk, F. van den Bosch, H. H. T. Prins, and H. de Kroon, "Vegetation pattern formation in semi-arid grazing systems," *Ecology* **82** (2001) 50–61.

[115] S. Kéfi, M. Rietkerk, C. L. Alados, Y. Pueyo, V. P. Papanastasis, A. ElAich, and P. C. de Ruiter, "Spatial vegetation patterns and imminent desertification in mediterranean arid ecosystems," *Nature* **449** (2007) 213–217.

[116] T. Scanlon, K. Caylor, S. Levin, and I. Rodriguez-Iturbe, "Positive feedbacks promote power-law clustering of Kalahari vegetation.," *Nature* **449** (2007), no. 7159, 209–12.

[117] K. Binder, "Theory of First-Order Phase Transitions," *Reports on Progress in Physics* (1987) 783–859.

[118] J. Sethna, *Statistical Mechanics: Entropy, Order Parameters, and Complexity*. Oxford University Press, Oxford, UK, 2006.

[119] M. Kot, M. Lewis, and P. van den Driessche, "Dispersal Data and the Spread of Invading Organisms," *Ecology* **77** (1996), no. 7, 2027–2042.

[120] J. Clark, C. Fastie, G. Hurtt, S. Jackson, C. Johnson, G. King, M. Lewis, J. Lynch, S. Pacala, C. Prentice, *et al.*, "Reids paradox of rapid plant migration: dispersal theory and interpretation of paleoecological records," *BioScience* **48** no. 1, 13–24.

[121] P. Turchin, *Quantitative Analysis of Movement: Measuring and Modeling Population Redistribution in Animals and Plants*. Sinauer Associates, 1998.

[122] J. Levine and D. Murrell, "The Community-Level Consequences of Seed Dispersal Patterns," *Annual Review of Ecology, Evolution and Systematics* **34** (2003) 549–574.

[123] R. Nathan, "Long distance dispersal of plants," *Science* **313** (2006) 786–788.

[124] A. Gandhi, S. Levin, and S. Orszag, ""Critical Slowing Down" in Time-to-extinction: an Example of Critical Phenomena in Ecology," *Journal of Theoretical Biology* **192** (1998), no. 3, 363–376.

[125] A. Gandhi, S. A. Levin, and S. Orszag, "Nucleation and Relaxation from Meta-stability in Spatial Ecological Models," *Journal of Theoretical Biology* **200** (1999) 121–146.

[126] V. Guttal and C. Jayaprakash, "Changing skewness: An early warning signal of regime shifts in ecological systems," *Ecology Letters* **11** (2008) 450–460.

[127] R. Rossi, D. Mulla, A. Journel, and E. Franz, "Geostatistical Tools for Modeling and Interpreting Ecological Spatial Dependence," *Ecological Monographs* **62** (1992) 277–314.

[128] J. Horne and D. Schneider, "Spatial Variance in Ecology," *Oikos* **74** (1995) 18–26.

[129] J. HORNE, "Spatial variance of mobile aquatic organisms: capelin and cod in Newfoundland coastal waters," *Philosophical Transactions of the Royal Society B: Biological Sciences* **352** (1997) 633–642.

[130] E. Logerwell, R. Hewitt, and D. Demer, "Scale-Dependent Spatial Variance Patterns and Correlations of Seabirds and Prey in the Southeastern Bering Sea as Revealed by Spectral Analysis," *Ecography* **21** (1998) 212–223.

[131] F. He and K. J. Gaston, "Scale-Dependent Spatial Variance Patterns and Correlations of Seabirds and Prey in the Southeastern Bering Sea as Revealed by Spectral Analysis," *The American Naturalist* **162** (2003) 366–375.

[132] N. Barbier, P. Couteron, J. Lejoly, V. Deblauwe, and O. Lejeune, "Self-organized vegetation patterning as a fingerprint of climate and human impact on semi-arid ecosystems," *Journal of Ecology* **94** (2006) 537–547.

[133] S. R. Carpenter, W. A. Brock, J. J. Cole, F. Ketchell, and M. L. Pace, "Leading indicators of trophic cascades," *Ecology Letters* **10** (2008) –.

[134] S. Levin, "Multiple Scales and the Maintenance of Biodiversity," *Ecosystems* **3** (2000), no. 6, 498–506.

[135] E. van Nes and M. Scheffer, "Implications of spatial heterogeneity for catastrophic regime shifts in ecosystems," *Ecology* **86** (2005), no. 7, 1797–1807.

[136] S. Altizer, A. Dobson, P. Hosseini, P. Hudson, M. Pascual, and P. Rohani, "Seasonality and the dynamics of infectious diseases.," *Ecology Letters* **2006** (2004) 467–484.

[137] B. Grenfell, B. Bolker, and A. Kleczkowski, "Seasonality and Extinction in Chaotic Metapopulations," *Proceedings: Biological Sciences* **259** (1995), no. 1354, 97–103.

[138] A. King and W. Schaffer, "The geometry of a population cycle: A mechanistic model of snowshow hare demography," *Ecology* **82** (2001), no. 3, 814–830.

[139] N. Stenseth, H. Viljugrein, T. Saitoh, T. Hansen, M. Kittilsen, E. Bolviken, and F. Glockner, "Seasonality, density dependence, and population cycles in Hokkaido voles," *Proceedings of the National Academy of Sciences* **100** (2003), no. 20, 11478–11483.

[140] N. M. Shnerb, P. Sarah, H. Lavee, and S. Solomon, "Reactive glass and vegetation patterns," *Physical Review Letters* **90** (2003) 038101.

[141] N. Ursino and S. Contarini, "Stability of banded vegetation patterns under seasonal rainfall and limited soil moisture storage capacity," *Advances in Water Resources* **29** (2006) 1556–1564.

[142] I. Rodriguez-Iturbe, A. Porporato, L. Ridolfi, V. Isham, and D. R. Cox, "Probabilistic modelling of water balance at a point: the role of climate, soil and vegetation," *Proceedings of the Royal Society A: Mathematical, Physical and Engineering Sciences* **455** (1999), no. 1990, 3789–3805.

[143] P. D'Odorico, F. Laio, A. Porporato, and I. Rodriguez-Iturbe, "Hydrologic controls on soil carbon and nitrogen cycles. II. A case study," *Advances in Water Resources* **26** (2003), no. 1, 59–70.

[144] V. Guttal and C. Jayaprakash, "Self-organization and productivity in semi-arid ecosystems: Implications of seasonality in rainfall," *Journal of Theoretical Biology* **248** (2007), no. 3, 490–500.

[145] J. M. Thiery, J. M. d'Herbés, and C. Valentin, "A model simulating the genesis of banded vegetation patterns in niger," *The Journal of Ecology* **83** (1995) 497–507.

[146] R. Lefever and O. Lejeune, "On the origin of tiger bush," *Bulletin of Mathematical Biology* **59** (1997), no. 2, 263–294.

[147] C. A. Klausmeier, "Regular and irregular patterns in semiarid vegetation," *Science* **284** (1999) 1826–1828.

[148] J. von Hardenberg, E. Meron, M. Shachak, and Y. Zarmi, "Diversity of vegetation patterns and desertification," *Physical Review Letters* **2001** (2001) 198101:1–4.

[149] T. Okayasu and Y. Aizawa, "Systematic Analysis of Periodic Vegetation Patterns," *Progress of Theoretical Physics* **106** (2001), no. 4, 705–720.

[150] O. Lejeune, M. Tlidi, and P. Couteron, "Localized vegetation patches: A self-organized response to resource scarcity," *Physical Review E* **66** (2002) 010901(R).

[151] E. Gilad, J. von Hardenberg, A. Provenzale, M. Shachak, and E. Meron, "Ecosystem Engineers: From Pattern Formation to Habitat Creation," *Physical Review Letters* (2004) 98105.

[152] J. Sherratt, "An Analysis of Vegetation Stripe Formation in Semi-Arid Landscapes," *Journal of Mathematical Biology* **51** (2005) 183–197.

[153] P. D'Odorico, F. Laio, and L. Ridolfi, "Vegetation patterns induced by random climate fluctuations," *Geophysical Research Letters* **33** (2006) L19404.

[154] J. Sherratt and G. Lord, "Nonlinear dynamics and pattern bifurcations in a model for vegetation stripes in semi-arid environments," *Theoretical Population Biology* **71** (2007) 1–11.

[155] M. Rietkerk, M. C. Boerlijst, F. van Langevelde, R. HilleRisLambers, J. van de Koppel, L. Kumar, H. H. T. Prins, and A. M. de Roos, "Self-organization of vegetation in arid ecosystems," *American Naturalist* **160** (2002) 524–530.

[156] H. Walter, *Ecology of tropical and subtropical vegetation*. Oliver and Boyd, Edinburgh, 1971.

[157] M. Evenari, "Adaptations of plants and animals to the desert environment," in *Hot Deserts and arid Shrublands*, M. Evenari, I. Noy-Meir, and D. W. Goodall, eds., ch. 12A, pp. 79–92. Elsevier, Amsterdam, 1985.

[158] D. Hillel, *Environmental soil physics*. Academic Press, CA, USA, 1998.

[159] R. L. Scott, W. J. Shuttleworth, D. C. Goodrich, and T. Maddock-III, "The water use of two dominant vegetation communities in a semiarid riparian ecosystem," *Agricultural and Forest Meterology* **105** (2000) 241–256.

[160] M. Galassi, J. Davies, J. Theiler, B. Gough, G. Jungman, M. Booth, and F. Rossi, *GNU Scientific Library Reference Manual*. revised 2nd edition ed., 2003.

[161] B. T. Bestelmeyer, J. P. Ward, and K. M. Harvstad, "Soil-geomorphic heterogeneity governs patchy vegetation dynamics at an arid ecotone," *Ecology* **87** (2006) 963–973.

[162] M. Holmgren, P. Stapp, C. R. Dickman, C. Gracia, S. Graham, J. R. Gutiérrez, C. Hice, F. Jaksic, D. A. Kelt, M. Letnic, M. Lima, B. C. López, P. L. Meserve, W. B. Milstead, G. A. Polis, , M. A. Previtali, M. Richter, S. Sabaté, and F. A. Squeo, "Extreme climatic events shape arid and semiarid ecosystems," *Frontiers in Ecology and the Environment* **4** (2006) 87–95.

[163] R. Katz and B. Brown, "Extreme events in a changing climate: Variability is more important than averages," *Climatic Change* **21** (1992), no. 3, 289–302.

[164] P. D'Odorico, F. Laio, and L. Ridolfi, "Noise-induced stability in dryland plant ecosystems," *Proceedings of the National Academy of Sciences* **102** (2005), no. 31, 10819–10822.

[165] M. Scheffer, M. Holmgren, V. Brovkin, and M. Claussen, "Synergy between small and large-scale feedbacks of vegetation on the water cycle," *Global Change Biology* **11** (2005) 1003–12.

[166] S. Dekker, M. Rietkerk, and M. Bierkens, "Coupling microscale vegetation-soil water and macroscale vegetation-precipitation feedbacks in semiarid ecosystems," *Global Change Biology* **13** (2007) 671–678.

[167] B. Obórny, G. Meszéna, and G. Szabó, "Dynamics of populations on the verge of extinction," *Oikos* **109** (2005), no. 2, 291–296.